THE DYNAMICS OF LIGAND EXCHANGE PROCESSES ON MAGNESIUM(II), SCANDIUM(III) AND YTTRIUM(III) IONS

A thesis submitted for the degree of

Doctor of Philosophy

by

DINO LUIGI PISANIELLO, B.Sc.(Hons.)

Department of Physical and Inorganic Chemistry

The University of Adelaide

October 1980

CONTENTS

CONTENTS (continued)

CONTENTS (continued)

SUMMARY

Variable temperature n.m.r. spectroscopy has been used to directly investigate unidentate ligand exchange processes on magnesium(II), scandium(III) and yttrium(III) ions in non-aqueous media. Sample solutions for the kinetic studies were usually composed of the ligand (e.g. dmf) and the corresponding metal complex (as the perchlorate salt, e.g. $[Mg(dmf)_6](ClO_4)_2$) dissolved together in a non-coordinating diluent. For many such samples the exchange of ligand between free and coordinated environments was conveniently monitored by the n.m.r. lineshape analysis technique. Assignments of the ligand exchange mechanisms were generally founded on the observed rate laws (reported for the first time) with respect to free ligand concentration.

In the case of those magnesium(II) ligand exchange systems studied in detail, reactions proceeded via dissociative-type pathways. The derived kinetic parameters are similar to those for other magnesium(II) systems in the literature. Substitution reactions at the scandium(III) centre were found to be extraordinarily sensitive to ligand and diluent properties and a variety of rates and mechanisms were observed. For example, formamide-type ligands exchanged at rates outside the ^1H n.m.r. time scale whereas the exchange rates of acetamide analogues (which characterized two term rate laws) fell conveniently within that scale. Furthermore, the lability of six-coordinate acetamide complexes of scandium(III) decreased as the sizes of the nitrogen substituents increased in the series N-methylacetamide, N,N-dimethylacetamide and N,N-diethylacetamide. Yttrium(III) complex species were generally more labile than their scandium(III) counterparts. An expected greater tendency for yttrium(III) to achieve a ground or transition state coordination number larger than six is thought to be

partly responsible for the behaviour. Nevertheless, lineshape analysis was readily applicable to the 1,1,3,3-tetramethylurea and methylmethylphenylphosphinate systems. An improved method of analysing kinetic data for a two term rate law has been developed from these investigations.

For the three metal ions examined, steric effects and interactions outside the first coordination sphere appear to significantly influence kinetic parameters in a complex manner. An extrathermodynamic linear relationship between $\Delta H^{\ddagger}$ and $\Delta S^{\ddagger}$ (which seems to arise from intimate characteristics of the ligand and diluent) was statistically confirmed for the scandium(III) data and probably also exists for other metal ions. Comparisons of metal ion lability may thus be meaningfully made on an empirical basis from plots of $\Delta H^{\ddagger}$ against $\Delta S^{\ddagger}$. Finally, simple electrostatic models of metal-ligand interaction are found to be surprisingly useful in describing ligand exchange phenomena on these hard metal ions.

DECLARATION

This thesis contains no material previously submitted for a degree or diploma in any university, and, to the best of the candidate's knowledge, contains no material written or devised by another person, except where an appropriate reference is made.

The author accepts full responsibility for any errors present in the treatise, regardless of their nature.

Dino Pisaniello

ACKNOWLEDGEMENTS

I extend genuine gratitude to my supervisor, Dr. S.F. Lincoln, who through his continual encouragement and guidance has contributed significantly to the essence of this research.

I am indebted to Dr. T.M. Spotswood and Mr. E.H. Williams for their enlightening discussions and assistance in technical matters. I wish to thank Dr. A. Jones of the Research School of Chemistry at the Australian National University, Canberra, for recording a series of 270 MHz ^{1}H n.m.r. spectra.

My thanks are also due to Professors D.O. Jordan and M.I. Bruce for making available to me the facilities of the Department. I acknowledge the financial assistance of a Commonwealth Postgraduate Research Award for the period of my candidature. A special mention must be given to my fellow students for their help and friendship. I also thank Mrs. Dawn Darwent and Mrs. Elaine Curran for typing the manuscript.

My final appreciation is directed to my wife, Lisa, and my parents for their interest and support.

LIGAND TERMINOLOGY

Acronym	*Structural Formula*	*Systematic or Trivial Name*
nmf	O:CH(NHMe)	N-methylformamide
nma	O:CMe(NHMe)	N-methylacetamide
dmf	O:CH(NMe_2)	N,N-dimethylformamide
dma	O:CMe(NMe_2)	N,N-dimethylacetamide
def	O:CH(NEt_2)	N,N-diethylformamide
dea	O:CMe(NEt_2)	N,N-diethylacetamide
dbf	O:CH($NnBu_2$)	N,N-di-n-butylformamide
npa	O:CMe(NHC_6H_5)	N-phenylacetamide (acetanilide)
dmso	O:S$\acute{M}e_2$	dimethylsulphoxide
tso	O:S(p-C_6H_4-Me)$_2$	4,4'-ditolylsulphoxide
dmmp	O:P(OMe)$_2$Me	dimethylmethylphosphonate
tmp	O:P(OMe)$_3$	trimethylphosphate
mmpp	O:P(OMe)Me(OC_6H_5)	methylmethylphenylphosphinate
tppo	O:P(C_6H_5)$_3$	triphenylphosphineoxide
hmpa	O:P(NMe_2)$_3$	hexamethylphosphoramide
dmadmp	O:P(OMe)$_2$(NMe_2)	N,N-dimethylamido-O,O'-dimethylphosphate
tmdamp	O:P(OMe)(NMe_2)$_2$	bis(N,N-dimethylamido)-O-methylphosphate
dmu	O:C(NHMe)$_2$	1,3-dimethylurea
tmu	O:C(NMe_2)$_2$	1,1,3,3-tetramethylurea
tmtu	S:C(NMe_2)$_2$	1,1,3,3-tetramethylthiourea

N.B. The colons in the structural formulae represent double bonds.

DEFINITIONS

k_{ex}	General rate constant for an exchange process.
k_1	Elementary rate constant pertaining to a ligand exchange process which is independent of free ligand concentration.
k_2	Elementary rate constant pertaining to a ligand exchange process in which the overall rate is directly proportional to the free ligand concentration.
K	Equilibrium constant associated with the interchange mechanism.
k_{int}	Rate constant for interchange of ligands between the first and second coordination spheres according to an interchange formalism.
[ligand]	Free ligand concentration; i.e. the concentration of ligand not in the first coordination sphere of the metal ion.

CHAPTER 1 INTRODUCTION

1.1 Preamble

The fundamental reaction for a metal cation in solution is considered to be the exchange of solvent molecules between the primary solvation shell of the cation and 'bulk' solvent. A solvent molecule in the first solvation or coordination shell is defined to be one which is within 'contact' or 'bonding' distance of the metal ion and whose residence time in the immediate vicinity of the metal ion is long compared with its correlation time in outer solvation shells and the bulk solvent. Strong evidence[1] exists to support the notion that a definite number (coordination number) of spatially ordered solvent molecules occupy the first coordination sphere of a metal ion in solution.

The chemical characteristics of the hydrated metal ion in dilute aqueous solution are thought to be satisfactorily explained by a model similar to that of Frank and Wen[2] in which the metal ion is at the centre of a series of concentric regions of water. This model is depicted in Figure 1.1. The innermost region, A, is the first coordination sphere (as defined above) and is the region of greatest importance as far as studies of reaction mechanisms are concerned. Region B is the second coordination sphere in which the metal ion orientates the water molecules directly through an electrostatic interaction and indirectly through the polarization of the water molecules in the first coordination sphere. In region C, the third hydration sphere, the water molecules are disordered as a consequence of competing orientation forces emanating from the second hydration sphere and bulk water (region D). The interface between regions A

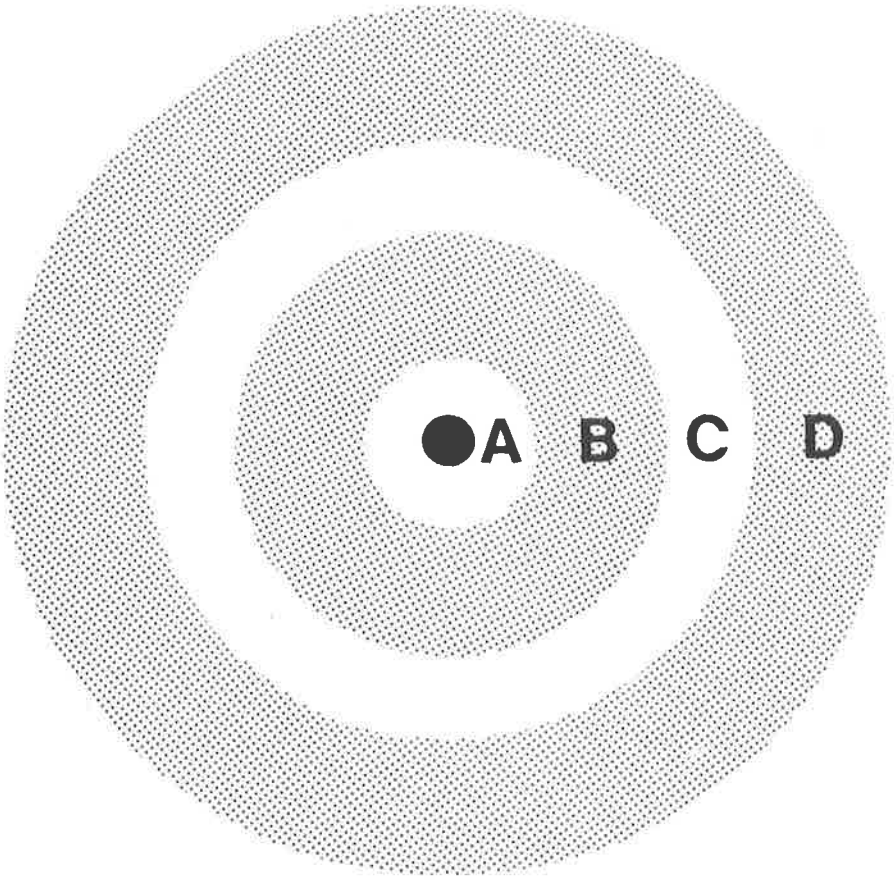

FIGURE 1.1 Structural model for a solvated metal ion.

and B is well defined for metals of high surface charge density. However, the 'boundaries' between regions B, C and D are indistinct[3] and in non-hydrogen bonding solvents such as N,N-dimethylacetamide regions B and C are probably indistinguishable from bulk solvent.

It is remarkable that the observed rate constants at room temperature for the unidentate solvent exchange reaction,

$$[MS_n]^{m+} + S^* \rightleftharpoons [MS_{n-1}S^*]^{m+} + S$$

(asterisk is typographical distinction only)

where S is a neutral solvent molecule (normally an oxygen donor ligand), span at least seventeen orders of magnitude. However, as will be discussed later, the major factors determining the rate of solvent exchange on a metal ion probably arise from the metal itself[4,5]. In particular, cation size and charge are important but equally important are crystal field effects. The influence of the latter factor may be gauged by the fact that the bivalent first row transition metal ions whose ionic radii are in the range 0.57 - 0.83 Å (enclosed by Co^{2+} and Mn^{2+} respectively) exhibit a water exchange rate constant variation of $\sim 10^9$ which shows little dependence upon ionic radius. Cations which have large crystal field stabilization energies are likely to have large crystal field activation energies with respect to substitution processes. On the other hand, transition metal ions may be particularly labile because of tetragonal distortions (e.g. Cu^{2+}).

This thesis deals with ligand exchange on spherical metal ions which are devoid of crystal field effects (hereafter referred to as closed shell ions) and specifically with neutral unidentate ligands (usually common organic solvents). Exchange of these ligands represents the simplest type of ligand exchange process.

1.2 Substitution on a solvated metal ion

Extensive investigation of the rudiments of multidentate complex formation processes (a subject which has relevance to metal oriented biological reactions) has been undertaken[6-8]. Eigen and coworkers[9,10] using relaxation methods have been particularly active in this area. Although these studies have been extensive it would appear that a more detailed examination of the precursive solvent exchange reaction is needed in order to explain observed variations in complex formation rates and to clarify proposed mechanisms which involve solvento complex species.

At the outset, measured enthalpies of solvation, molecular orbital calculations and simple electrostatic models[11] suggest that the bond between solvent and metal is very strong indeed (typically > 100 kJ mol^{-1}). The fact that many solvated ions are labile (k_{ex}(300 K) > 0.1 s^{-1}) towards ligand substitution through a variety of exchange mechanisms implies that the strength of a single metal-solvent bond is only one of the factors determining the substitution kinetics and that a fine balance exists between these factors.

The best experimental strategy for tackling the solvent exchange problem *ab initio* is to systematically change as many physico-chemical variables as possible and observe the effects on rates. Perhaps the most important of such variables for solvent exchange on a given metal ion are the concentration and the identity of the exchanging solvent. Another variable of seemingly lesser importance is the nature of the non-coordinating counter ion (usually ClO_4^-, PF_6^- etc.). However, if the metal ion is a solute in the pure solvent it is not experimentally possible to achieve a large solvent concentration range and the kinetics will be inevitably first order.

In principle, variation of the coordinating solvent concentration by the addition of a non-coordinating diluent (other variables are now created) should permit the determination of the complete solvent exchange rate law and thereby provide a strong indication of the exchange mechanism. This technique has been adopted by many workers who still refer to the ligand exchange process occurring in solvento complex/solvent/diluent mixtures as solvent exchange.

Before reviewing some experimental results it would be appropriate to consider what kinds of mechanisms one would expect for the solvent exchange (ligand exchange) reaction. Langford and Gray[12] have examined the early data on ligand substitution and have formulated four mechanisms, namely the dissociative (D), dissociative interchange (I_D), associative interchange (I_A) and associative (A) mechanisms. The D and A mechanisms may be considered equivalent to the limiting versions of the classical S_N1 and S_N2 mechanisms[13,14] respectively. However, the dynamics of the interchange mechanisms are conceptually more sophisticated: Here, an outer sphere or 'encounter' complex is initially formed and interchange of ligand molecules then proceeds through the interface of first and second coordination spheres. The leaving and entering ligands move synchronously. Whilst an intermediate capable of independent existence is not formed during the interchange of ligands between the first and second coordination spheres, the degree of bond making and breaking in the formation of the transition state may, in principle, show a continuous gradation from that observed with the D mechanism to that observed with the A mechanism. In the case of the I_D mechanism the predominant contribution to the exchange energetics is the breaking of a metal-solvent bond.

$$[MS_n]^{m+} + S^* \overset{K}{\rightleftharpoons} [MS_n]^{m+}.....S^* \overset{k_{int}}{\rightleftharpoons} [MS_{n-1}S^*]^{m+}.....S$$

encounter complex

The observed rate constant, k_{ex}, is given by Equation 1.1

$$k_{ex} = \frac{k_{int}K[S]}{1 + K[S]} \qquad (1.1)$$

where [S] is the concentration of solvent which is not in the first coordination sphere, k_{int} is the rate constant characterizing the interchange step and K is the equilibrium constant for the formation of the encounter complex. If $K[S] \ll 1$ (limit (a)), k_{ex} approximates to $k_{int}K[S]$ and a rate dependence on [S] will be observed. Alternatively, if K is very large such that $K[S] \gg 1$ (limit (b)), k_{ex} will approximate to k_{int}. Hence, over a sufficiently large concentration range of solvent a plot of k_{ex} versus [S] will appear initially linearly dependent on [S] but eventually (at high [S]) becomes asymptotic to k_{int}. It is implicit in this mechanism that k_{int} should not be much different from the rate constant for a D mechanism, k_1, since bond breaking is the most important process in both mechanisms. For the I_A mechanism, bond formation between the metal and a solvent molecule residing in the second coordination sphere is the energetically dominant step. The variation of k_{ex} with [S] for the I_A mechanism is of the same form as that in Equation 1.1. Few examples of this mechanism are known[12,15] and several of the assignments have been made on the basis of measured volumes of activation[16,17]. One of the major difficulties with the assignment of interchange mechanisms is the experimental problem in evaluating K. Estimates of K from the Fuoss-Eigen[3] expression for ions such as Mg^{2+} in most non-aqueous solvents have an upper limit

of about unity. However, some experimental estimates are significantly higher ($\approx$ 10 dm^3 mol^{-1})[18] than this theoretical limit.

Finally, another associative-type mechanism has been postulated[19] in which the diluent, X, does enter the first coordination sphere to produce the reactive species $[MS_nX]^{m+}$ and $[MS_{n-1}X]^{m+}$ (which are consequently present in low concentration) according to the scheme,

$$[MS_n]^{m+} + X \underset{}{\overset{k_X}{\rightleftharpoons}} [MS_nX]^{m+} \underset{\text{slow}}{\overset{\text{fast}}{\rightleftharpoons}} [MS_{n-1}X]^{m+} + S$$

where k_X characterizes the rate determining step for the exchange of S. This mechanism, first proposed for ligand substitution reactions on square planar platinum(II) species[20], is unlikely to be operative in weakly coordinating diluents. Furthermore, a variation in coordination number for six-coordinate metal ions seems energetically less drastic than for four-coordinate platinum(II) so that this mechanism appears unnecessarily complicated for $[MS_6]^{m+}$.

1.3 Solvent exchange studies

There have been numerous studies of solvent exchange on closed shell metal ions (with and without the presence of an inert diluent) reported in the literature, albeit with differing levels of kinetic thoroughness. From a review of the experimental results one can begin to appreciate the relative importance of the physico-chemical variables concerned. Table 1.1 lists some of the results and mechanistic conclusions reached for many of the better characterized solvent exchange systems.

One feature of the Table is that exchange rates are particularly dependent on the metal ion. Unidentate solvent exchange data for the alkali metals and the latter members of the alkaline earth group are

TABLE 1.1 *Kinetic parameters for solvent exchange on various metal ions*

Metal ion	Diluent	k_{ex}(298.2 K) s^{-1} or $dm^3\ mol^{-1}\ s^{-1}$	$\Delta H^{\ddagger}$ kJ mol^{-1}	$\Delta S^{\ddagger}$ J K^{-1} mol^{-1}	Assigned mechanism	Reference
Beryllium(II)						
$[Be(H_2O)_4]^{2+}$	-	1800	42	-44	I_A?	21
$[Be(dmf)_4]^{2+}$	?	310	61	11	D?	22
$[Be(dmmp)_4]^{2+}$	CH_3NO_2	0.81[a]	60	-44	A	23
$[Be(dmadmp)_4]^{2+}$	CH_3NO_2	7.3×10^{-3}	89	13	D	23
$[Be(dmadmp)_4]^{2+}$	pc*	9×10^{-2}	77	-5	D	23
$[Be(tmdamp)_4]^{2+}$	pc	6.9×10^{-3}	89	13	D	23
$[Be(hmpa)_4]^{2+}$	pc	2.7×10^{-4}	117	78	D	23
$[Be(tmp)_4]^{2+}$	CH_3NO_2	1.5[a]	56	-54	A	23
$[Be(tmp)_4]^{2+}$	CH_2Cl_2	3.6	57	-44	D	24
Aluminium(III)						
$[Al(H_2O)_6]^{3+}$[b]	-	16	65.3	0	D?	25
$[Al(dmso)_6]^{3+}$	CD_3NO_2	0.3	83	22	D	26
$[Al(tmp)_6]^{3+}$	CH_3NO_2	0.38	98	76	D	27
$[Al(tmp)_6]^{3+}$	CD_3NO_2	0.78	85	38	D	26
$[Al(tmp)_6]^{3+}$	CD_3NO_2	0.36	87	35	D	28
$[Al(dmf)_6]^{3+}$	CD_3NO_2	0.05	93	43	D	26
$[Al(dmmp)_6]^{3+}$	CH_3NO_2	5.1	84	48	D	27
$[Al(dmmp)_6]^{3+}$	CH_3NO_2	5.0	75	18	D	27
$[Al(hmpa)_4]^{3+}$	CH_3NO_2	4800[a]	32	-43	A	27

TABLE 1.1 *(cont.)*

Metal ion	Diluent	k_{ex}(298.2 K) s^{-1} or $dm^3\ mol^{-1}\ s^{-1}$	$\Delta H^{\ddagger}$ kJ mol^{-1}	$\Delta S^{\ddagger}$ J K^{-1} mol^{-1}	Assigned mechanism	Reference
Gallium(III)						
$[Ga(H_2O)_6]^{3+}$ [c]	-	760	69	42	?	25
$[Ga(dmso)_6]^{3+}$	CD_3NO_2	1.9	73	4	D	26
$[Ga(tmp)_6]^{3+}$	CD_3NO_2	6.4	74	19	D	26
$[Ga(tmp)_6]^{3+}$	CD_3NO_2	5.0	88	63	D	29
$[Ga(dmf)_6]^{3+}$	CD_3NO_2	1.7	86	46	D	26
Indium(III)						
$[In(H_2O)_6]^{3+}$	-	40 000 [a]	19	-96	A	25
$[In(tmp)_6]^{3+}$	CD_3NO_2	34 [a]	29	-117	A	26
$[In(tmp)_6]^{3+}$	CD_3NO_2	7.2 [a]	36	-109	A	29
Zinc(II)						
$[Zn(tmtu)_4]^{2+}$	CD_2Cl_2	9×10^6	65	106	D	30
Magnesium(II)						
$[Mg(H_2O)_6]^{2+}$ [d]	-	5×10^5	42.7	8.4	?	31

* pc = propylene carbonate $MeCOC(O)OCH_2$

a Second order rate constant.

b 0.55 molal Mn^{2+} present.

c 0.60 molal Mn^{2+} present.

d Approximately 12% w/w $Mn(ClO_4)_2 \cdot 6H_2O$ in sample.

not presented but all rate constants at room temperature are in excess of 10^7 s^{-1} [4] and some rates are virtually diffusion controlled. In a broad sense, the trend (cf. $[Al(H_2O)_6]^{3+}$, $[Ga(H_2O)_6]^{3+}$, $[In(H_2O)_6]^{3+}$) is such that as the surface charge density of the metal cation increases, the rate constant at room temperature decreases. This has been explained in terms of the simple ion-dipole model[32,33] and the hard/soft/acid/base model[34] of solvent-metal ion interaction.

Another salient feature of the Table is the arguably lesser dependence of rate constant upon ligand identity for a given metal ion (k_{ex}(298 K) for Be^{2+} covers seven orders of magnitude). Now, if steric effects are ignored then, intuitively, the electron pair donating ability of the ligand towards the metal should determine to a large extent the strength of the metal-ligand bond and hence strongly influence the kinetics. There are various ligand basicity scales available[34-39] but the Gutmann donor number scale[38] provides, perhaps, the best indication of relative metal-ligand bond strength in the absence of steric effects. One problem with the Gutmann scale is that the measured bonding interaction is between the ligand and the relatively soft acid[34,39] $SbCl_5$. Hence, there is some uncertainty as to its reliability when applied to hard acids such as Al^{3+} or Be^{2+}. From the limited data there appears to be no meaningful correlation between donor number (or donicity) and kinetic parameters. This observation is possibly due (as intimated) to the fact that a range of potentially important steric interactions are not being taken into consideration. It has been recognized that for some ligands an increase in molecular bulk is accompanied by an increase in basicity, via inductive effects, and that it is often impossible to segregate the two individual contributions to the energetics of exchange.

Other trends which may be discerned from Table 1.1 include the frequency of dissociative kinetics and the dominance of six-coordination except for the small Be^{2+} ion or for complexes with bulky ligands such as hmpa[27]. Perhaps the most intriguing observation, however, is the effect of diluent on the kinetics of tmp exchange on $[Be(tmp)_4]^{2+}$. It is evident that a completely different exchange rate law operates in CH_2Cl_2 compared to that in CD_3NO_2. Therefore, interactions outside the first coordination sphere may be important[40]. Finally, it seems that as the metal ion size increases so does the likelihood of second order kinetic behaviour (cf. $[Al(tmp)_6]^{3+}$, $[Ga(tmp)_6]^{3+}$ and $[In(tmp)_6]^{3+}$). The rationale[29], here, stems from the idea that steric crowding around a larger metal ion is less and therefore this permits a transition state of higher coordination number.

1.4 Objectives of this research

From analysis of the results in Table 1.1 it is clear that the chemistry of solvent exchange reactions is not fully understood. This situation is not aided by the disagreement on the precise magnitudes of rates and activation parameters for ostensibly the same system by different laboratories especially when the technique of variable temperature n.m.r. spectroscopy is employed. Recently, however, the predicament has become less embarrassing through the use of more sophisticated instrumentation and the complete lineshape analysis method. It seems that further systematic solvent exchange investigations with a wider variety of metal ions and solvents are required. In particular, the effect of small molecular structural variations (e.g. -methyl for -ethyl groups) in the solvent, and possibly diluent, on the kinetics of solvent exchange is a virtually unexplored area and should be very informative.

Assuming that metal-solvent electrostatic interactions are energetically dominant, it follows that ions of similar surface charge density will exchange a given ligand at approximately the same rate. Hence, on the strength of this argument, solvent exchange reactions on the little-known Sc^{3+} and Y^{3+} ions appear suitable for n.m.r. study since the surface charge densities of these ions are comparable with those of two of the ions mentioned in Table 1.1, namely Ga^{3+} and In^{3+}.

The object of this thesis was to elucidate the fundamentals of solvent exchange on some spherically symmetrical closed shell metal ions. The ions which are dealt with in detail are magnesium(II), scandium(III) and yttrium(III). Very little was known about the kinetic behaviour of these ions (especially the latter two) in solution prior to the commencement of the project in 1977. One by-product of this kind of research into metal-solvent interaction is expected to be a greater understanding of the physical organic chemistry of the solvents themselves.

CHAPTER 2 DERIVATION OF KINETIC PARAMETERS

2.1 Techniques for studying solvent exchange

There are a number of different experimental techniques that may be adopted in order to directly or indirectly investigate solvent exchange processes on metal ions. The most commonly used ones have been the isotope dilution[41,42], flow[43-45], relaxation[43,46-49] and resonance methods[7,33,50]. Additional or more accurate information is sometimes afforded by combining two or more techniques. As an example, the use of stopped flow n.m.r. spectroscopy[51] has recently effected an extension of the temperature range over which kinetic data may be reliably obtained (and so improving the accuracy of $\Delta H^{\ddagger}$ and $\Delta S^{\ddagger}$ measurements) for certain aluminium(III) and gallium(III) solvent exchange systems that had been previously studied by ^{1}H n.m.r. alone.

Without question, nuclear magnetic resonance spectroscopy is by far the most powerful single technique available for the study of labile closed shell metal ions in solution. If the frequency of solvent exchange is comparable to the frequency difference between the relevant n.m.r. signals (in the absence of exchange) within the experimentally accessible temperature or pressure range, a significant absorption mode lineshape modification due to the exchange process will be evidenced. It is this lineshape modification of the frequency domain spectrum which will be discussed now. Pulse n.m.r. methods (e.g. for $T_{1\rho}$ measurements[52,53]) and spin saturation transfer procedures (for the time domain spectra)[54,55] have also been employed but are not dealt with here.

2.2 Lineshape analysis

The absorption mode (v) lineshape of a n.m.r. signal under continuous wave (CW) slow passage conditions is given by[53]

$$v = \frac{-M_{z\,eq}\ \gamma\ B_1 T_2}{1 + T_2^2(\omega_0 - \omega)^2 + \gamma^2\ B_1^2 T_1 T_2} \qquad (2.1)$$

where ω = the angular radiofrequency of the n.m.r. probe

ω_0 = the angular resonance frequency of the nucleus under a large static field $\vec{B}_0$

B_1 = the magnitude of small oscillating magnetic field associated with ω

γ = the magnetogyric ratio of the observed nucleus

T_2 = the observed transverse relaxation time

T_1 = the spin-lattice relaxation time

and $M_{z\,eq}$ = the component of magnetization (at thermal equilibrium) along the direction of $\vec{B}_0$.

Usually under these conditions B_1 is so small that $\gamma^2\ B_1^2 T_1 T_2$ can be neglected. In this case v becomes Lorentzian* in character:

$$v = \frac{-M_{z\,eq}\ \gamma\ B_1 T_2}{1 + T_2^2(\omega_0 - \omega)^2} \qquad (2.2)$$

The extension of the classical relations above to incorporate exchange between uncoupled magnetic sites A and B (e.g. coordinated

---

* The experimental n.m.r. lineshape deviates[56-58] slightly from true Lorentzian character but this has been found to introduce no significant errors in lineshape analysis.

and free ligand sites) has been given by several authors[59-64]. The n.m.r. absorption lineshape is then proportional to v below[65,66].

$$v = \frac{-\gamma M_{z\,eq} B_1 \{Y[1 + \tau(P_B/T_{2A} + P_A/T_{2B})] + QR\}}{Y^2 + R^2} \qquad (2.3)$$

$$\tau = P_B\tau_A = P_A\tau_B \qquad (2.4)$$

where τ_A and P_A represent the mean site lifetime of the exchanging species and mole fraction respectively for site A, τ_B and P_B represent the lifetime and mole fraction respectively for site B and:

$$\Delta\omega = \omega_{0A} - \omega_{0B} \qquad (2.5)$$

$$\delta\omega = \tfrac{1}{2}|\omega_{0A} - \omega_{0B}| - \omega \qquad (2.6)$$

$$Y = \tau\left[\frac{1}{T_{2A}T_{2B}} - \delta\omega^2 + \frac{\Delta\omega^2}{4}\right] + \frac{P_B}{T_{2B}} + \frac{P_A}{T_{2A}} \qquad (2.7)$$

$$R = \delta\omega[1 + \tau(1/T_{2A} + 1/T_{2B})] + \frac{\Delta\omega}{2}\tau(1/T_{2B} - 1/T_{2A}) + \frac{\Delta\omega}{2}(P_A - P_B) \qquad (2.8)$$

$$Q = \tau(\delta\omega - \frac{\Delta\omega}{2}(P_A - P_B)). \qquad (2.9)$$

This general lineshape expression may be simplified under a series of limiting conditions.

Very slow exchange

If τ_A^{-1}, $\tau_B^{-1} \ll |\omega_{0A} - \omega_{0B}|$, T_{2A}^{-1}, T_{2B}^{-1} we may approximate Equation 2.3 to

$$v = \frac{-\gamma B_1 P_A M_{z\,eq} T_{2A}^{-1}}{T_{2A}^{-2} + (\omega_{0A} - \omega)^2} + \frac{-\gamma B_1 P_B M_{z\,eq} T_{2B}^{-1}}{T_{2B}^{-2} + (\omega_{0B} - \omega)^2} \qquad (2.10)$$

Since v does not contain any τ terms it gives no kinetic information. It represents two Lorentzian lineshapes centred at ω_{0A} and ω_{0B}.

Slow exchange

If τ_A^{-1}, $\tau_B^{-1} \ll |\omega_{0A} - \omega_{0B}|$ with $\tau_A^{-1} \approx T_{2A}^{-1}$ and $\tau_B^{-1} \approx T_{2B}^{-1}$

$$v = \frac{-\gamma B_1 P_A M_{z\,eq} (T_{2A}^{-1} + \tau_A^{-1})}{(T_{2A}^{-1} + \tau_A^{-1})^2 + (\omega_{0A} - \omega)^2} + \frac{-\gamma B_1 P_B M_{z\,eq} (T_{2B}^{-1} + \tau_B^{-1})}{(T_{2B}^{-1} + \tau_B^{-1})^2 + (\omega_{0B} - \omega)^2} \qquad (2.11)$$

This corresponds to two Lorentzian lineshapes at ω_{0A} and ω_{0B}. Now $1/T_{2A\,obs} = 1/T_{2A} + 1/\tau_A$ and $1/T_{2B\,obs} = 1/T_{2B} + 1/\tau_B$ and hence the signals are "exchange broadened".

Fast exchange

If τ_A^{-1}, $\tau_B^{-1} \gg |\omega_{0A} - \omega_{0B}|$ a single Lorentzian signal centred at $(P_A\omega_{0A} + P_B\omega_{0B})$ is observed. "Exchange broadening" is again exhibited and

$$1/T_{2\,obs} = \frac{P_A}{T_{2A}} + \frac{P_B}{T_{2B}} + P_A^2 P_B^2 (|\omega_{0A} - \omega_{0B}|)^2 (\tau_A + \tau_B). \qquad (2.12)$$

Very fast exchange

If τ_A^{-1}, $\tau_B^{-1} \gg |\omega_{0A} - \omega_{0B}|$, T_{2A}^{-1}, T_{2B}^{-1} Equation 2.3 simplifies to

$$v = \frac{-\gamma B_1 M_{z\,eq} (P_A T_{2A}^{-1} + P_B T_{2B}^{-1})}{(P_A T_{2A}^{-1} + P_B T_{2B}^{-1})^2 + (P_A\omega_{0A} + P_B\omega_{0B} - \omega)^2} \qquad (2.13)$$

Equation 2.13 represents a single Lorentzian signal centred at $(P_A\omega_{0A} + P_B\omega_{0B})$ with $1/T_{2\,obs} = P_A/T_{2A} + P_B/T_{2B}$ and v contains no kinetic information.

Practical examples of slow, fast and intermediate exchange conditions are depicted in Figure 3.3. The initial doublet under slow exchange conditions is seen to coalesce to a singlet at higher rates of exchange. For spectra composed of more than one independent

'coalescing doublet' it is apparent that the total lineshape is the sum of all the individual doublet contributions. In particular, if spin-spin coupling occurs in an exchanging molecule (e.g. $^{31}P - ^{1}H$ in tmp) the classical equations are still valid and one logically treats the total lineshape as the sum of more than one coalescing doublet[53].

The lineshape 'fitting' computer program, MATCH[67], based on a program developed by Nakagawa[68] with modifications by Siddall, Stewart and Knight[69], was utilized to simulate experimental lineshapes for some of the two site exchange systems in this report. MATCH is a non-interactive computer program and was run on the University of Adelaide's CYBER 173 computer in batch mode. However, an interactive program, LINSHP[70] derived from MATCH (and which was used almost exclusively) proved to be more convenient for analyses since it employs the Nicolet BNC-12 minicomputer of the HX-90-E spectrometer (see Section 7.5) and provides a visual display of the fit.
When chemical exchange occurs between more than two uncoupled sites the Kubo-Sack method[56,62-64,71] may be applied to introduce exchange effects into the classical lineshape equations. Appendix 2 deals with the three site exchange situation.

Lineshape analysis was performed on both pulsed free precession (equivalent to CW) and Fourier transform n.m.r. spectra during the course of this research. Since the computer programs used are derived from a continuous wave treatment, this raises the question of whether continuous wave and Fourier transform lineshapes are indeed equivalent. In fact, the transient and steady state solutions of the modified Bloch equations[53] in the case of an uncoupled spin system undergoing chemical exchange between two non-equivalent sites form a Fourier transform pair[72]. Hence, Fourier transformation of the free induction decay of an exchanging system gives the continuous wave lineshape.

2.3 Some problems associated with the variable temperature n.m.r. lineshape analysis procedure

As previously intimated, the method used here to determine exchange rates hinges on analysis of the coalescence of n.m.r. signals caused by increase in temperature. Some problems associated with the procedure are now discussed.

It is evident from Equation 2.3 that the total n.m.r. lineshape under any exchange condition is dependent on transverse relaxation times, mole fractions and chemical shifts. If these parameters are temperature dependent the magnitude of the variation with temperature needs to be established. As a rule, extrapolation of transverse relaxation times, mole fractions and chemical shifts[53,73] (calculated from spectra in the very slow exchange limit) into the temperature region of interest should be carried out to avoid potentially large errors in computed lifetimes. The extrapolations, however, are not easily accomplished for many exchange systems. Hence, in these cases relaxation times, mole fractions and chemical shifts must be regarded as variable input parameters for lineshape fitting programs.
It can be shown that if $|\Delta\omega| \gg T_{2A}^{-1}, T_{2B}^{-1}$ (which is usually the case for exchange systems in this thesis) then minor ($\sim$10%) errors in relaxation times make little impact on the total kinetic uncertainty associated with the lineshape analysis. (For this reason linewidths will not normally be quoted later.) More often than not, the largest contributions to the total uncertainty arise from errors in mole fractions and chemical shifts. The lineshape is most sensitive to exchange perturbation when site populations are equal and at intermediate rates of exchange.

A further difficulty encountered in variable temperature n.m.r. work is the control of the sample temperature itself. The kinetic uncertainties associated with the use of many commercial high resolution n.m.r. temperature control units should not be underestimated[73]. Depending on the values of activation parameters for the exchange process, variations of one or two degrees in temperature may produce quite substantial errors in rates (i.e. of the order of 30% or more). The use of a calibrated copper constantan thermocouple in the variable temperature work here has limited the uncertainty in temperature to approximately 0.5 K.

Problems of a (usually) lesser nature in variable temperature n.m.r. lineshape analysis include field inhomogeneity, spectral phasing, baseline irregularities, saturation, 'ringing' and superimposed inert diluent signals. Most of these may be alleviated by the employment of Fourier transform n.m.r. and an interactive fitting program equipped with a 'difference spectrum' display.

2.4 Calculation of activation enthalpies and entropies

According to the transition state theory[74], the dependence of the rate constant for an elementary exchange process on temperature is given by the Eyring expression

$$k_{ex} = (k_B T/h)\ \exp(-\Delta G^{\ddagger}/RT)$$

$$= (k_B T/h)\ \exp(-\Delta H^{\ddagger}/RT + \Delta S^{\ddagger}/R) \qquad (2.14)$$

where k_B = Boltzmann's constant

h = Planck's constant

and R = the gas constant.

The transmission coefficient is assumed to be unity for our purposes. Although the mechanistic interpretation of experimental $\Delta H^{\ddagger}$ and $\Delta S^{\ddagger}$ values derived using the Eyring expression above has generated some controversy[15,75,76] it is still desirable where possible to quote parameters which define the temperature dependence of k_{ex}. Kinetic data may be fitted to the Eyring relationship in exponential form or in the convenient linear form below

$$\ln(T/k_{ex}) = (\Delta H^{\ddagger}/R)1/T + (\ln(h/k_B) - \Delta S^{\ddagger}/R). \qquad (2.15)$$

A number of elaborate computer programs are available for the computation of activation enthalpies and entropies using the Eyring relationship above. One such program employed by the author was ACTENG[77].

When the observed exchange rate constant is composed of two or more elementary rate constants the evaluation of activation parameters pertaining to the elementary processes becomes more involved. Let us consider a two term rate law, for solvent exchange on a six-coordinate complex, arising from the simultaneous operation of two different exchange mechanisms (for sake of argument, dissociative and associative mechanisms).

$$\text{rate} = 6k_{ex}[MS_6^{m+}] = 6(k_1 + k_2[S])[MS_6^{m+}] \qquad (2.16)$$

From a mathematical standpoint, plots of $\ln(T/k_{ex})$ versus $1/T$ will not necessarily be linear since there are now two parameters, viz. $\Delta H_1^{\ddagger}$ and $\Delta H_2^{\ddagger}$, which determine the 'slope'. Alternatively, writing the appropriate Eyring relationship in exponential form,

$$k_{ex} = k_1 + k_2[S] = (k_B T/h)\left\{\exp\left(\frac{\Delta S_1^{\ddagger}}{R} - \frac{\Delta H_1^{\ddagger}}{RT}\right) + [S]\exp\left(\frac{\Delta S_2^{\ddagger}}{R} - \frac{\Delta H_2^{\ddagger}}{RT}\right)\right\} \qquad (2.17)$$

one is dealing with two exponentials here instead of one. From

Equations 2.16 and 2.17 it is apparent that one exchange pathway will be favoured to a greater or lesser degree over the other depending on the temperature and [S]. In general, if $\Delta H_1^{\ddagger}$ is much different from $\Delta H_2^{\ddagger}$ and measurements are made over a large temperature range (>50 K) plots of $\ln(T/k_{ex})$ versus 1/T will exhibit a substantial deviation from linearity as in Figures 2.1 and 2.2. Theoretically, the non-linearity of plots of $\ln(T/k_{ex})$ versus 1/T (obtainable from n.m.r. lineshape analysis data) is not a problem in the calculation of the four activation parameters associated with two term rate law above: It should be possible to directly evaluate k_{ex} for any physically realistic value of [S] or T. In practice, the effective lineshape simulation temperature range for one sample solution is not always the same as that for another (cf. Figure 4.16). Furthermore, experimental error often masks the systematic curvature of the plots. The first practical limitation has, up till now, necessitated the extrapolation of rate values into a 'common temperature region'. The rate data for this region have then been used to evaluate activation parameters by a method described elsewhere[78]. The second limitation makes the extrapolation difficult. If $\Delta H_1^{\ddagger}$ is not exceptionally larger or smaller than $\Delta H_2^{\ddagger}$ (i.e. $\Delta H_1^{\ddagger}/\Delta H_2^{\ddagger}$ lies between, say, 0.5 and 2) it is unlikely any curvature will be discernible unless the temperature range is very large. Interpolation and extrapolation of k_{ex} values assuming linearity will therefore wipe out some intrinsic information on the ratio of activation enthalpies and contribute to the total error. One way to overcome this problem is to use activation parameters obtained by the linear interpolation and extrapolation procedure[78] as initial estimates only and then try to simulate the experimental plots of $\ln(T/k_{ex})$ versus 1/T according to Equation 2.17. Having done so more accurate

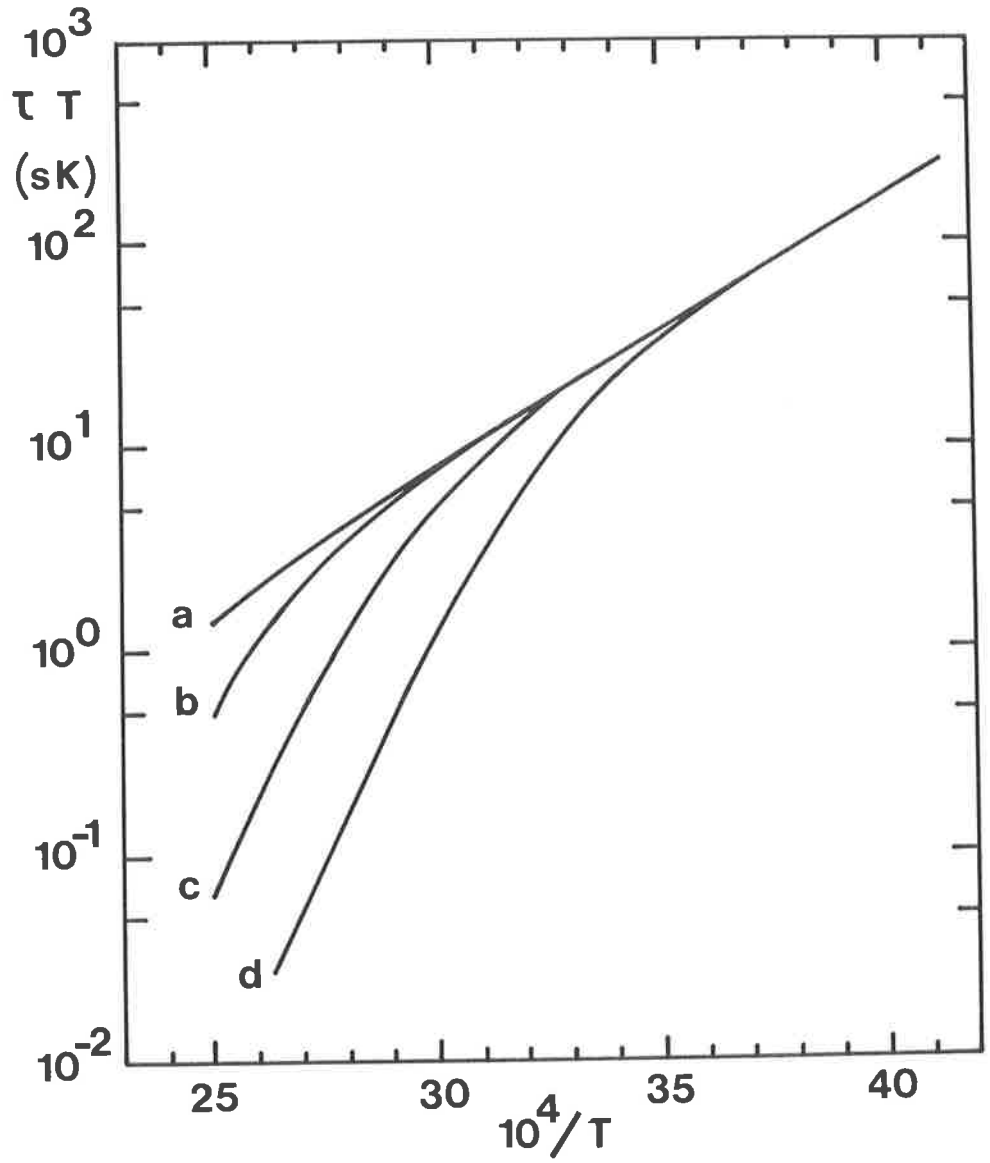

FIGURE 2.1 Semilogarithmic plots of T/k_{ex} (= τT) versus $1/T$ calculated according to Equation 2.17. $\Delta H_1^{\ddagger}$ = 25 kJ mol^{-1}, $\Delta S_1^{\ddagger}$ = -140 J K^{-1} mol^{-1}, $\Delta H_2^{\ddagger}$ = 90 kJ mol^{-1} and $\Delta S_2^{\ddagger}$ = 50 J K^{-1} mol^{-1}. [S] = 0.01 mol dm^{-3} (a), 0.1 mol dm^{-3} (b), 1.0 mol dm^{-3} (c) and 10.0 mol dm^{-3} (d).

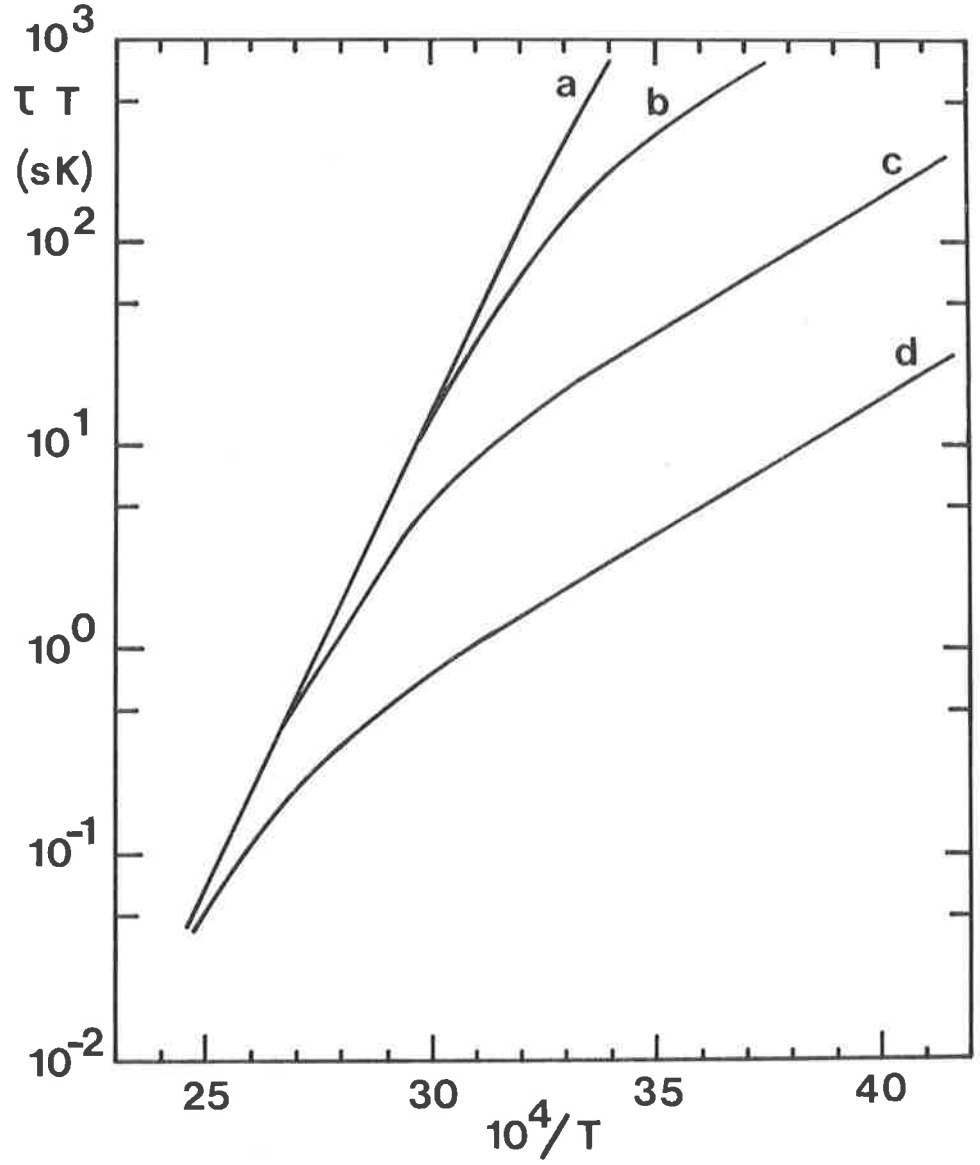

FIGURE 2.2 Semilogarithmic plots of T/k_{ex} (= τT) versus $1/T$ calculated according to Equation 2.17. $\Delta H_1^{\ddagger}$ = 90 kJ mol^{-1}, $\Delta S_1^{\ddagger}$ = 50 J K^{-1} mol^{-1}, $\Delta H_2^{\ddagger}$ = 25 kJ mol^{-1} and $\Delta S_2^{\ddagger}$ = -140 J K^{-1} mol^{-1}. [S] = 0.01 mol dm^{-3} (a), 0.1 mol dm^{-3} (b), 1.0 mol dm^{-3} (c) and 10.0 mol dm^{-3} (d).

(non-linear) interpolated and extrapolated rates are obtained and these can be subsequently used to refine activation parameters. This kind of iterative procedure is cumbersome and does not provide good estimates of the total errors[78] which presumably comprise (amongst other things) errors in sample temperature, concentrations and computed lifetimes. The method developed in this thesis for calculating activation enthalpies and entropies associated with two term rate laws is now described.

In essence, the 'surface' defined by experimental (temperature, [S], k_{ex}) coordinates is simulated. Using a weighted non-linear least squares computer program, DATAFIT, the parameters $\Delta H_1^{\ddagger}$, $\Delta H_2^{\ddagger}$, $\Delta S_1^{\ddagger}$ and $\Delta S_2^{\ddagger}$ are derived according to Equation 2.17. DATAFIT minimizes the residuals between the experimental and calculated surfaces by method number five of Pitha and Jones[79] keeping the fractional change of any of the four parameters to within 0.001 at convergence. The standard deviations for activation parameters which may be quoted from the output of the program serve as genuine measures of the total statistical uncertainties since account is taken of estimated experimental errors in the individual input variables. Equation 2.17 may also be formulated in terms of activation enthalpies and elementary rate constants (k_1 and k_2) at a desired temperature. In this case, DATAFIT furnishes rates and their standard deviations for that temperature. This facility is very convenient since it enables, under certain circumstances, previously difficult mechanistic decisions to be made quite easily. For example, if plots of k_{ex} versus [S] are linear but uncertainty exists as to whether small positive intercepts (arising from an exchange pathway independent of [S]) are statistically 'real' it may be possible from the DATAFIT results to reject one

mechanism solely on statistical grounds. Of course, it is necessary to establish that the intercept is indistinguishable from zero over the whole experimental temperature range.

One final (perhaps obvious) point must be made. The observation of a linear (within experimental error) plot of k_{ex} versus [S] from experimental data does not mean that the activation parameters derived through the mathematical procedures above adequately describe the actual kinetics of the exchange system under all possible conditions of [S] and temperature. For example, the data treatment does not allow for specific effects that may manifest themselves more clearly outside the [S] range examined. In particular, above a certain free solvent concentration, the numerical value of [S] no longer accurately represents the probability of collision between $[MS_6]^{m+}$ and S species. Hence, any computer program which evaluates kinetic parameters from experimental data is subject to the limitations of its mathematical model (which attempts to describe a complicated real system).

CHAPTER 3 LIGAND EXCHANGE ON MAGNESIUM(II)

3.1 Introduction

Since the sixties, when the first measurements of the rates of water and methanol exchange on magnesium(II) were made[80,81], there have been surprisingly few direct studies of ligand exchange processes on this ion[31,82-85]. The early investigations were rather limited in scope and it was not feasible, at the time, to make extensive kinetic comparisons with other exchange systems. Table 3.1 lists some of the kinetic results obtained.

TABLE 3.1 *Data for ligand exchange on magnesium(II)*

Complex ion	k_{ex}(225 K)[a] s^{-1}	$\Delta H^{\ddagger}$ kJ mol^{-1}	$\Delta S^{\ddagger}$ J K^{-1} mol^{-1}	Reference
$[Mg(H_2O)_6]^{2+}$	1585	42.7	8.4	31
$[Mg(MeOH)_6]^{2+}$	0.324	69.9	58.6	82
$[Mg(EtOH)_6]^{2+}$	108.4	74.0	125.5	83
$[Mg(acetone)_6]^{2+}$	264	50	26	84

a Calculated from activation parameters

One aim of this project, therefore, was to supplement the existing knowledge and, indeed, more detailed and informative solvent exchange studies are reported herein.

3.2 Exchange of trimethylphosphate on $[Mg(tmp)_6]^{2+}$

Crea, Lincoln and West[85] have investigated the exchange of tmp on $[Mg(tmp)_6]^{2+}$ in dichloromethane and acetone diluents using ^1H n.m.r. In their study a small chemical shift separation between coordinated and free ligand signals (ca. 0.07 p.p.m. in CH_2Cl_2 and ca. 0.18 p.p.m. in acetone) was observed, giving rise to relatively large experimental errors in the reported kinetic data. Furthermore, the tmp exchange rate law was not determined although a dissociative exchange mechanism was, tentatively, proposed. However, with ^{31}P n.m.r. spectroscopy, the chemical shift separation between coordinated and free tmp signals is very much larger (ca. 5.5 p.p.m. in CD_2Cl_2 and ca. 4.9 p.p.m. in $(CD_3)_2CO$). This feature promotes the achievement of greater accuracy in the kinetic parameters. In this Section the rate law is established using ^{31}P n.m.r. and the postulated dissociative mechanism confirmed.

Using a synthetic procedure similar to that of Crea, Lincoln and West a perchlorate salt of the formula $[Mg(tmp)_{5.75}](ClO_4)_2$ was isolated. The infra-red spectrum of the complex showed neither a hydroxyl stretching band nor bands attributable to coordinated perchlorate or lattice tmp of crystallization. Therefore, the non-stoichiometric formula arising from the elemental analyses (Table 7.1) suggests the co-existence of both $[Mg(tmp)_5]^{2+}$ and $[Mg(tmp)_6]^{2+}$ ions in the solid state. As the crystal structures of the species $[Mg(OAs(Me)_3)_5](ClO_4)_2$ [86] and $[Mg(OP(Me)_3)_5](ClO_4)_2$ [87], in which the ligands are in a square-based pyramidal array about magnesium(II), have been published, the proposition of $[Mg(tmp)_5]^{2+}$ is in accord with these known structures. Crea, Lincoln and West reported a tmp complex with 2.33% Mg. The calculated magnesium

content for $[Mg(tmp)_6](ClO_4)_2$ is 2.29%. It therefore appears that their compound may also have been non-stoichiometric.

The proton decoupled 36.43 MHz ^{31}P FT n.m.r. spectrum of a 0.034 mol dm^{-3} solution of $[Mg(tmp)_{5.75}](ClO_4)_2$ in d_2-dichloromethane at 167 K exhibited three singlets; (a), (b) and (c) (Figure 3.1). The singlets (a) and (b) are assigned to $[Mg(tmp)_5]^{2+}$ but spectral resolution did not permit a distinction to be drawn between the square-based pyramidal and trigonal bipyramidal geometries which represent the most probable structures for this species. (There may be a minor resonance occurring between (a) and (b) but it proved impossible to improve resolution beyond that in Figure 3.1.) Singlet (c) is assigned to $[Mg(tmp)_6]^{2+}$ and the ratio of the concentration of this species to that of $[Mg(tmp)_5]^{2+}$ was found to be $\sim$3:1 (in agreement with the analyses above). With increase in temperature singlets (a), (b) and (c) coalesced until at 185 K a solitary singlet was observed. This phenomenon is consistent with rapid interconversion of the five- and six-coordinate species. The addition of free tmp ligand induced (at 175 K) singlets (a) and (b) to simultaneously decrease in intensity and a new singlet assigned to free tmp to appear downfield. This observation is compatible with a shift in the tacit equilibrium towards $[Mg(tmp)_6]^{2+}$. Of solutions (i) to (v) only solution (v) exhibited small signals (which made up <1% of the total coordinated tmp signal area) attributable to $[Mg(tmp)_5]^{2+}$. Within the experimental error, the number of tmp molecules in the first coordination sphere of magnesium(II) was six in solutions (i) to (v) (see Table 3.2).

The proton decoupled ^{31}P FT n.m.r. spectrum of a 0.028 mol dm^{-3} solution of $[Mg(tmp)_{5.75}](ClO_4)_2$ in d_6-acetone at 176 K consisted of five resolved coordinated tmp singlets and one free tmp singlet,

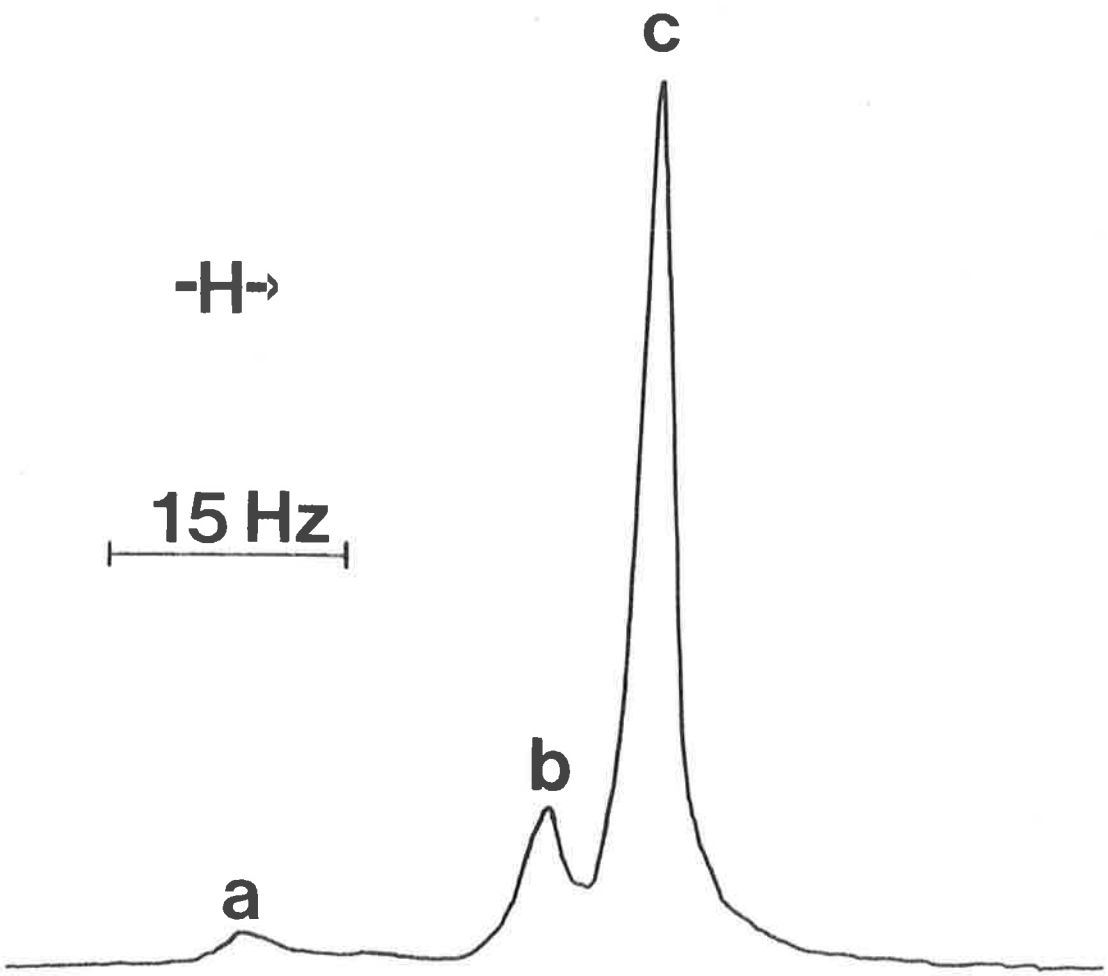

FIGURE 3.1 Proton decoupled ^{31}P FT n.m.r. spectrum of a 0.034 mol dm^{-3} solution of $[Mg(tmp)_{5.75}](ClO_4)_2$ in d_2-dichloromethane at 167 K. Singlets (a) and (b) are assigned to $[Mg(tmp)_5]^{2+}$ and singlet (c) to $[Mg(tmp)_6]^{2+}$.

TABLE 3.2 *Solution compositions and kinetic parameters for the* $[Mg(tmp)_6]^{2+}$ *system*

Solution	$[Mg(tmp)_6^{2+}]$ mol dm^{-3}	[tmp] mol dm^{-3}	$[CD_2Cl_2]$ mol dm^{-3}	$[(CD_3)_2CO]$ mol dm^{-3}	C.N.[a]	k_{ex}(225 K)[b] s^{-1}	$\Delta H^{\ddagger}$[c] kJ mol^{-1}	$\Delta S^{\ddagger}$[c] J K^{-1} mol^{-1}
(i)	0.299	2.51	7.07	-	5.9 ± 0.1	442 ± 27	54.1 ± 0.4	48.6 ± 1.9
(ii)	0.160	1.61	10.3	-	5.8 ± 0.2	630 ± 41	53.4 ± 0.4	48.1 ± 2.0
(iii)	0.185	0.970	11.4	-	5.9 ± 0.1	689 ± 47	50.8 ± 0.5	37.2 ± 2.0
(iv)	0.116	0.604	12.7	-	6.1 ± 0.1	683 ± 47	51.3 ± 0.5	39.5 ± 2.0
(v)	0.064	0.327	13.8	-	6.0 ± 0.1	707 ± 42	50.5 ± 0.4	36.2 ± 1.9
(vi)	0.278	1.59	-	8.06	5.9 ± 0.1	587 ± 57	51.2 ± 0.7	38.1 ± 3.3
(vii)	0.188	0.842	-	10.3	5.8 ± 0.2	495 ± 53	53.8 ± 0.8	48.2 ± 3.4

a C.N. = number of coordinated ligand molecules as determined from integration of the ^{31}P n.m.r. signals of free and coordinated tmp in the temperature range 175 - 195 K. The quoted errors represent one standard deviation.

b k_{ex}(225 K) interpolated from the Eyring plots. The quoted errors represent one standard deviation.

c $\Delta H^{\ddagger}$ and $\Delta S^{\ddagger}$ determined from the Eyring plots. The quoted errors represent one standard deviation (ACTENG).

indicating the presence of several magnesium(II) species in solution (Figure 3.2). The appearance of free tmp demonstrates the ability of d_6-acetone to displace coordinated tmp and it is probable that as d_6-acetone is in excess concentration ($[Mg(acetone)_6]^{2+}$ [84,88] has been reported under such conditions) a coordination number of six is retained in species of stoichiometry $[Mg(tmp)_{6-n}(d_6\text{-acetone})_n]^{2+}$ in this system. Direct confirmation of the presence of coordinated acetone was obtained from the ^1H n.m.r. spectrum of a 0.034 mol dm^{-3} solution of $[Mg(tmp)_{5.75}](ClO_4)_2$ in a d_6-acetone/acetone mixture in which a broad signal arising from coordinated acetone was observed 42 Hz downfield from the free acetone signal at 185 K. In solutions (vi) and (vii) a single ^{31}P singlet was observed for coordinated tmp at 185 K and the integrations were consistent with $[Mg(tmp)_6]^{2+}$ being the predominant magnesium(II) species in solution (for the integrations of ^{31}P signals: ^{31}P nuclei were fully relaxed prior to each new pulse and no significant nuclear Overhauser enhancement difference between coordinated and free ^{31}P nuclei is expected).

Rate constants for intermolecular exchange ($k_{ex} = 1/\tau_c$ where τ_c is the coordinated tmp lifetime) at specific temperatures were obtained by lineshape analysis of the ^{31}P FT n.m.r. spectra (Figure 3.3). As the effective temperature range for analysis (198 - 256 K) employing ^{31}P n.m.r. for this system is much greater than those ranges of Crea, Lincoln and West (188 - 198 K in CH_2Cl_2 and 193 - 208 K in acetone in their ^1H study), the results here are considered to be more reliable.

The composition of each solution and the derived kinetic parameters are given in Table 3.2. Semilogarithmic plots of $\tau_c T$ (= T/k_{ex}) versus 1/T are shown in Figure 3.4. The rate constants

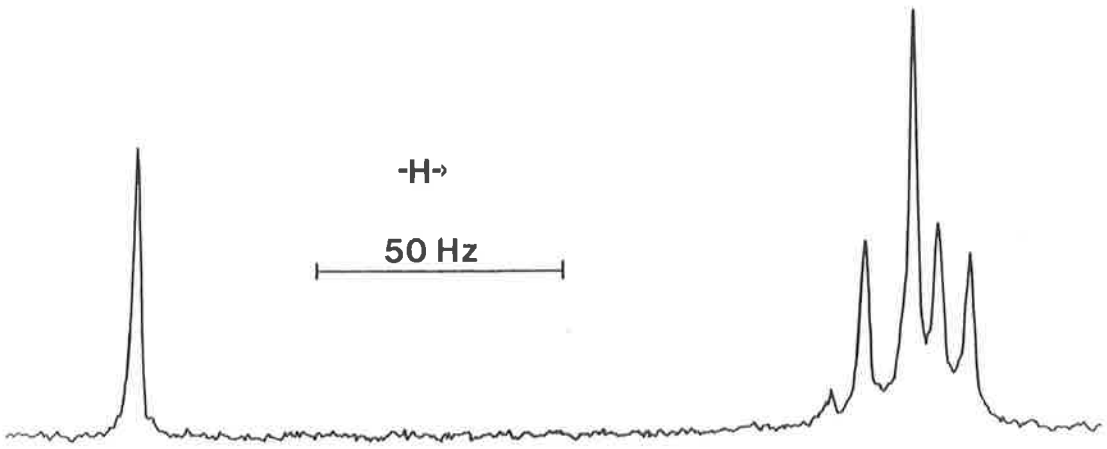

FIGURE 3.2 Proton decoupled ^{31}P FT n.m.r. spectrum of a 0.028 mol dm^{-3} solution of $[Mg(tmp)_{5.75}](ClO_4)_2$ in d_6-acetone at 176 K. The downfield singlet arises from free tmp.

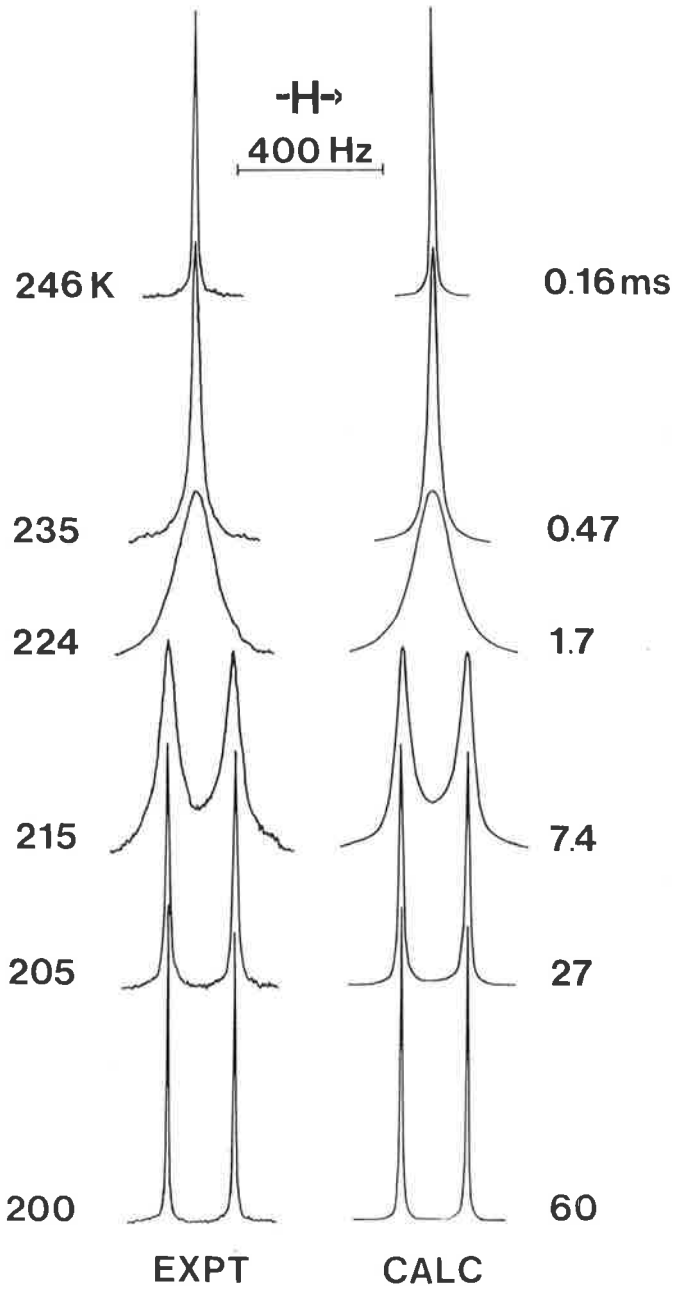

FIGURE 3.3 Experimental and computed best fit ^{31}P FT n.m.r. line-shapes of a $[Mg(tmp)_6]^{2+}$(0.278 mol dm^{-3}), tmp (1.59 mol dm^{-3}) and d_6-acetone (8.06 mol dm^{-3}) solution. The experimental temperatures and best fit τ_c (coordinated ligand lifetime) values appear to the left and right of the Figure respectively. The free tmp signal is downfield.

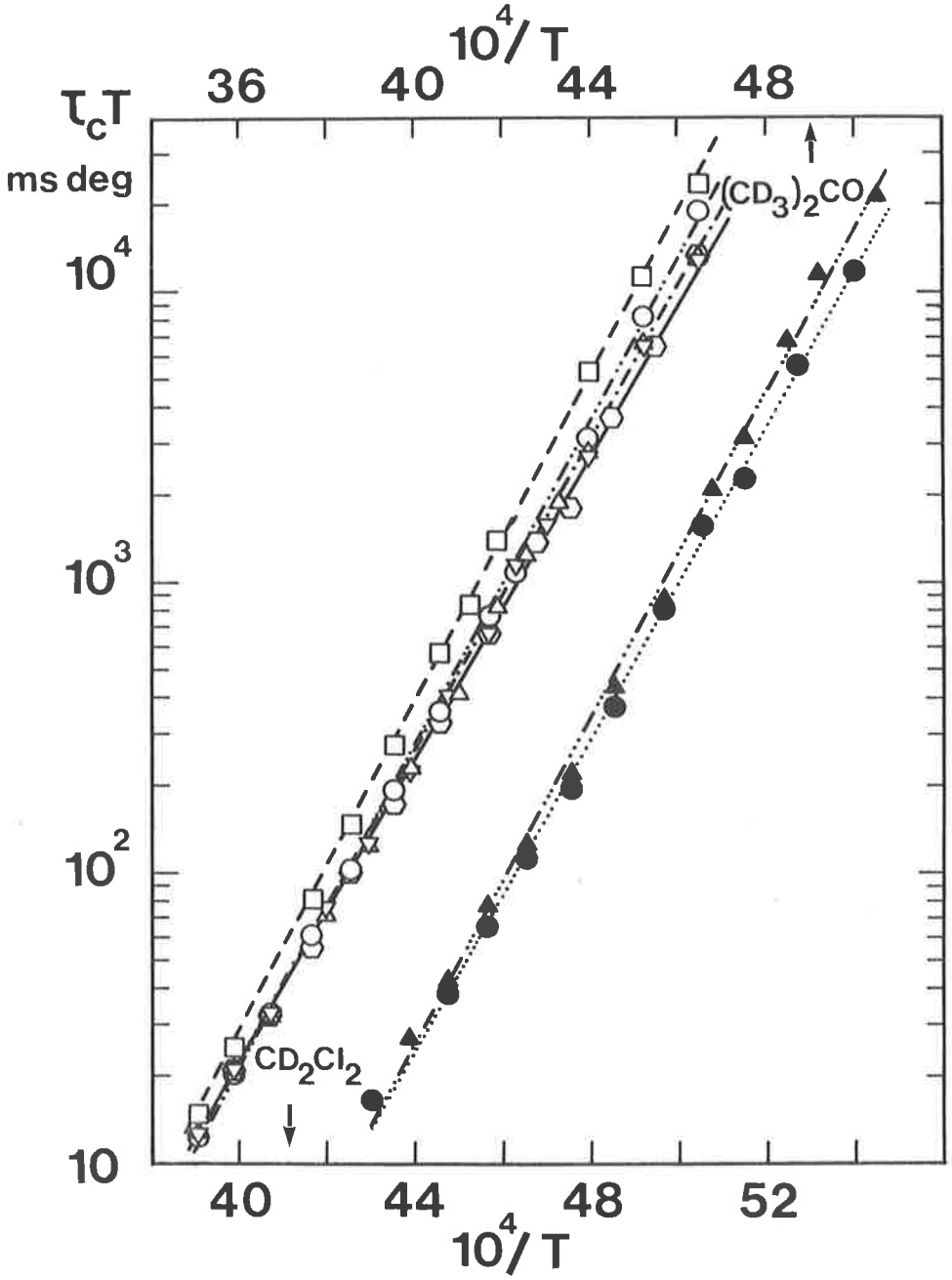

FIGURE 3.4 Semilogarithmic plots of $\tau_c T$ against 1/T for the $[Mg(tmp)_6]^{2+}$ system. The individual data points for solutions (i) - (vii) are represented as (i)□, (ii)○, (iii)▽, (iv)△, (v)⬡, (vi)●, (vii)▲ and the corresponding linear least-squares lines (the line for solution (iii) is omitted for clarity) as — — —, ··—··—··, ·—·—·, ———, ····· and ···—···—···. The bottom scale refers to solutions (i) - (v) while (vi) and (vii) are referred to the upper scale.

derived in the midst of the n.m.r. signal coalescence phenomenon (which occurs at ~225 K in this system) are the most accurate[53] and hence k_{ex}(225 K) values are quoted. The k_{ex}(225 K) values for solutions (ii) to (v) are identical within two standard deviations over a 4.9-fold variation in [tmp] and the variation in k_{ex}(225 K) over the 7.6-fold variation in [tmp] encompassed by solutions (i) to (v) is a factor of 1.6. Thus, the rate of tmp exchange on $[Mg(tmp)_6]^{2+}$ is not markedly dependent on [tmp] in d_2-dichloromethane diluent. Space filling models indicate that approximately twenty dichloromethane molecules or ten trimethylphosphate molecules can fill the second coordination sphere of $[Mg(tmp)_6]^{2+}$. Hence, on a statistical basis, the number of tmp molecules in the second coordination sphere of $[Mg(tmp)_6]^{2+}$ will vary from less than one for solution (v) to four or more in solution (i). Unless there is a very high degree of preferential occupancy of the second coordination sphere by tmp such that this occupancy is almost invariant under the experimental conditions reported here, it appears that the lability of tmp in the first coordination sphere is not modified to a major extent by the composition of the second coordination sphere. This is supported by the observation that the kinetic parameters derived from solutions (vi) and (vii) in d_6-acetone may not be meaningfully distinguished from those observed in d_2-dichloromethane diluent.

Overall, these rate phenomena are consistent with a tmp exchange mechanism in which bond breaking constitutes the predominant contribution to the observed $\Delta H^{\ddagger}$ and $\Delta S^{\ddagger}$ values. The observation of $[Mg(tmp)_5]^{2+}$ in d_2-dichloromethane diluent lends support to the postulation of a dissociative (D) tmp exchange process for $[Mg(tmp)_6]^{2+}$. The kinetic data for the $[Mg(tmp)_6]^{2+}$ system may now be compared with

those data in Table 3.1. Disregarding the results for $[Mg(MeOH)_6]^{2+}$, all rate constants at 225 K lie in the range 100 - 1600 s^{-1}. The dissociative mechanism is also thought to be operative for the systems in Table 3.1.

3.3 Exchange of N,N-dimethylformamide on $[Mg(dmf)_6]^{2+}$

The hygroscopic perchlorate salt $[Mg(dmf)_6](ClO_4)_2$ afforded using the preparative method described in Section 7.2 was employed for the ligand exchange investigation. This complex has been previously mentioned in the literature[22] but no detailed kinetic study involving it has been reported.

Anhydrous solutions of $[Mg(dmf)_6](ClO_4)_2$ and dmf in d_2-dichloromethane or d_6-acetone whose compositions are given in Table 3.3 exhibited N-methyl proton (90 MHz) resonances of coordinated dmf downfield from those of the analogous resonances of free dmf under slow exchange conditions at 180 K. In the d_2-dichloromethane solution (iii) the N-methyl resonances of coordinated dmf were separated by 15.3 Hz, and those of free dmf by 9.7 Hz. The high-field coordinated dmf resonance was 5.5 Hz downfield from that of the corresponding high-field free dmf resonance. Similar chemical shift separations were observed in the other d_2-dichloromethane solutions. In the d_6-acetone solution (vi) the analogous separations were 14.6, 16.1 and 13.1 Hz, and similar values were observed in the other $(CD_3)_2CO$ solutions. A comparison of the integrated areas of these coordinated and free resonances showed that $[Mg(dmf)_6]^{2+}$ was the predominant magnesium(II) species present in solutions (i) - (viii).

The effective temperature range for lineshape analysis ($N-CH_3$ resonances; minor coupling with formyl proton was ignored) in this

TABLE 3.3 *Solution compositions and kinetic parameters for dmf exchange on* $[Mg(dmf)_6]^{2+}$

Solution	$[Mg(dmf)_6^{2+}]$ mol dm^{-3}	[dmf] mol dm^{-3}	$[CD_2Cl_2]$ mol dm^{-3}	$[(CD_3)_2CO]$ mol dm^{-3}	C.N.[a,b]	k_{ex}(215 K)[c,d] s^{-1}	$\Delta H^{\ddagger}$[d] kJ mol^{-1}	$\Delta S^{\ddagger}$[d] J K^{-1} mol^{-1}
(i)	0.199	1.17	12.6	-	5.9 ± 0.1	17.2 ± 2.3	71.9 ± 2.3	116 ± 11
(ii)	0.101	0.508	13.8	-	5.8 ± 0.2	17.7 ± 2.0	72.3 ± 1.8	118 ± 8
(iii)	0.0768	0.397	13.9	-	5.8 ± 0.2	23.5 ± 3.2	77.8 ± 3.0	146 ± 14
(iv)	0.0523	0.326	14.1	-	6.1 ± 0.2	25.2 ± 2.5	81.0 ± 2.3	161 ± 10
(v)	0.0354	0.239	14.1	-	5.9 ± 0.2	22.5 ± 2.5	72.4 ± 2.6	120 ± 12
(vi)	0.118	0.801	-	11.6	6.1 ± 0.2	61.7 ± 5.3	54.2 ± 1.5	44 ± 7
(vii)	0.0505	0.243	-	12.7	5.9 ± 0.2	76.2 ± 6.3	56.2 ± 1.1	55 ± 5
(viii)	0.0301	0.205	-	12.8	5.9 ± 0.2	65.3 ± 3.1	53.0 ± 0.6	39.1 ± 2.9

a C.N. = the number of dmf ligands in the first coordination sphere as determined from a comparison of the integrated areas of the resonances of free and coordinated dmf in the temperature range 180 - 200 K.

b The errors represent the maximum observed deviation from the mean value.

c The k_{ex}(215 K) values were interpolated from the Eyring plots.

d The errors represent one standard deviation.

study was 205 - 235 K and rate constants are quoted at 215 K, the middle coalescence temperature. Over the 4.9- and 3.9-fold range of [dmf] in CD_2Cl_2 and $(CD_3)_2CO$* respectively, k_{ex}, exhibits a small non-linear variation with [dmf]. The k_{ex} values observed in $(CD_3)_2CO$ are approximately three times larger than those observed in CD_2Cl_2. This sensitivity of k_{ex} to the nature of the diluent may to some extent explain the small variation of k_{ex} observed in a given diluent since a change in [dmf] may be expected to modify the environment of $[Mg(dmf)_6]^{2+}$. Nevertheless, the small variation of k_{ex} with [dmf] in both diluents indicates that the predominant path for ligand exchange on $[Mg(dmf)_6]^{2+}$ is independent of [dmf] and is thus consistent with bond rupture being the major process in the formation of the transition state. In principle, either a dissociative mechanism or a dissociative interchange mechanism (in the limit where all of the magnesium(II) is in the form of the encounter complex, $[Mg(dmf)_6]^{2+}$.... dmf) is compatible with the observed ligand exchange kinetics.

When $[dmf]_{total}$ (= $[dmf] + [dmf]_{coord}$) was reduced beyond approximately 0.4 mol dm^{-3} in d_2-dichloromethane (i.e. by dilution of solutions (i) - (v) in Table 3.3) integrations of coordinated and free dmf resonances yielded coordination number values for magnesium(II) that were less than six: The apparent coordination number had levelled out to five at $[dmf]_{total} \simeq 0.02$ mol dm^{-3}. This trend is consistent with a shift in equilibrium towards $[Mg(dmf)_5]^{2+}$ (like the tmp system). Unfortunately, the ^1H resonances arising from the proposed five-coordinate magnesium(II) species were found to have the same chemical

---

* Deuterated acetone is expected to coordinate to magnesium(II) under conditions of low $[dmf]_{total}$. Hence, only a small [dmf] range is feasible for a study in d_6-acetone.

shifts (within spectral resolution) as those from $[Mg(dmf)_6]^{2+}$. The observed rate constants for exchange of dmf on the five-coordinate species (over a small concentration range) were roughly three to five times larger than those for dmf exchange on $[Mg(dmf)_6]^{2+}$ in CD_2Cl_2 diluent.

On the basis of the observations above and the data in Table 3.3 it seems likely that a dissociative rather than a dissociative interchange mechanism is operating in both diluents for $[Mg(dmf)_6]^{2+}$. The observed variation of k_{ex}, $\Delta H^{\ddagger}$ and $\Delta S^{\ddagger}$ with the nature of the diluent indicates that changes in the environment external to the first coordination sphere significantly modify the enthalpy and entropy differences between the ground state and transition state in the $[Mg(dmf)_6]^{2+}$ system. This modification appears to be minimal in the case of $[Mg(tmp)_6]^{2+}$.

3.4 Exchange of triphenylphosphineoxide on magnesium(II)

A magnesium(II) complex of stoichiometry $[Mg(tppo)_4](ClO_4)_2$ has been reported by Karayannis and coworkers[89]. (The bulk of the tppo ligand probably precludes the formation of $[Mg(tppo)_6](ClO_4)_2$.) They concluded from infra-red evidence that the ligand bonds to the metal via the phosphoryl oxygen and also intimated that at least two of the three aromatic rings are not coplanar with the plane of symmetry of the electron cloud of the P = O ⇈ bond. The complex was air-stable and there was no evidence for coordinated perchlorate in the solid state or in CH_2Cl_2 solution.

^1H n.m.r. was not employed in the ligand exchange study since the aromatic region is far too complex for lineshape analysis.

Rather, ^{31}P was the nucleus of choice because of its proximity to magnesium in the complex and because it gives rise to simple spectra (when ^{1}H decoupled). One major disadvantage is the poor signal to noise induced by the low sensitivity of ^{31}P nuclei and the low percentage of phosphorus by weight in the complex ion. Nevertheless, the complex and ligand were sufficiently soluble in CD_2Cl_2 to permit a reasonable concentration range of tppo (7.5-fold) for the determination of the exchange rate law in this diluent.

The ^{1}H decoupled 36.43 MHz ^{31}P n.m.r. spectrum of tppo in CD_2Cl_2 consisted of a single sharp peak throughout the liquid temperature range of CD_2Cl_2. Similarly, the ^{1}H decoupled ^{31}P spectrum of $[Mg(tppo)_4](ClO_4)_2$ in CD_2Cl_2 consisted of a single sharp peak which was displaced 301 Hz downfield at 200 K. However, when complex and ligand were mixed together such that $[tppo]_{total}/[Mg^{2+}] > 5$ the coordinated tppo signal was only 157 Hz downfield from the free tppo signal at 200 K. Integration of the coordinated and free ligand resonances revealed that $[Mg(tppo)_5]^{2+}$ is the much preferred magnesium(II) entity under these conditions. In principle, the non-equivalence of ligands in the possible trigonal bipyramidal or square-based pyramidal structures of $[Mg(tppo)_5]^{2+}$ should result in two singlets of different resonant frequencies; one characterizing the axial ligands and the other the equatorial ligands. In practice, this was not observed, indicating that either the chemical shift separation between the two expected singlets is too small for detection at 36.43 MHz or that the intramolecular tppo exchange between the two sites is in the fast exchange limit down to 180 K, the lowest temperature studied. In CD_2Cl_2 the following equilibrium exists.

$$[Mg(tppo)_4]^{2+} + tppo \overset{K_{eq}}{\rightleftharpoons} [Mg(tppo)_5]^{2+}$$

The stability of $[Mg(tppo)_5]^{2+}$ is such that over the whole magnesium(II) concentration range examined, 0.0813 - 0.0108 mol dm^{-3} (Table 3.4), in which the formal $[tppo]_{total}/[Mg^{2+}]$ ratio > 5 only singlets arising from $[Mg(tppo)_5]^{2+}$ and free tppo were observed. When this ratio was between four and five, singlets arising from $[Mg(tppo)_5]^{2+}$ and $[Mg(tppo)_4]^{2+}$ only were observed. The limit of detection of the least concentrated of the three species under either of these concentration ratio conditions was about 5% (*vide infra*) and on this basis the apparent equilibrium constant, K_{eq}, has a lower limit of $\sim$500 dm^3 mol^{-1}.

If the dissociation of a tppo ligand is the sole rate determining process leading to tppo exchange on $[Mg(tppo)_5]^{2+}$, the lifetime of magnesium(II) in $[Mg(tppo)_5]^{2+}$, τ_{Mg}, and the lifetime of a single ligand in $[Mg(tppo)_5]^{2+}$, τ_c, (which will bear the relationship $\tau_{Mg} = \tau_c/5$) will be independent of all reactant concentrations. The k_{ex} (= $1/\tau_c$), $\Delta H^{\ddagger}$ and $\Delta S^{\ddagger}$ values for solutions (i) - (iii), which were derived by complete lineshape analysis of the coalescence of the $[Mg(tppo)_5]^{2+}$ and free tppo ^{31}P singlets over the temperature range 210 - 245 K (Table 3.4), are seen to be internally similar and are also comparable to the kinetic parameters characterizing solution (iv) which were derived from the coalescence of the ^{31}P singlets of $[Mg(tppo)_5]^{2+}$ and $[Mg(tppo)_4]^{2+}$ over the temperature range 205 - 240 K. For solutions (i) - (iv) [tppo] ranges from 0.276 - ca. 0.01 mol dm^{-3} and $[Mg(tppo)_4^{2+}]$ ranges from 0.05 - ca. 0.0005 mol dm^{-3} (the lower concentration limit being estimated for both of these species on the grounds that the limit of detection would require a signal intensity of approximately 5% of that of the major species present). It is

TABLE 3.4 *Solution compositions and kinetic parameters for triphenylphosphineoxide exchange on magnesium(II) in CD_2Cl_2 diluent*

Solution	$[Mg(tppo)_5^{2+}]$ mol dm^{-3}	[tppo] mol dm^{-3}	k_{ex}(220 K) s^{-1}	$\Delta H^{\ddagger}$ kJ mol^{-1}	$\Delta S^{\ddagger}$ J K^{-1} mol^{-1}
(i)	0.0813	0.276	38 ± 4	73.7 ± 1.8	123 ± 8
(ii)	0.0465	0.128	37 ± 5	69.0 ± 2.1	101 ± 9
(iii)	0.0108	0.0368	56 ± 4	69.6 ± 1.2	107 ± 5
		$[Mg(tppo)_4^{2+}]$			
(iv)	0.050	0.050	[a] 200 ± 20	73.0 ± 1.6	[a] 133 ± 7
			[b] 40 ± 4	73.0 ± 1.6	[b] 120 ± 7
	$[Zn(tppo)_4^{2+}]$	[tppo]			
from ref. 90:	0.0202	0.079		31.7 ± 0.3	-29.6 ± 1.6

a k_{ex} and $\Delta S^{\ddagger}$ refer to the interconversion of $[Mg(tppo)_5]^{2+}$ to $[Mg(tppo)_4]^{2+}$ such that the ligand exchange rate = $\tau_{Mg}^{-1}[Mg(tppo)_5^{2+}]$.

b k_{ex} and $\Delta S^{\ddagger}$ refer to the exchange of one tppo ligand on $[Mg(tppo)_5]^{2+}$ such that the ligand exchange rate = $5\tau_c^{-1}[Mg(tppo)_5^{2+}]$.

Quoted errors on all parameters represent one standard deviation using ACTENG.

apparent from these data that ligand exchange on $[Mg(tppo)_5]^{2+}$ proceeds predominantly through a D mechanism.

An A mechanism necessarily provides one ligand exchange path for the $[Mg(tppo)_4]^{2+}$ species according to the equilibrium above. In addition, the invariance of the width of the $[Mg(tppo)_4]^{2+}$ singlet upon dilution of solution (iv) and the broadening* of the tppo singlet upon dilution of solutions (i) - (iii) (in the temperature range 180 - 200 K where the $[Mg(tppo)_5]^{2+}$ singlet was not significantly broadened by the ligand exchange), suggests the operation of a D ligand exchange mechanism at a rate (at 200 K) which is below the fast exchange limit of the n.m.r. time scale.

Due to the disparate concentrations of $[Mg(tppo)_4]^{2+}$ and tppo existing in solution, as discussed earlier, quantitative ligand exchange data were unobtainable for this ligand exchange process, but the dilution experiments provided good estimates of the temperature dependent linewidth variations arising from this process in solutions (i) - (iii) so that the small allowances for these variations were readily made in the derivation of the $[Mg(tppo)_5]^{2+}$ exchange parameters.

It is interesting to note that zinc(II) also forms a four-coordinate complex with tppo in the solid state but the predominant zinc(II) species in $[Zn(tppo)_4](ClO_4)_2$/tppo/CD_2Cl_2 mixtures[90] is

---

*This is consistent with an increase in the ratio $[Mg(tppo)_4^{2+}]/[tppo]$ upon dilution. The mean lifetime of tppo in $[Mg(tppo)_4]^{2+}$, τ_c', which appeared to be independent of [tppo] in the temperature range 180 - 200 K (since tppo exchange on $[Mg(tppo)_4]^{2+}$ through an A mechanism is relatively slow), is related to the mean lifetime of free tppo, τ_F, as below.

$$\tau_c'/P_c' = \tau_F/P_F$$

$[Zn(tppo)_4]^{2+}$. Given that the crystallographic and effective ionic radii of both four- and five-coordinate magnesium(II) and zinc(II) are almost identical[91] it is concluded that steric effects are unlikely to produce the coordination number differences between the tppo complexes of magnesium(II) and zinc(II) observed in solution. Therefore, an alternative origin of these differences must be sought.

Magnesium(II) has the neon electronic configuration whereas zinc(II) is characterized by $[Ne]3s^23p^63d^{10}$ and this is reflected on an empirical basis by magnesium(II) behaving as a hard acid whilst zinc(II) exhibits characteristics between those of a hard and a soft acid[92]. As a consequence, magnesium(II) is expected to form some of its most stable complexes with oxygen donor ligands whereas zinc(II) is expected to form more stable complexes with ligands bonding through sulphur. These expectations may partly explain why magnesium(II) achieves the five-coordinate state in $[Mg(tppo)_5]^{2+}$ in CD_2Cl_2 solution whilst zinc(II) only achieves four-coordination in $[Zn(tppo)_4]^{2+}$ under similar conditions.(It is also implied that crystal packing forces cause $[Mg(tppo)_4]^{2+}$ to be more stable than $[Mg(tppo)_5]^{2+}$ in the solid state.) The harder acid nature of magnesium(II) compared to zinc(II) again probably manifests itself in the $\Delta H^{\ddagger}$ and $\Delta S^{\ddagger}$ values for tppo exchange,which are substantially larger in the case of magnesium(II) (Table 3.4).

3.5 ^{1}H n.m.r. studies of N-methylformamide and N-methylacetamide complexes of magnesium(II)

The solvents nmf and nma exist in two isomeric forms, viz.

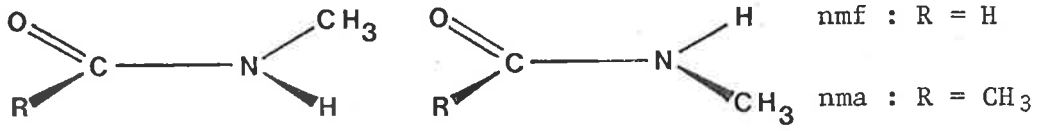

I ⇌ II

which interconvert very slowly below room temperature. It has been shown by a variety of spectroscopic methods that the *trans* (I) form predominates over the *cis* (II) form. In addition, if the N-methyl group is *cis* to the carbonyl group (I) then the N-CH_3 ^{1}H n.m.r. resonances will occur at a higher field compared to those resonances for a N-methyl group *trans* to the carbonyl group.

In 1964, La Planche and Rogers[93] determined the proportion of *cis* : *trans* to be 8 : 92 in the case of nmf. They were not able to detect any *cis* isomer at all for nma. However, Barker and Boudreaux[94] later reported 3% *cis* isomer in aqueous nma solution and ten percent *cis* isomer of nmf was found in neat or aqueous nmf samples at 35°C. The proportion of *cis* amide increased only slightly with temperature.

$[Mg(nmf)_6](ClO_4)_2$ was easily prepared using a slight variation of the general synthetic procedure described in Chapter 7. It was mildly hygroscopic with poor solubility in CD_2Cl_2. 90 MHz ^{1}H n.m.r. spectra of samples of the complex in $(CD_3)_2CO$/nmf mixtures at temperatures below 200 K were consistent with the occurrence of slow intermolecular nmf exchange been free and coordinated sites. Approximately 10% of the nmf was in the *cis* form for both free and coordinated environments. Comparisons of the relative areas of all

resonances implied that $[Mg(nmf)_6]^{2+}$ was the predominant magnesium(II) species in solution. Coalescence of the N-methyl resonances took place at about 215 K in accord with the kinetic behaviour of the $[Mg(dmf)_6]^{2+}$ system. Due to the complexity of the coalescence phenomenon which involves two isomers of nmf, kinetic parameters were not obtained.

$[Mg(nma)_5](ClO_4)_2$ was a hygroscopic (possibly non-stoichiometric) complex and was only sparingly soluble in CD_2Cl_2. Studies of this system were, as in the nmf case, confined to $(CD_3)_2CO$ diluent. Approximately 3% *cis* isomer was observed for the free ligand in $(CD_3)_2CO$. The same percentage of *cis* isomer seemed to be maintained when nma was coordinated to magnesium(II), as determined from ^1H n.m.r. spectra of the complex in $(CD_3)_2CO$. However, at temperatures close to the freezing point of $(CD_3)_2CO$ the N-methyl resonances of coordinated *trans* nma appeared to possess an upfield shoulder. This observation could be due to either the displacement of a significant amount of nma from the first coordination sphere (*vide infra*), or the slowing down of intramolecular ligand exchange in $[Mg(nma)_5]^{2+}$ to a point where separate n.m.r. signals are evidenced for axial and equatorial ligands (cf. Sections 3.2 and 3.4). In the latter event, the upfield shoulder arises from the axial ligands. The spectral resolution under these conditions was, unfortunately, not very good. (The presence of proton signals from incompletely deuterated diluent precluded proper measurements in the acetyl region but, at low temperature, splitting of the *trans* amide acetyl signal was observed.)

^1H n.m.r. spectra of $[Mg(nma)_5](ClO_4)_2$ and nma together in $(CD_3)_2CO$ at room temperature were consistent with the occurrence of very fast intermolecular exchange. When the solutions were cooled

below 200 K significant exchange broadening was observed. At about 180 K the intermediate ('flat top') intermolecular exchange condition was satisfied and there were signs of splitting in the N-methyl region. Further cooling induced a prohibitively large increase in viscosity. Coordination numbers and quantitative kinetic data were unobtainable.

It would appear that the intermolecular exchange of nma on magnesium(II) is too fast for accurate ^{1}H lineshape analysis at 90 MHz. Ligand exchange is therefore substantially more rapid for nma than for nmf, dmf, tmp or tppo. Rationalization of this kinetic phenomenon in terms of relative ligand basicities or sizes seems impossible.

CHAPTER 4 LIGAND EXCHANGE ON SCANDIUM(III)

4.1 Introduction

The rate of murexide substitution into the first coordination sphere of the aquascandium(III) ion has been measured (k_2(285 K) = 4.8×10^7 dm^3 mol^{-1} s^{-1}) using the T-jump technique[95] and is unexpectedly high for a trivalent metal ion occurring early in the periodic table. More recently, in another study[96] of multidentate complex formation involving the aquascandium(III) ion, the lowest rate constant observed was 3.3×10^6 s^{-1} (298 K). It has been suggested that these observations may be a consequence of there being more than six aqua ligands in the first coordination sphere of scandium(III) in solution[10,95], but only 5.1 aqua ligands have been directly detected by ^1H n.m.r. in that environment, possibly as a result of some of the first coordination sphere sites being occupied by anionic ligands[97]. ^{45}Sc n.m.r. studies[98] of various scandium salts in aqueous solution have provided no hard evidence as to the stoichiometries of the scandium(III) species present. In scandium perchlorate solutions, for example, the observed changes in chemical shift and linewidth may be due to the formation of hydrolysis products[99,100] or contact ion pair formation. A comparison of the experimental free energy of hydration to values calculated for various coordination numbers[101] suggests that $[Sc(H_2O)_6]^{3+}$ should be the dominant scandium(III) species. On the other hand, it is known from crystal structure determinations that scandium(III) can form six-[102], seven-[103], eight-[104] and nine-[105] coordinate complexes with various ligands in the solid state and hence, possibly in solution. Moreover, scandium(III) is able to vary its coordination number by two (six to

eight) in the presence of the same ligand[102,104].

Along with the mystique which surrounds ligand substitution processes on scandium(III) in aqueous solution, there is a paucity of kinetic data with respect to non-aqueous scandium(III) systems. This Chapter provides further insight into the dynamics of ligand exchange on scandium(III) through n.m.r. investigations of the more general and possibly simpler non-aqueous systems.

4.2 Exchange of trimethylphosphate on $[Sc(tmp)_6]^{3+}$

The mildly hygroscopic complex, $[Sc(tmp)_6](ClO_4)_3$, was soluble in CD_3CN, CD_3NO_2, $C_2H_2Cl_4$ and $(CD_3)_2CO$ but insoluble in CD_2Cl_2. Slow decomposition of d_6-acetone solutions containing Sc^{3+} was seen to occur (yellow after thirty minutes) in accordance with observations made by Crea[67] of the behaviour of acetone solutions containing Al^{3+}.* A study in this diluent was, therefore, not attempted. Solutions of $[Sc(tmp)_6](ClO_4)_3$ and tmp in CD_3CN, CD_3NO_2 or $C_2H_2Cl_4$ exhibited a ^1H n.m.r. doublet for coordinated tmp ($J(^1H - ^{31}P)$ = 11.4 Hz) downfield from the doublet of free tmp ($J(^1H - ^{31}P)$ = 11.1 Hz) under conditions of slow exchange between coordinated and free sites. The slow exchange condition was satisfied in all the CD_3CN and $C_2H_2Cl_4$ solutions (Table 4.1) below 250 and 260 K respectively. In CD_3NO_2 solutions the onset of the slow exchange condition occurred at progressively higher temperatures as [tmp] decreased; thus slow exchange was observed at and below 265 and 305 K respectively for the concentration extremes

---

* Decomposition of acetone solutions containing Mg^{2+} (Chapter 3) is very much slower (yellow after two weeks). Hence over the period required for data accumulation (ca. two hours) the extent of decomposition is negligible for magnesium(II) systems.

TABLE 4.1 *Solution compositions and kinetic parameters for tmp exchange on* $[Sc(tmp)_6]^{3+}$

Solution	$[Sc(tmp)_6^{3+}]$ mol dm^{-3}	[tmp] mol dm^{-3}	$[CD_3CN]$ mol dm^{-3}	$[C_2H_2Cl_4]$ mol dm^{-3}	$[CD_3NO_2]$ mol dm^{-3}	C.N.[a]	k_{ex}(300 K)[b,c] s^{-1}	$\Delta H^{\ddagger}$[c,d] kJ mol^{-1}	$\Delta S^{\ddagger}$[c,d] J K^{-1} mol^{-1}
(i)	0.110	0.693	15.0	-	-	5.9 ± 0.1	65.7 ± 2.6	29.8 ± 0.4	-111 ± 2
(ii)	0.0503	0.147	17.3	-	-	5.8 ± 0.2	36.5 ± 0.7	31.3 ± 0.2	-111 ± 1
(iii)	0.0174	0.109	17.7	-	-	6.0 ± 0.2	33.9 ± 1.2	32.7 ± 0.3	-107 ± 1
(iv)	0.0153	0.0448	17.7	-	-	5.8 ± 0.2	33.4 ± 1.1	33.2 ± 0.4	-105 ± 2
(v)	0.00307	0.0193	18.1	-	-	6.1 ± 0.1	36.3 ± 1.2	28.9 ± 0.3	-119 ± 1
(vi)	0.00109	0.0069	18.1	-	-	6.0 ± 0.2	49.2 ± 2.3	29.4 ± 0.6	-115 ± 2
(vii)	0.113	0.864	-	7.32	-	6.0 ± 0.1	42.4 ± 1.3	41.3 ± 0.5	-76.0 ± 1.8
(viii)	0.0579	0.386	-	8.11	-	6.1 ± 0.2	42.7 ± 1.6	43.4 ± 0.5	-69.1 ± 1.8
(ix)	0.125	0.892	-	-	14.0	5.9 ± 0.1			
(x)	0.107	0.595	-	-	14.9	5.9 ± 0.1	k_2(300 K)[e] = 51.3 ± 1.8 dm^3 mol^{-1} s^{-1}		
(xi)	0.0612	0.312	-	-	16.1	6.0 ± 0.1	$\Delta H^{\ddagger}$[e] = 26.0 ± 0.9 kJ mol^{-1}		
(xii)	0.0279	0.199	-	-	16.9	6.1 ± 0.2	$\Delta S^{\ddagger}$[e] = -126 ± 3 J K^{-1} mol^{-1}		
(xiii)	0.0044	0.0315	-	-	17.7	6.0 ± 0.2			

a C.N. = number of coordinated tmp molecules. The errors represent the maximum observed deviation from the mean value.

b k_{ex}(300 K) interpolated from the Eyring plots.

c The errors represent one standard deviation (ACTENG).

d $\Delta H^{\ddagger}$ and $\Delta S^{\ddagger}$ determined from the Eyring plots.

e Determined from DATAFIT. The errors quoted represent one standard deviation.

represented by solutions (ix) and (xiii). In every case only one coordinated tmp doublet was observed and a comparison of the integrated areas of the coordinated and free tmp doublets indicated that, within experimental error, six tmp ligands occupy the first coordination sphere of scandium(III). Coalescence of the coordinated and free tmp doublets occurred as the temperature was raised, and is exemplified by the $[Sc(tmp)_6]^{3+}/tmp/CD_3CN$ system in Figure 4.1. Complete lineshape analysis of the coalescence phenomenon yielded τ_c, the lifetime of a single ligand coordinated to scandium(III). A semilogarithmic plot of $\tau_c T$ versus 1/T for the CD_3CN and $C_2H_2Cl_4$ solutions is shown in Figure 4.2 and the derived kinetic parameters are given in Table 4.1.

From the data it is seen that k_{ex}(300 K) in CD_3CN solutions varies by a factor of two in a non-linear manner over a hundred-fold variation in [tmp] which indicates that the rate of the predominant exchange process is virtually independent of [tmp]. This observation is typical of a dissociative mechanism in which the rate determining step is the breaking of a metal-ligand bond to produce a reactive intermediate, $[Sc(tmp)_5]^{3+}$. (As will be noted later, the dynamics of tmp exchange on $[Sc(tmp)_6]^{3+}$ appear to be dictated by the nature of the diluent and it is therefore likely that a part of the observed variation in k_{ex}(300 K) for solutions (i) - (vi) reflects composition changes in bulk solvent as both [tmp] and $[Sc(tmp)_6{}^{3+}]$ are varied.)

Alternatively, the dissociative interchange mechanism can give rise to the observed exchange rate law,

$$\text{exchange rate} = 6k_1[Sc(tmp)_6^{3+}]$$

if the pre-equilibrium constant, K, is very large such that $K[tmp] \gg 1$ (limit (b)) even for solution (vi). An inspection of the relative tmp and CD_3CN concentrations in Table 4.1 suggests that a high degree

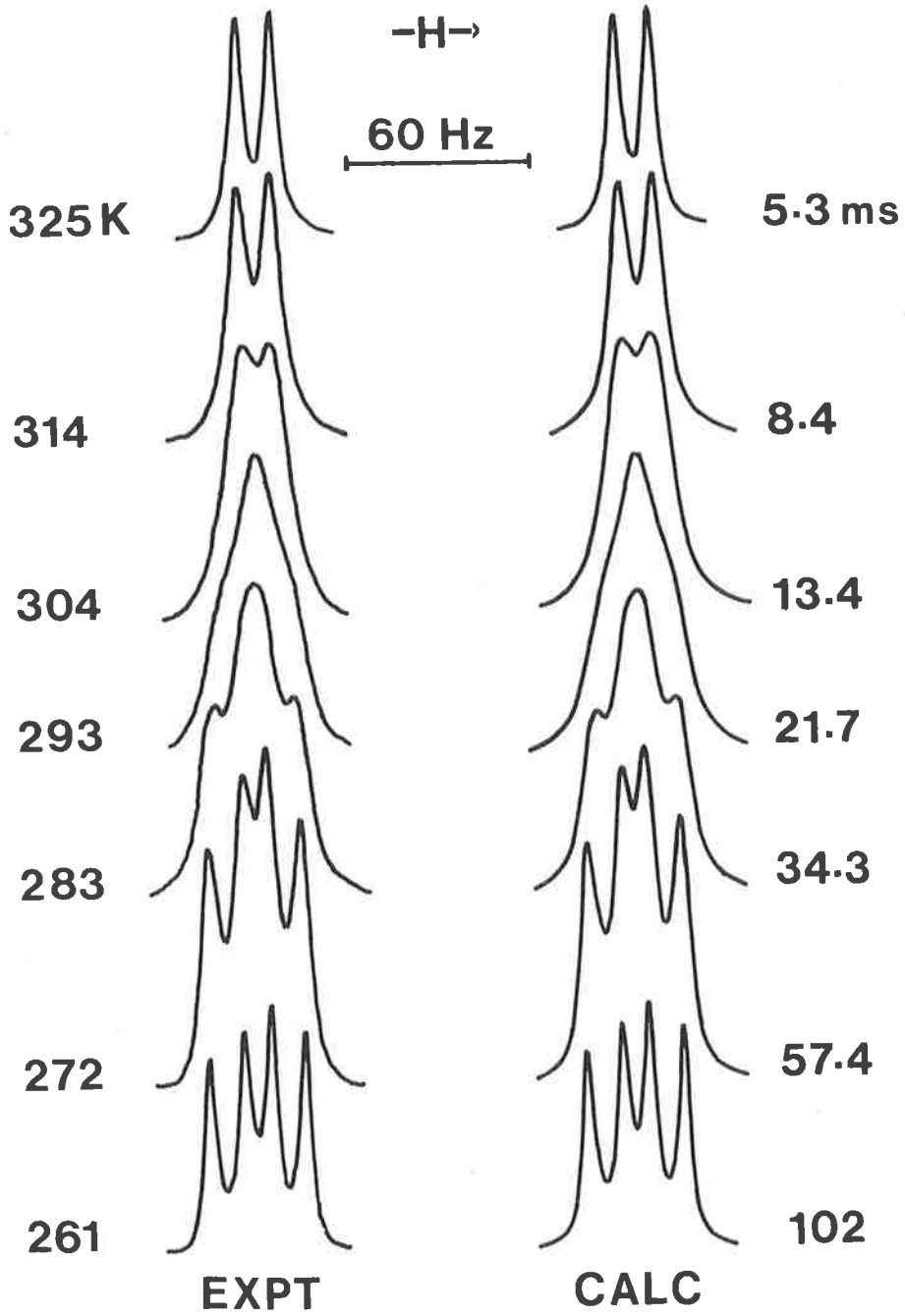

FIGURE 4.1 Experimental and computed best fit ^{1}H n.m.r. lineshapes for solution (i). The experimental temperatures and best fit τ_c values appear to the left and right of the Figure respectively. The coordinated tmp signal is downfield.

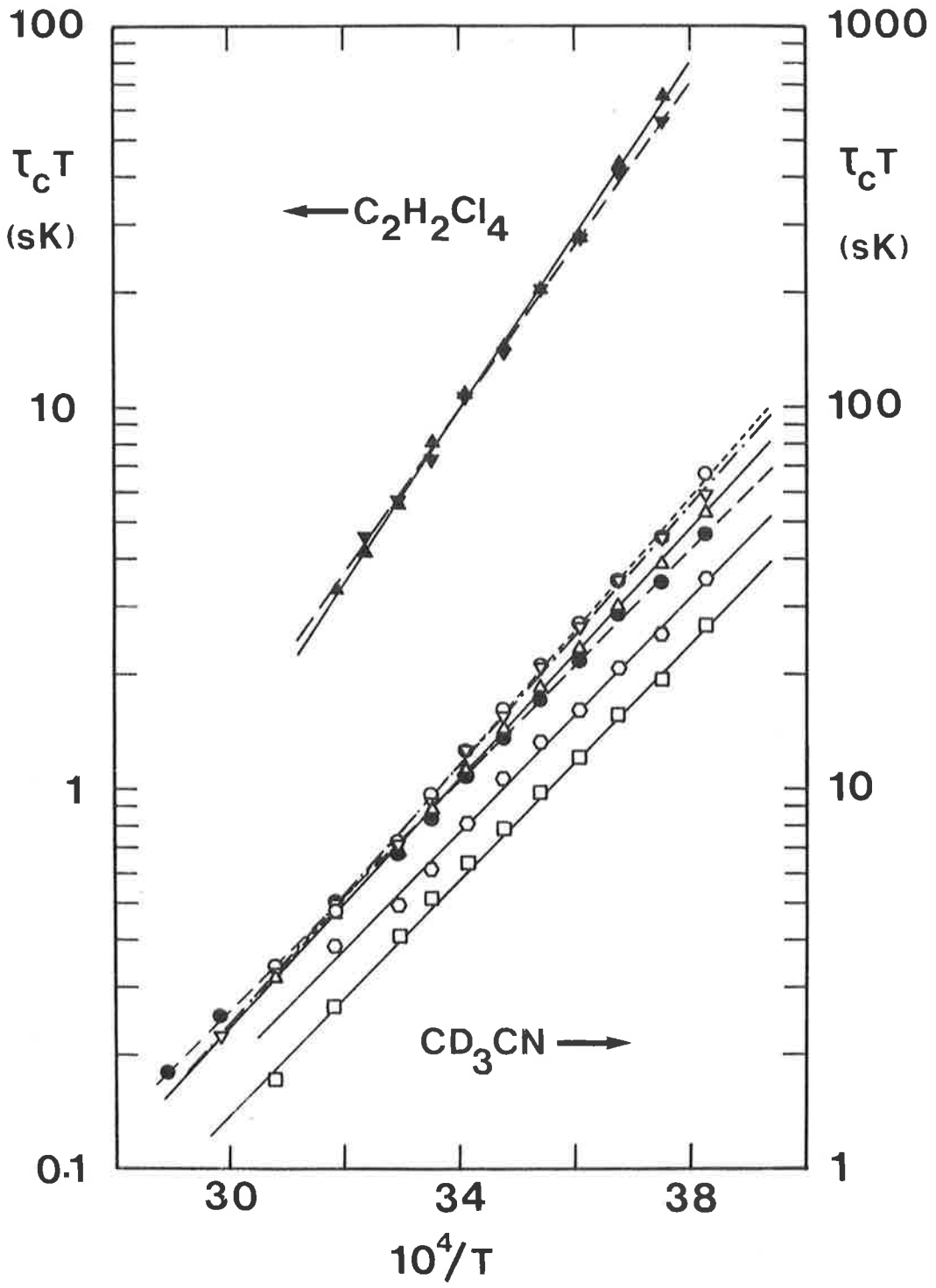

FIGURE 4.2 Semilogarithmic plots of $\tau_c T$ against 1/T for the $[Sc(tmp)_6]^{3+}$/tmp/CD_3CN and $[Sc(tmp)_6]^{3+}$/tmp/$C_2H_2Cl_4$ systems. Data for solutions (i) - (viii) are represented as (i) —□—, (ii) —△—, (iii) —·▽—·—, (iv) ----○----, (v) —●— —, (vi) —⬡—, (vii) —▼— — and (viii) —▲—.

of preferential occupancy of the second coordination sphere of scandium(III) by tmp would be necessary for the limiting condition above to hold over the entire experimental concentration range. There is no experimental evidence that such preferential occupancy occurs in this system.

Two solutions in 1,1,2,2-tetrachloroethane were studied in detail (Table 4.1) and the derived $\Delta H^{\ddagger}$ and $\Delta S^{\ddagger}$ values are seen to be markedly different from those associated with the CD_3CN samples. Unfortunately, the lineshape coalescence phenomenon for less concentrated solutions was irreproducible after they had been taken above 320 K, thus precluding exchange studies over a large concentration range. It is possible that some decomposition of $C_2H_2Cl_4$ occurred, leading to the generation of chloride ions which subsequently coordinated to scandium(III). The coalescence phenomenon for the two solutions (vii) and (viii) was, however, reproducible after several days at room temperature. The rate constants for these solutions appear to be independent of [tmp] but the twofold concentration range is too small to base a definite mechanistic conclusion on.

In CD_3NO_2 solutions, the dynamics of the tmp exchange process were characterized by a second order rate law,

$$\text{exchange rate} = 6k_2[\text{tmp}][Sc(\text{tmp})_6^{3+}]$$

over the 28.3-fold variation in [tmp] examined (Figure 4.3). Derived kinetic parameters (DATAFIT) for this second order process are given in Table 4.1. The rate law above is compatible with either an I_D mechanism in the limit where $K[\text{tmp}] \ll 1$ (limit (a)), or an associative mechanism in which the rate determining step is the formation of a transition state or reactive intermediate of stoichiometry $[Sc(\text{tmp})_7]^{3+}$.

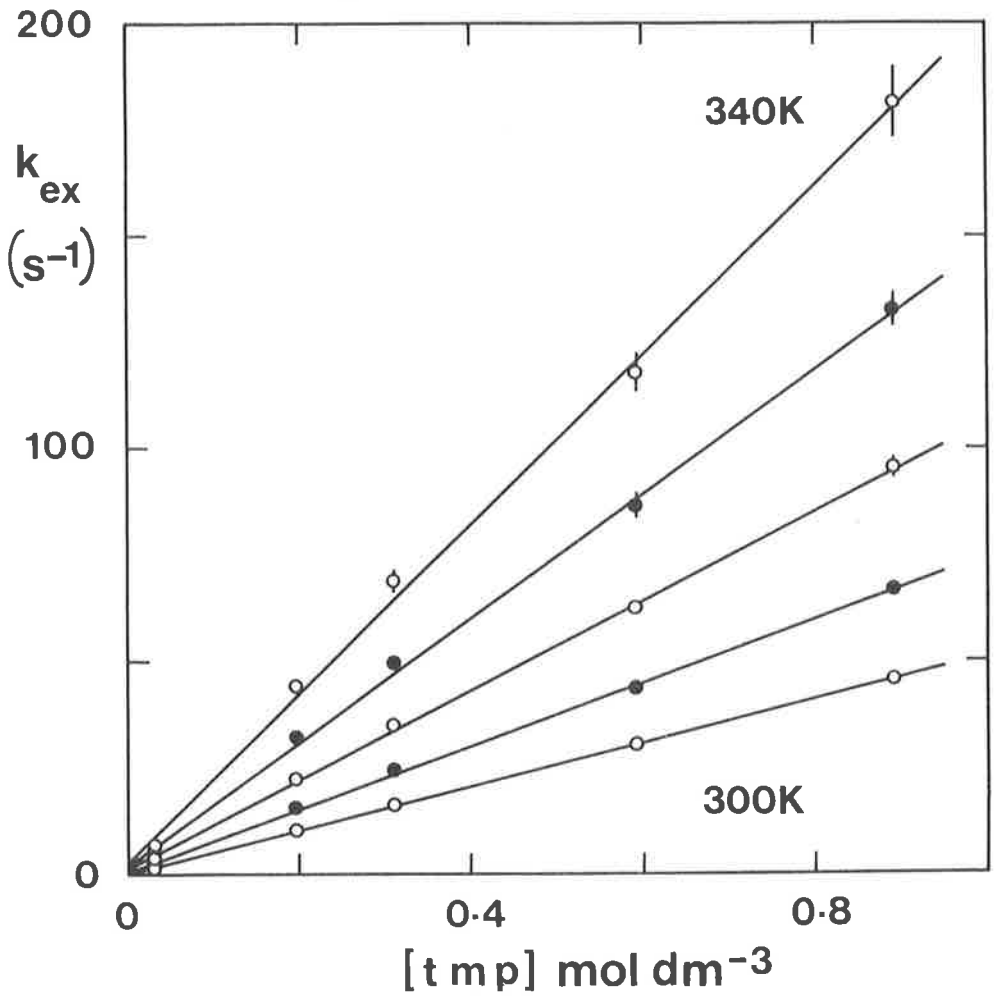

FIGURE 4.3 Plots of k_{ex} data sets against [tmp] for the $[Sc(tmp)_6]^{3+}/tmp/CD_3NO_2$ system. The solid lines represent linear regression lines. k_{ex} was interpolated at each temperature (300, 310, 320, 330, 340 K) from the linear regression line of $\ln(\tau_c T)$ against 1/T for each of the solutions (ix) - (xiii).

In view of their similar molecular sizes and dielectric constants (35.9 and 36.2 for their respective proton analogues at 298 K) it is surprising that different tmp exchange rate laws should be observed in the diluents CD_3CN and CD_3NO_2. The least mechanistic difference arises if the I_D mechanism in the limits (b) and (a) operates in CD_3CN and CD_3NO_2 respectively, whereas the greatest mechanistic difference arises if D and A mechanisms operate in these diluents respectively. However, it is clearly not possible to test for an A mechanism in this type of ligand exchange system by observing the effect of variation in the character of an incoming ligand upon the substitution rate.

Obviously the nature of the diluent has a profound effect upon the kinetics of the tmp exchange process, but low temperature ^1H n.m.r. spectra of $[Sc(tmp)_6](ClO_4)_3$ in mixtures of CD_3CN and CH_3CN, or CD_3NO_2 and CH_3NO_2, exhibited no resonances attributable to either diluent being present in the first coordination sphere of scandium(III). This observation in conjunction with the observed constancy of the coordination number of scandium(III) (Table 4.1) with respect to tmp over extended concentration ranges indicates that the entry of diluent into the first coordination sphere is probably not a significant consideration. Nevertheless, the diluent does have a marked effect upon the chemical shift of $[Sc(tmp)_6]^{3+}$ relative to the resonance of free tmp. In CD_3CN, $C_2H_2Cl_4$ and CD_3NO_2 and with ^1H n.m.r., the above-mentioned chemical shift (which was slightly temperature dependent) ranged from 0.224 - 0.199 p.p.m. for solutions (i) - (vi) (240 K); 0.221 - 0.216 p.p.m. for solutions (vii) - (viii) (240 K); and 0.329 - 0.337 p.p.m. for solutions (ix) - (xiii) (260 K). In CD_3CN and $C_2D_2Cl_4$ respectively the ^{31}P chemical shift of $[Sc(tmp)_6]^{3+}$

was 7.46 and 7.60 p.p.m. upfield from the free tmp signal (Figure 4.4) at 235 K whereas in CD_3NO_2 it was 1.98 p.p.m. downfield at 260 K. The CD_3NO_2 solutions froze below 250 K but since the ^{31}P chemical shifts had only a small temperature variation the resonance position of $[Sc(tmp)_6]^{3+}$ extrapolated to 235 K would be close to 1.98 p.p.m. downfield from that of free tmp. The $[Sc(tmp)_6]^{3+}$ ^{31}P resonance was a broad octuplet (I = 7/2 for ^{45}Sc) when proton decoupled for which $J(^{45}Sc - ^{31}P)$ was ca. 35 Hz. The different chemical shift separations observed are indicative of marked differences in diluent interaction with coordinated and free tmp and it is particularly interesting that the chemical shift separations in CD_3NO_2, in which second order kinetics dominate, are distinctly dissimilar to those observed in the other two diluents.

The maximum difference between the interactions of CD_3NO_2 and CD_3CN with the spherical array of methyl groups presented by the first coordination sphere of scandium(III) arises if the $-NO_2$ and -CN groups of these diluents are oriented towards the scandium(III) centre. The electrostriction of the first and second coordination spheres may well cause the stereochemical characteristics of the $-NO_2$ and -CN groups to be crucial in determining the orientation of the methyl groups at the surface of the first coordination sphere and therefore the relative energies of $[Sc(tmp)_6]^{3+}$ and the $[Sc(tmp)_5]^{3+}$ and $[Sc(tmp)_7]^{3+}$ intermediate or transition state species. Evidently, the effect of diluent upon the free energies of ground and transition states for the $[Sc(tmp)_6]^{3+}$ and $[Be(tmp)_4]^{2+}$ systems[23,24] may be sufficient to cause a change from a D to an A mechanism. When the degree of steric crowding in the primary coordination sphere is high or low, the tendency for a change in mechanism should not depend critically on a change in the

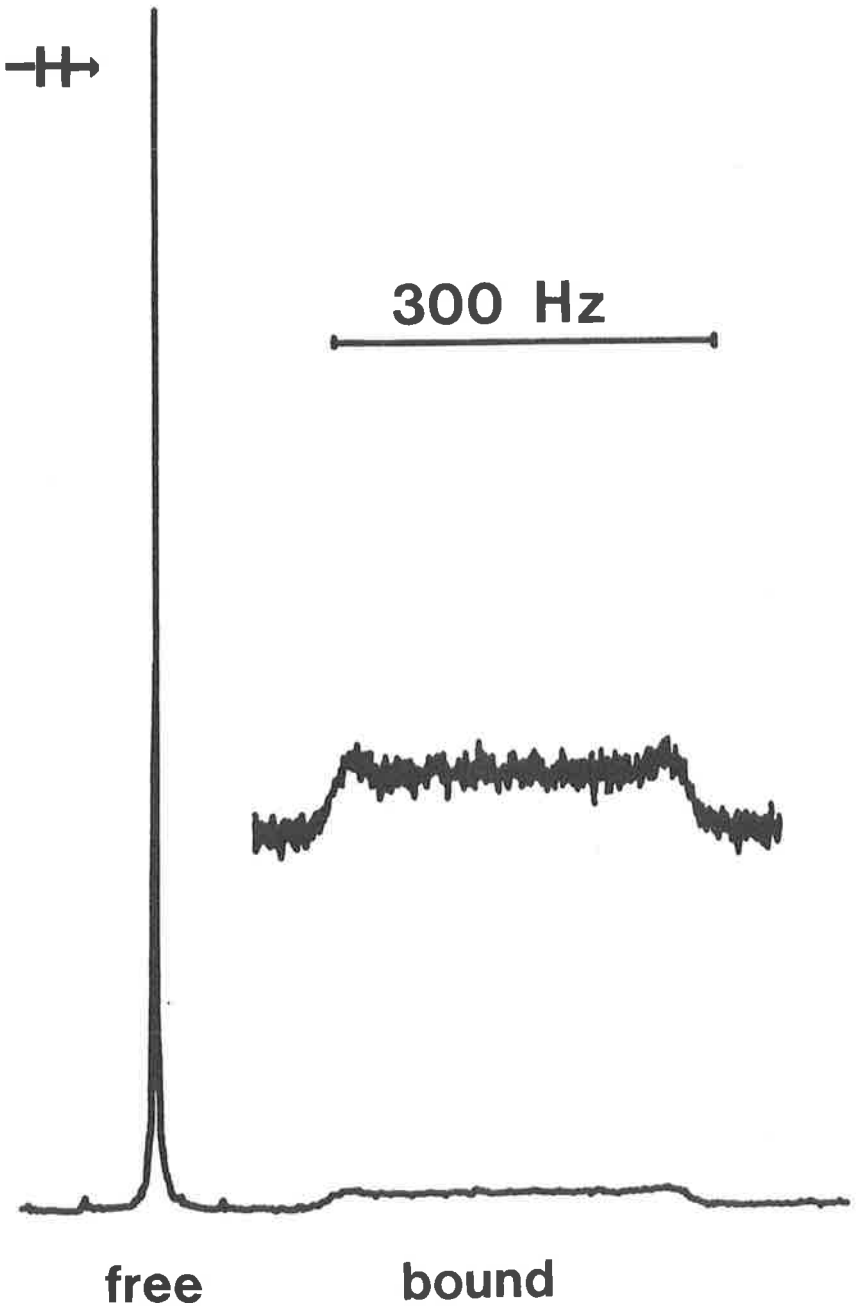

FIGURE 4.4 ^{1}H decoupled ^{31}P (36.43 MHz) FT n.m.r. spectrum of a CD_3CN solution of $[Sc(tmp)_6]^{3+}$ (0.110 mol dm^{-3}) and tmp (0.693 mol dm^{-3}) at 235 K. The tmp singlet appears downfield from the broad $[Sc(tmp)_6]^{3+}$ octuplet, which is also displayed at a higher amplitude in the inset.

diluent but nevertheless some disparity may be expected in activation parameters (cf. $[Mg(dmf)_6]^{2+}$). In intermediate steric crowding cases, which $[Be(tmp)_4]^{2+}$ and $[Sc(tmp)_6]^{3+}$ (and $[Sc(dmmp)_6]^{3+}$ also; see Section 4.3) evidently are, a change in diluent may cause a change in mechanism. On the basis of the limited data available (*vide infra*) it appears that the CD_3NO_2 diluent favours the A mechanism to a greater extent than does CD_3CN.

From an inspection of the kinetic data in Tables 1.1, 3.2 and 4.1, it is clear that $[Sc(tmp)_6]^{3+}$ is not unexpectedly labile by comparison with its magnesium(II), aluminium(III), gallium(III) and indium(III) analogues. However, it is pertinent to note the mechanistic differences between the six-coordinate tmp systems. The complex $[Sc(tmp)_6]^{3+}$ is similar in size to $[Al(tmp)_6]^{3+}$ and $[Ga(tmp)_6]^{3+}$ and it is therefore improbable, in CD_3NO_2, that tmp will preferentially enter the second coordination sphere of the aluminium(III) and gallium(III) species. This indicates that the least difference in mechanism between these three systems is between the D mechanism for $[Al(tmp)_6]^{3+}$ and $[Ga(tmp)_6]^{3+}$ and the I_D mechanism for $[Sc(tmp)_6]^{3+}$. The larger ionic radius[91] of scandium(III) will presumably cause $[Sc(tmp)_5]^{3+}$ and $[Sc(tmp)_7]^{3+}$ to be respectively less and more stable (on steric grounds) than their aluminium(III) and gallium(III) analogues. Consequently, $[Sc(tmp)_6]^{3+}$ will have a greater tendency to undergo ligand exchange through either an I_D or an A mechanism. Indium(III), which is even larger than scandium(III) in terms of ionic radius, is expected to strongly favour seven-coordination over five-coordination and this expectation is supported by the fact that tmp exchange on $[In(tmp)_6]^{3+}$ in CD_3NO_2 is seen to occur by an A mechanism (Table 1.1). At this point it is interesting to speculate

on the behaviour of $[Al(tmp)_6]^{3+}$, $[Ga(tmp)_6]^{3+}$ and $[In(tmp)_6]^{3+}$ in CD_3CN diluent. The degree of steric crowding in the first coordination sphere of aluminium(III) is probably higher than that of scandium(III). In contrast, $[In(tmp)_6]^{3+}$ is likely to be less sterically crowded than $[Sc(tmp)_6]^{3+}$. Hence, one might expect (using the steric crowding argument presented above) that a change in mechanism on going from CD_3NO_2 to CD_3CN will be observed for $[Ga(tmp)_6]^{3+}$ but not for $[Al(tmp)_6]^{3+}$ or $[In(tmp)_6]^{3+}$.

4.3 Exchange of dimethylmethylphosphonate on $[Sc(dmmp)_6]^{3+}$

The air stable compound $[Sc(dmmp)_6](ClO_4)_3$ was soluble in CD_3CN and CD_3NO_2 but, like the tmp complex, virtually insoluble in CD_2Cl_2. Under conditions of slow exchange the ^1H decoupled ^{31}P octuplet resonance arising from coordinated dmmp ($J(^{45}Sc - ^{31}P) \approx 35$ Hz) was observed downfield from the singlet resonance of free dmmp (Figure 4.5) in both CD_3CN and CD_3NO_2 diluents. Partial overlap of the two ^{31}P resonances prevented a reliable estimate (by integration) of the number of dmmp ligands coordinated to scandium(III). The ^1H doublet resonance from the O-Me groups* of coordinated dmmp was observed downfield from the analogous doublet for free dmmp in solutions (i) - (xi) (Table 4.2) under conditions of slow exchange. Comparisons of the integrated areas of coordinated and free doublets (Figure 4.6) showed $[Sc(dmmp)_6]^{3+}$ to be the dominant scandium(III) species in solution. In both CD_3CN and CD_3NO_2 diluents the slow exchange condition was observed at increasingly

---

* The doublets arising from the P-Me groups of coordinated and free dmmp appeared upfield of the O-Me doublets but superimposition of the proton impurity resonances of incompletely deuterated CD_3CN on the former doublets rendered quantitative study impossible and consequently the ^1H study was confined to the O-Me doublets.

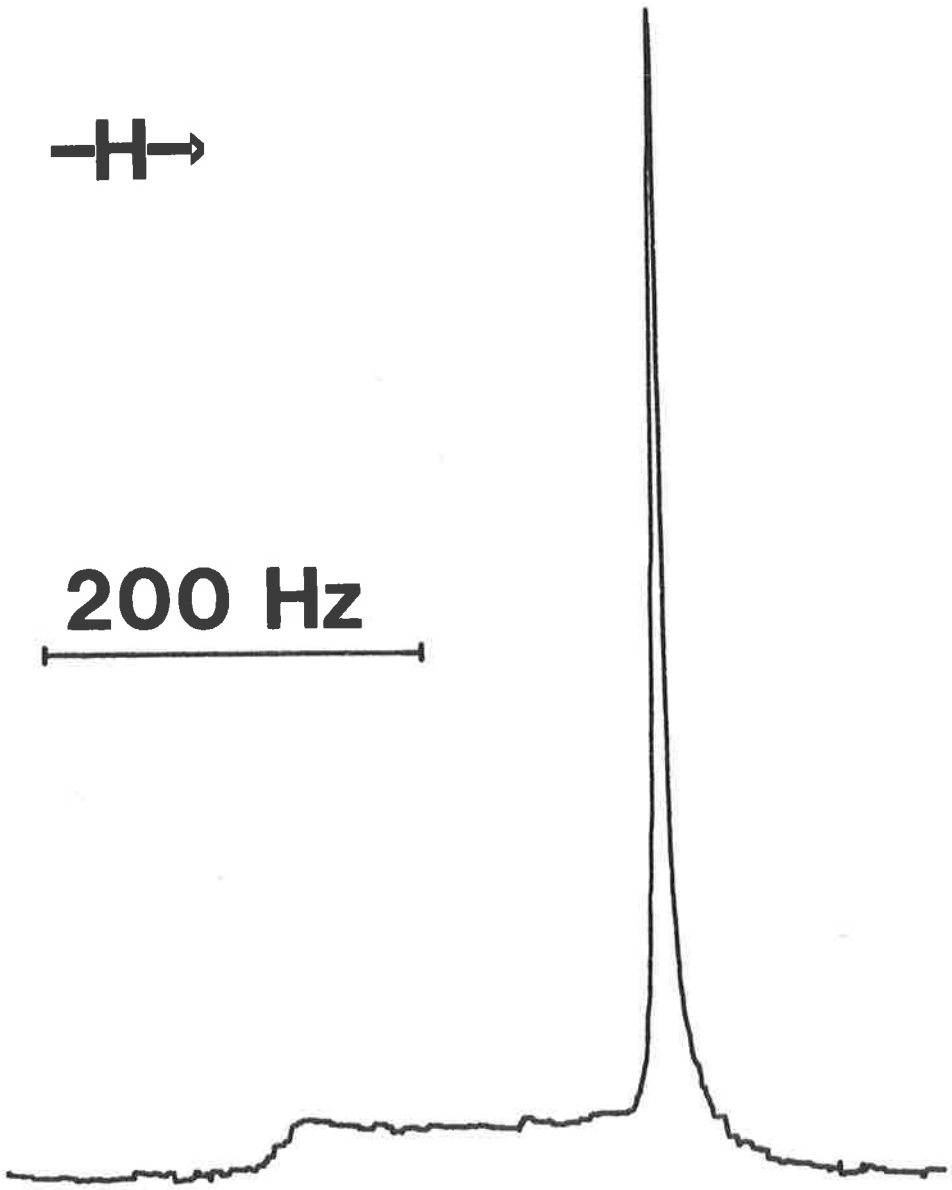

FIGURE 4.5 A ^{1}H decoupled ^{31}P (36.43 MHz) FT n.m.r. spectrum of a solution of $[Sc(dmmp)_6](ClO_4)_3$ (0.0657 mol dm^{-3}) and dmmp (0.3607 mol dm^{-3}) in CD_3CN diluent at 250 K.

TABLE 4.2 *Solution compositions for the* $[Sc(dmmp)_6]^{3+}$ *studies*

Solution	$[Sc(dmmp)_6^{3+}]$ mol dm^{-3}	[dmmp] mol dm^{-3}	$[CD_3CN]$ mol dm^{-3}	$[CD_3NO_2]$ mol dm^{-3}	C.N.[a]
(i)	0.134	0.887	13.4	-	6.1 ± 0.1
(ii)	0.0657	0.361	16.7	-	6.0 ± 0.1
(iii)	0.0308	0.203	17.6	-	6.0 ± 0.1
(iv)	0.0089	0.0487	18.2	-	5.9 ± 0.1
(v)	0.0060	0.0396	18.2	-	6.0 ± 0.2
(vi)	0.0014	0.0075	18.5	-	5.9 ± 0.1
(vii)	0.165	1.042	-	12.7	5.9 ± 0.2
(viii)	0.166	0.791	-	14.1	5.9 ± 0.1
(ix)	0.0783	0.373	-	16.3	5.8 ± 0.2
(x)	0.0377	0.238	-	16.7	6.0 ± 0.1
(xi)	0.0261	0.124	-	17.2	5.8 ± 0.2

a C.N. = number of coordinated dmmp molecules; determined by integration. The errors represent the maximum observed deviation from the mean value.

TABLE 4.3 *Kinetic parameters for ligand exchange on* $[Sc(dmmp)_6]^{3+}$

Diluent	k_1(300 K) s^{-1}	k_2(300 K) $dm^3\ mol^{-1}\ s^{-1}$	$\Delta H^{\ddagger}$ kJ mol^{-1}	$\Delta S^{\ddagger}$ J $K^{-1}\ mol^{-1}$
CD_3NO_2		13.3 ± 0.3	29.5 ± 0.6	-125 ± 2
CD_3CN	3.2 ± 0.06		42.8 ± 0.4	-92.4 ± 1.4
CD_3CN		14.8 ± 0.4	26.0 ± 0.9	-136 ± 3

All parameters determined from DATAFIT analysis.
The quoted errors represent one standard deviation.

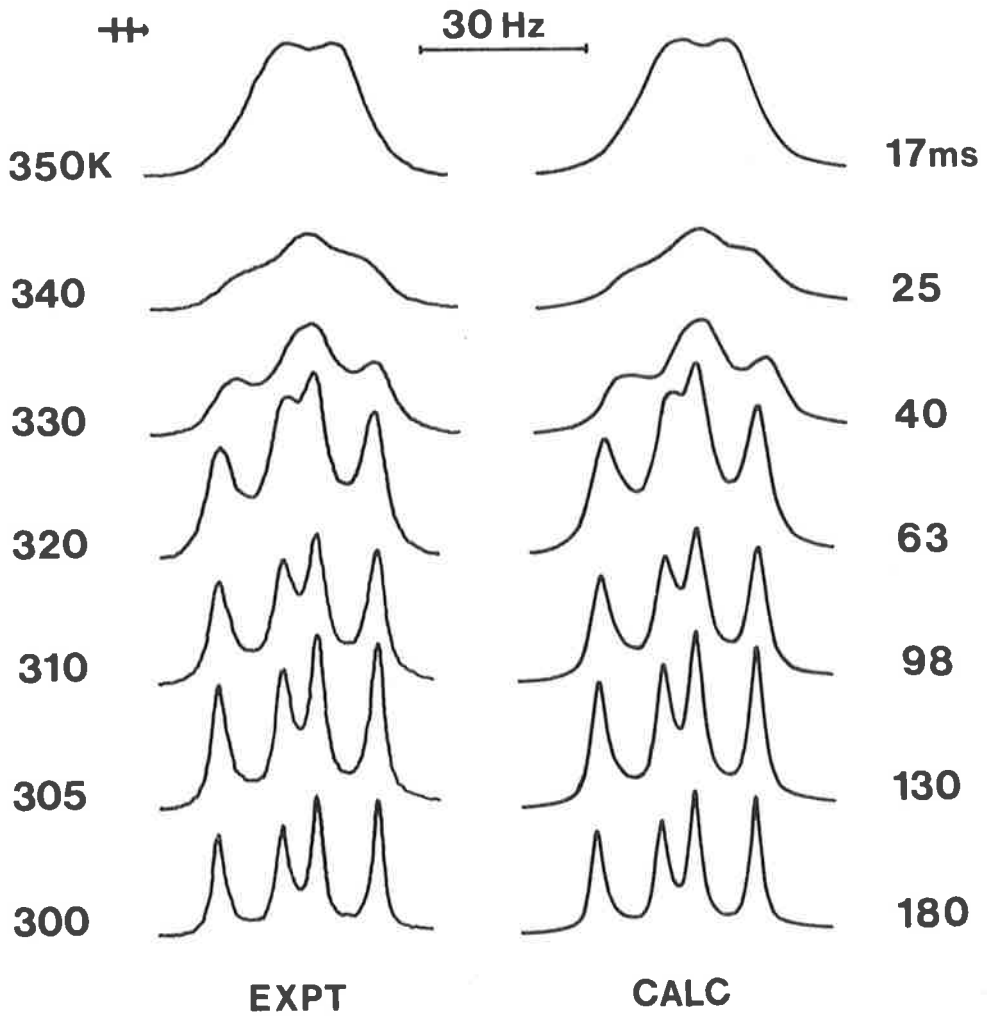

FIGURE 4.6 90 MHz ^{1}H spectra from a solution of $[Sc(dmmp)_6](ClO_4)_3$ (0.0308 mol dm^{-3}) and dmmp (0.203 mol dm^{-3}) in CD_3CN diluent. Experimental temperatures appear to the left of the Figure and the best fit τ_c values appear to the right. The doublet arising from coordinated dmmp appears downfield.

greater temperatures as the free dmmp concentration was decreased. In CD_3CN, slow exchange conditions applied at and below 280 K and 300 K respectively for solutions (i) and (vi) which represent the extremes of the concentration range, and the analogous temperatures were 275 K and 300 K respectively for the CD_3NO_2 solutions (vii) and (xi). Above these temperatures, a coalescence of the doublet signals was observed consistent with the occurrence of ligand exchange on $[Sc(dmmp)_6]^{3+}$ (Figure 4.6).

A rapid assessment of the kinetic results, obtained from ^1H n.m.r. lineshape analysis, may be made from Figure 4.7. This Figure shows plots of exchange rate constants, k_{ex}, (interpolated from plots of $\ln(\tau_c T)$ versus $1/T$, which were reasonably linear over the experimental temperature range) versus [dmmp]. It is apparent from Figure 4.7 that in CD_3CN $k_{ex} = k_1 + k_2[dmmp]$ whereas in CD_3NO_2, $k_{ex} = k_2[dmmp]$ (the apparent small positive intercept at [dmmp] = 0 observed in CD_3NO_2 does not differ significantly from zero). The kinetic parameters characterizing the $[Sc(dmmp)_6]^{3+}$ system in both diluents were obtained using DATAFIT and are presented in Table 4.3. The k_1 term observed for $[Sc(dmmp)_6]^{3+}$ in CD_3CN can be attributed to a dissociative ligand exchange process. However, in contrast to $[Sc(tmp)_6]^{3+}$/tmp/CD_3CN, a second ligand exchange pathway, characterized by k_2, becomes competitive. The slightly smaller size and anticipated greater electron donating power (one less electron withdrawing oxygen atom) of dmmp relative to tmp might be expected to cause the formation of a dissociative transition state and a transition state involving the incoming ligand with $[Sc(dmmp)_6]^{3+}$ to be respectively less and more favoured than the analogous transition states arising from $[Sc(tmp)_6]^{3+}$. The k_2 terms in CD_3CN and CD_3NO_2 may, in principle,

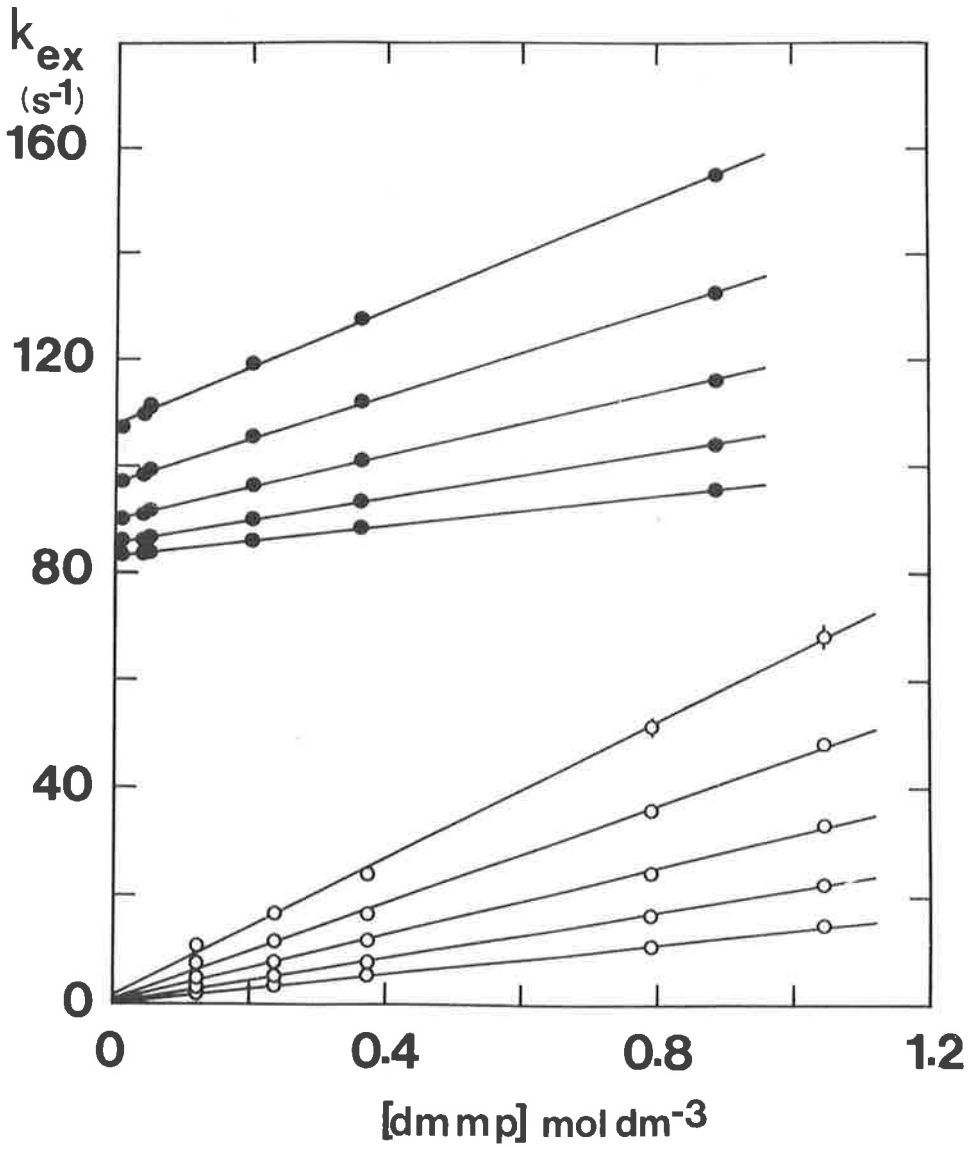

FIGURE 4.7 Plots of interpolated k_{ex} values for ligand exchange on $[Sc(dmmp)_6]^{3+}$ against [dmmp]. The upper data set (●) was obtained in CD_3CN diluent while the lower data set (○) refers to solutions in CD_3NO_2. The temperatures range in 10 K intervals from 340 K (upper line in each set) to 300 K (lower line). The lines represent linear regression lines.

Note: The upper data set has been translated up the k_{ex} axis by 80 s^{-1}.

arise from an I_D or A mechanism as described in the preceding Section. Limiting condition (a) would need to hold in both diluents for the I_D mechanism to be operative in both diluents. This seems highly unlikely to be the case, especially in CD_3CN solutions, because k_2 (= $k_{int}K$ under condition (a)) is about five times larger than k_1 in the same diluent at 300 K. The major contribution to the energetics in both the D and I_D mechanism is, after all, the breaking of a metal-ligand bond and so k_2 should be $\lesssim k_1$ if an I_D mechanism is operative in CD_3CN. Furthermore, from Figure 4.7 there is no indication of k_{ex} reaching a limiting value at high [dmmp]. The existence of a two term rate law for dmmp exchange indicates that the k_1 and k_2 transition states possess similar free energies and, like the tmp system, a significant component of these free energies arises from interactions in the second coordination sphere.

4.4 The scandium(III)/hexamethylphosphoramide system

Hexamethylphosphoramide is a particularly powerful base by a number of standards (e.g. Gutmann donor number = 38.8) and this feature coupled with its molecular bulk makes it an unusual ligand.

Since 1975, when the syntheses for $[Sc(hmpa)_4](ClO_4)_3$ and $[Sc(hmpa)_6](ClO_4)_3$ were expounded by Scholer and Merbach[106], there have been no reports of the solution behaviour of these hmpa complexes. Attempts to prepare either of these complexes according to the literature procedures did not yield the expected complex stoichiometries. Instead, apparently non-stoichiometric hmpa complexes were obtained. Infra-red spectra of $[Sc(hmpa)_{4.32}](ClO_4)_3$ and $[Sc(hmpa)_{4.97}](ClO_4)_3$ (Appendix 1) showed signals assignable to the characteristic absorption frequencies of both ionic and unidentate coordinated perchlorate[106] and

no signals due to water. Each complex was soluble in CD_2Cl_2 and CD_3CN thus facilitating the observation, by ^1H and ^{31}P n.m.r., of low temperature solution properties.

90 MHz ^1H n.m.r. spectra of $[Sc(hmpa)_{4.97}](ClO_4)_3$ in CD_2Cl_2 and CD_3CN at temperatures below 270 K exhibited at least three overlapping doublets. Corresponding 36.43 MHz ^{31}P (with ^1H broad-band decoupling) n.m.r. spectra were more informative. Figure 4.8 shows two ^{31}P resonances attributable to coordinated hmpa and one resonance due to free hmpa. In order to be consistent with the observed solid state stoichiometry the major coordinated hmpa signal is assigned to $[Sc(hmpa)_4]^{3+}$ and the minor signal to $[Sc(hmpa)_5]^{3+}$. Solutions of $[Sc(hmpa)_{4.32}](ClO_4)_3$ in CD_2Cl_2 and CD_3CN showed ^1H and ^{31}P n.m.r. signals consistent with the assignments above. It should be noted that coupling between ^{31}P and ^{45}Sc is not evident for either coordinated hmpa resonance and that the resonance for $[Sc(hmpa)_5]^{3+}$ appears to be a singlet (the five-coordinate complex should have magnetically inequivalent sites, namely for axial and equatorial environments).

The equilibrium between $[Sc(hmpa)_4]^{3+}$ and $[Sc(hmpa)_5]^{3+}$ was such that the former species became even more favoured at higher temperatures. At room temperature, slow intermolecular exchange between free and coordinated sites was evidenced. When extra free hmpa was added, ^1H n.m.r. spectra suggested that the equilibrium was displaced in favour of $[Sc(hmpa)_5]^{3+}$ but no new signals (e.g. for $[Sc(hmpa)_6]^{3+}$) seemed to appear. Lineshape analysis for this system was complicated due to the presence of more than one scandium(III) species and the temperature dependence of the relative populations. Hence, no attempt was made to obtain kinetic parameters. (However, the hmpa exchange processes occurring at the scandium(III) centre are slow

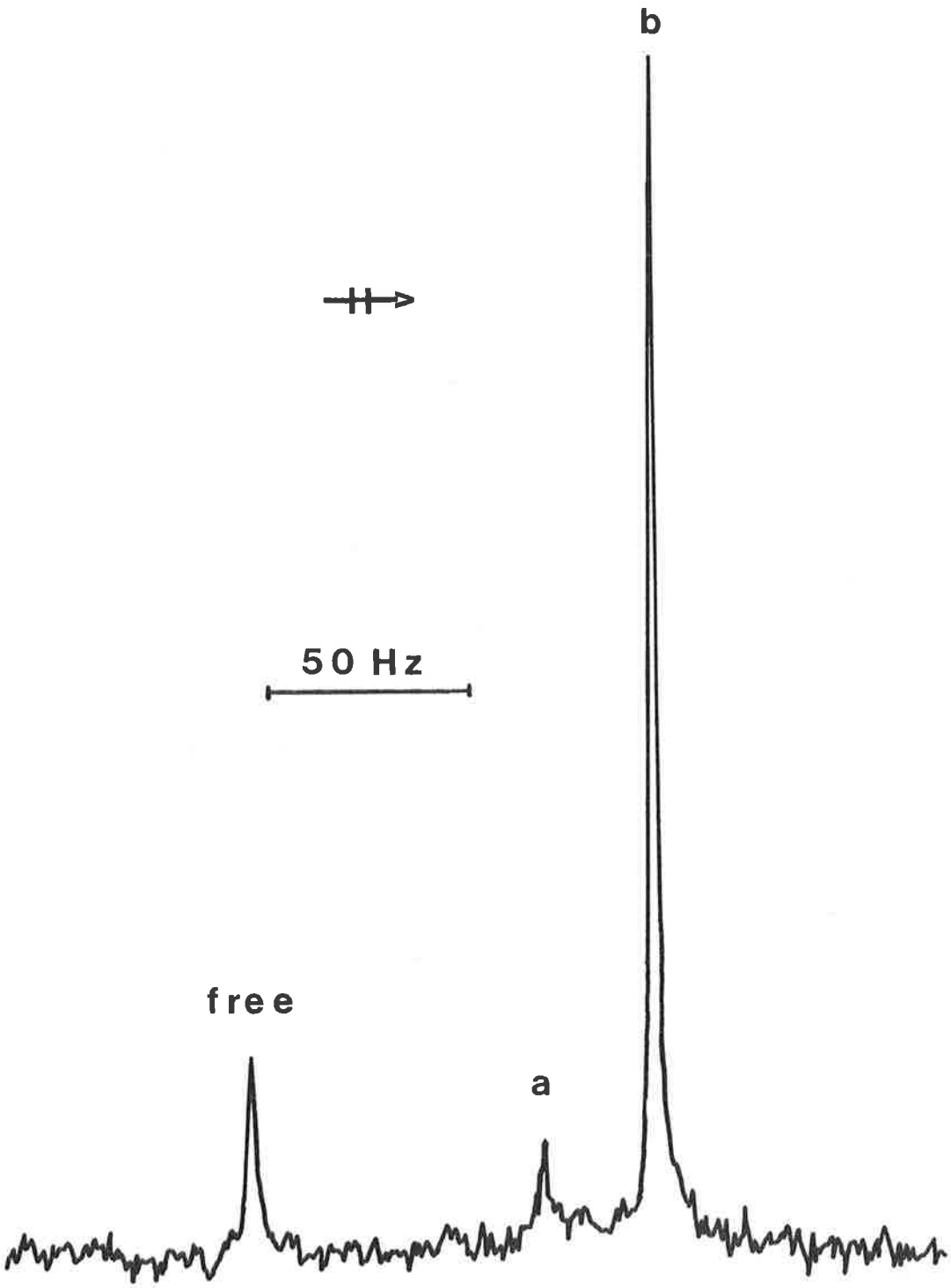

FIGURE 4.8 ^{1}H decoupled ^{31}P FT n.m.r. spectrum of a solution of $[Sc(hmpa)_{4.97}](ClO_4)_3$ (44 mg/ml) in CD_2Cl_2 at 206 K. Singlet (a) is assigned to $[Sc(hmpa)_5]^{3+}$ and singlet (b) is assigned to $[Sc(hmpa)_4]^{3+}$.

in relation to their tmp and dmmp counterparts.) A similar solution behaviour has recently been observed for gallium(III), indium(III)[107] and thorium(IV)[108] analogues. In contrast, aluminium(III)[27] and beryllium(II)[23] have only one complex species in solution, presumably due to the greater steric requirements for these two smaller ions.

4.5 Dimethylsulphoxide and 4,4'-ditolylsulphoxide complexes of scandium(III)

The complex $[Sc(dmso)_6](ClO_4)_3$ has been mentioned in several papers in the literature[109,110] but, like the new air stable complex $[Sc(tso)_6](ClO_4)_3$, nothing has been reported of its solution chemistry. ^1H n.m.r. spectra of solutions of $[Sc(dmso)_6](ClO_4)_3$ and dmso (covering a wide [dmso] range) in CD_3NO_2 ($[Sc(dmso)_6](ClO_4)_3$ was insoluble in CD_2Cl_2 and CD_3CN) exhibited a single peak over the entire liquid temperature range of the diluent. The singlets for coordinated and free dmso, under slow exchange conditions, should be well separated (>10 Hz) on the basis of shift measurements of complex and ligand in isolation. This expectation requires the dmso exchange rate constant to be greater than 40 s^{-1} at the lowest temperature examined (245 K).

Similar observations were made with the tso complex in tso/CD_2Cl_2 mixtures. Even at 180 K the 90 MHz ^1H and 22.625 MHz ^{13}C n.m.r. spectra of these solutions were consistent with the rate of tso exchange being outside the n.m.r. time scale. As the slow exchange limit was not reached it was not possible to assign a value of n in the species $[Sc(dmso)_n]^{3+}$ and $[Sc(tso)_n]^{3+}$. However, a high (i.e. >6) ground state or transition state coordination number with the bulky tso ligand is not expected.

4.6 Exchange of 1,1,3,3-tetramethylurea on $[Sc(tmu)_6]^{3+}$

Tetramethylurea undergoes rapid internal rotation at room temperature. The barrier to rotation about the C(central) - N bonds has been estimated to be 25.5 kJ mol^{-1} [111] with an approximate n.m.r. (100 MHz) signal coalescence temperature of 123 K. Ureas, in general, have a lower barrier to rotation than amides. This phenomenon has been explained[112,113] in terms of competitive conjugation; steric effects which prevent coplanarity of the carbonyl group with both nitrogen atoms and their substituents; and conjugation effects in the transition state. The energetics of internal rotation, however, are not as yet well understood. In a crystal structure determination of dichlorobis(tetramethylthiourea)copper(II)[114] the coordinated tmtu molecules were found to be distorted from planarity (11 - 32° about C(central) - N bond) due to methyl-methyl repulsions. Based on this information steric interactions between methyl groups in the first coordination sphere could be important when tmu is coordinated to a metal ion and these interactions may result in a retardation of the rate of internal rotation. Indeed, an increase in rotational barrier height has been observed upon coordination to UO_2^{2+} [115] and the increase was ascribed, in part, to steric restrictions. However, the effect of the metal on the electron distribution in tmu must also be considered[115].

$[Sc(tmu)_6](ClO_4)_3$ was easily isolated as an air stable crystalline salt. It was moderately soluble in CD_3CN and CD_3NO_2 and virtually insoluble in CD_2Cl_2. Solutions of $[Sc(tmu)_6](ClO_4)_3$ and tmu in CD_3CN or CD_3NO_2 exhibited a ^1H resonance arising from coordinated ligand downfield from that of the free ligand under conditions of slow exchange. Comparisons of the integrated areas of

the two resonances for the nine solutions whose compositions are given in Table 4.4 showed that $[Sc(tmu)_6]^{3+}$ was the predominant scandium(III) species. Singlet resonances were observed for both coordinated and free tmu (the separation varied somewhat with temperature; for example, 17.1 Hz (250 K) - 17.9 Hz (290 K) in solution (ii) and 5.9 Hz (250 K) - 7.9 Hz (310 K) in solution (vii)) in the region of the freezing point of the solutions. This observation is consistent with rotation about the C-N bonds in tmu being in the fast exchange limit of the n.m.r. time scale at these temperatures (225 K for CD_3CN, 245 K for CD_3NO_2).

From the kinetic data in Table 4.4, rate constants at 350 K for tmu exchange on $[Sc(tmu)_6]^{3+}$ in CD_3NO_2 (solutions (i) - (vi)) show only a small variation with [tmu]. In fact, k_{ex} exhibits a 1.8-fold increase over the 63-fold decrease in [tmu]. Hence, the rate of the dominant ligand exchange process is virtually independent of free ligand concentration and this is characteristic of a dissociative exchange mechanism. The rate determining step would be the formation of the reactive intermediate $[Sc(tmu)_5]^{3+}$. The 1.8-fold variation with k_{ex} with [tmu] may, as previously mentioned, reflect to some extent minor changes in the immediate environment of $[Sc(tmu)_6]^{3+}$ as the concentration of the exchanging species is altered. If the postulated intermediate, $[Sc(tmu)_5]^{3+}$ is insufficiently stable for a short, but independent, existence the observed exchange kinetics could be alternatively explained by the I_D mechanism. However, to reproduce the observed kinetics practically all of the $[Sc(tmu)_6]^{3+}$ units would need to exist in encounter complex form in solutions (i) - (vi) implying a high degree of preferential occupation of the second coordination sphere by tmu. On balance, therefore, it seems probable that a D mechanism is operating.

TABLE 4.4 *Solution compositions and kinetic parameters for tmu exchange on* $[Sc(tmu)_6]^{3+}$

Solution	$[Sc(tmu)_6^{3+}]$ mol dm^{-3}	[tmu] mol dm^{-3}	$[CD_3NO_2]$ mol dm^{-3}	$[CD_3CN]$ mol dm^{-3}	C.N.[a]	k_{ex}(350 K)[b,d] s^{-1}	$\Delta H^{\ddagger}$[c,d] kJ mol^{-1}	$\Delta S^{\ddagger}$[c,d] J K^{-1} mol^{-1}
(i)	0.124	0.682	14.9	-	5.9 ± 0.1	34.2 ± 1.5	99.1 ± 1.0	66.2 ± 2.8
(ii)	0.0724	0.535	15.7	-	6.0 ± 0.2	33.5 ± 1.6	101 ± 1	70.7 ± 3.1
(iii)	0.0534	0.294	15.8	-	5.9 ± 0.1	35.6 ± 1.5	92.7 ± 1.0	48.4 ± 2.8
(iv)	0.0123	0.0907	17.6	-	6.0 ± 0.1	45.5 ± 2.8	105 ± 2	84.7 ± 4.7
(v)	0.00249	0.0184	17.6	-	6.1 ± 0.1	57.4 ± 3.1	94.0 ± 1.4	56.1 ± 4.1
(vi)	0.00145	0.0108	17.7	-	5.8 ± 0.2	55.9 ± 5.7	91.2 ± 2.3	47.8 ± 6.7
(vii)	0.0385	0.266	-	17.3	5.9 ± 0.2	53.1 ± 1.2	80.5 ± 0.7	16.7 ± 2.2
(viii)	0.0138	0.0732	-	17.4	5.8 ± 0.2	63.1 ± 3.6	70.7 ± 1.6	-9.8 ± 4.8
(ix)	0.00742	0.0513	-	17.4	5.8 ± 0.2	64.1 ± 3.0	68.6 ± 1.3	-15.7 ± 3.8

a C.N. = coordination number of scandium(III) with respect to tmu. The errors represent the maximum observed deviation from the mean value.

b k_{ex}(350 K) interpolated from the Eyring plots.

c $\Delta H^{\ddagger}$ and $\Delta S^{\ddagger}$ values determined from the Eyring plots.

d The errors represent one standard deviation.

Studies of the tmu exchange process in CD_3CN diluent were confined to a relatively small concentration range (solutions (vii) - (ix)) as a consequence of the limited solubility of $[Sc(tmu)_6](ClO_4)_3$ in CD_3CN and the appearance of small extraneous ^1H resonances in the region of interest at low concentration and temperature. The extraneous resonances could be due, perhaps, to scandium(III) species of different coordination number or coordination of acetonitrile to scandium(III). In solution (ix) the extraneous signal area was less than two percent of the main signal of $[Sc(tmu)_6]^{3+}$. None the less, the dominant path for ligand exchange appears to be independent of [tmu] and this behaviour is consistent with a D mechanism. The systematic variation of k_{ex} in solutions (vii) - (ix) is presumably related to the environmental changes mentioned above.

A comparison of $\Delta H^{\ddagger}$ and $\Delta S^{\ddagger}$ values for solutions (i) - (ix) suggests that a major environmental modification has occurred on going from CD_3NO_2 as diluent to CD_3CN whilst still maintaining a dissociative mechanism over the concentration ranges in Table 4.4 (cf. $[Mg(dmf)_6]^{2+}$ system). Molecular models suggest that in comparison to $[ScS_6]^{3+}$ where S = tmp or dmmp, $[Sc(tmu)_6]^{3+}$ is more sterically crowded. As discussed in Section 4.2, a significant destabilization of $[Sc(tmu)_7]^{3+}$ by steric interactions could be responsible for the dominance of the dissociative type mechanism despite the major environmental modifications above.

4.7 The 1,3-dimethylurea complex of scandium(III)

A n.m.r. study of dmu in aqueous solution has been reported. Under the experimental conditions of the investigation[116] there was no evidence for the occurrence of slow internal rotation for the urea molecule. Dmu was only moderately soluble in CD_3CN (<20 mg/ml at

260 K) and ^1H n.m.r. spectra of dmu in CD_3CN (with or without a trace of pyridine[117]) in the temperature range 230 - 320 K were consistent with rapid internal rotation. Nevertheless, three distinct 'rotamers' are possible by virtue of rotation about the two equivalent C(central) - N bonds.

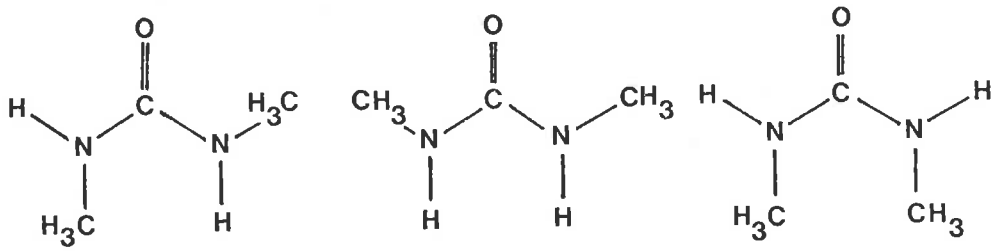

I II III

The dmu complex of scandium(III) which was obtained through the usual preparative procedure analysed as $[Sc(dmu)_6](ClO_4)_3 \cdot EtOH$. When this compound was recrystallized from $CH_3CN/dmu/CH_2Cl_2$ the product obtained was $[Sc(dmu)_6](ClO_4)_3 \cdot CH_2Cl_2$. The solution kinetic properties of the two complexes were found to be identical, strongly suggesting that neither EtOH nor CH_2Cl_2 is directly coordinated to scandium(III) in solution. Furthermore, EtOH or CH_2Cl_2 was easily removed from the crystal lattice by subjecting the appropriate solid to a rarefied atmosphere for several hours. This behaviour suggests EtOH and CH_2Cl_2 are not within bonding distance of scandium(III) in the solid state. The two complexes were only mildly hygroscopic and were more soluble in CD_3CN than was dmu.

^1H n.m.r. spectra of $[Sc(dmu)_6](ClO_4)_3 \cdot CH_2Cl_2$ (or EtOH) in CD_3CN at temperatures below about 250 K indicated that slow internal

rotation for coordinated dmu was occurring. The N-methyl region appeared to consist of two overlapping doublets (separation ca. 3 Hz) whilst the N-H region was composed of two major quartets of approximately equal area and a minor quartet resonance between them. Decoupling of the N-CH_3 protons from the N-H protons reduced the quartets to singlets and more clearly exposed the minor resonance. (The relative areas were identical with or without homonuclear decoupling.) The coalescence of the N-CH_3 decoupled N-H resonances with increase in temperature is depicted in Figure 4.9. Since there appears to be only three peaks, the two major ones being of equal area, the implications are that the two major peaks arise from rotamer I and that the minor one is due to II or III. The assignment of the minor peak to either II or III from its observed chemical shift is, however, equivocal. Intuitively, II should generate more steric crowding near the metal centre than III when coordinated. Nevertheless, crystallographic studies[118] of the coordination of N-methylurea and dmu to cobalt(II) and manganese(II) respectively have shown that the methyl groups are oriented towards the metal centre.

It is interesting to note that the N-H signals of coordinated dmu were narrower than the N-H signal of free dmu at any particular temperature. The presence of the metal seems to have a profound effect upon the nuclear relaxation times of the quadrupolar ^{14}N nuclei. (N-H protons coupled to ^{14}N nuclei in coordinated amides can also display this behaviour.)

In this rotational exchange system there are evidently three N-H magnetic environments giving rise to the coalescence phenomenon in Figure 4.9. The two sites in isomer I can only exchange through the third site in isomer II or III. Because of a number of difficulties,

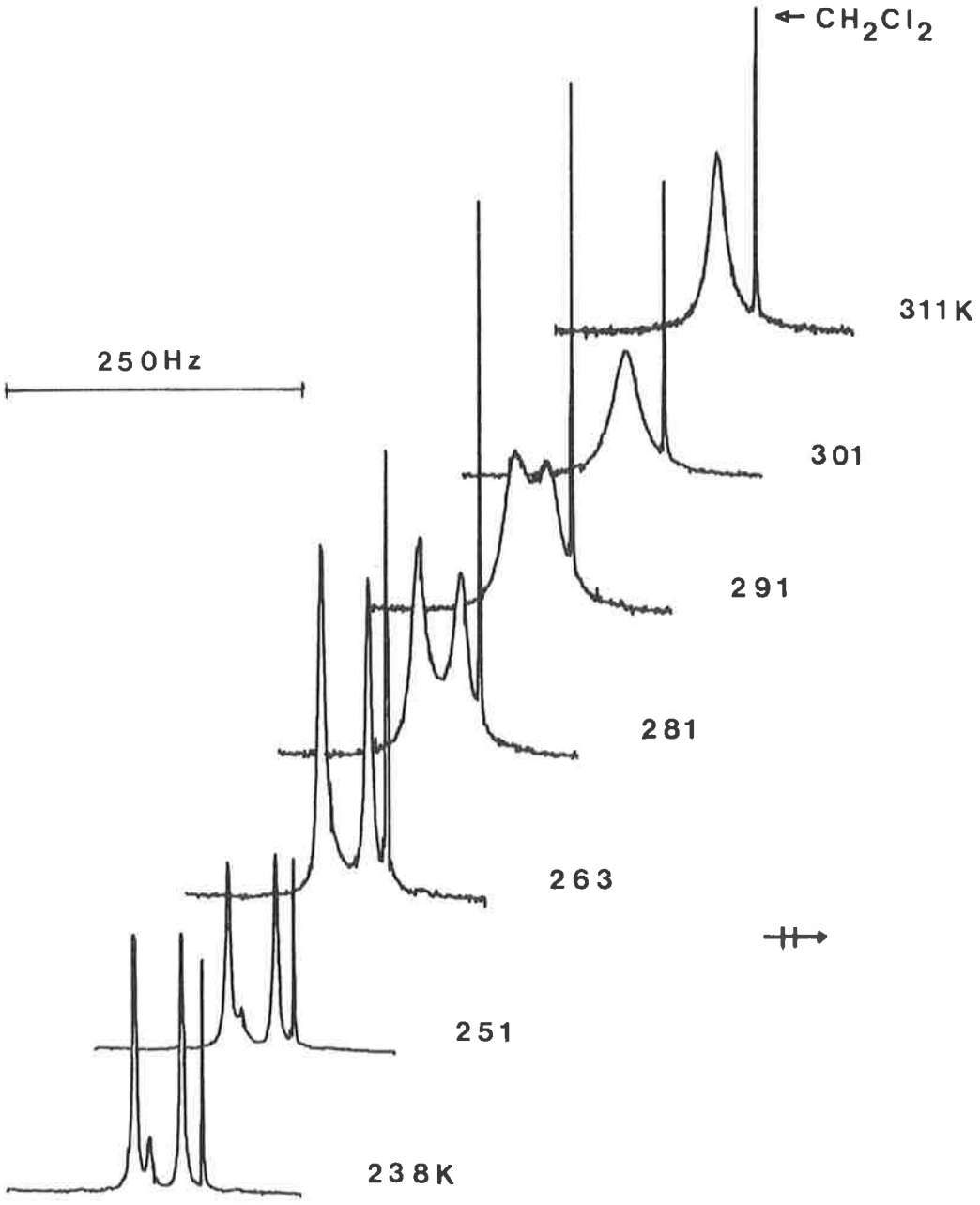

FIGURE 4.9 N-H ($N-CH_3$ decoupled) ^1H n.m.r. lineshapes for a solution of $[Sc(dmu)_6](ClO_4)_3 \cdot CH_2Cl_2$ (110 mg/ml) in CD_3CN. The experimental temperatures appear to the right of the Figure.

for example, the unfavourable temperature dependence of the N-H linewidths (increasing with increase in temperature), chemical shifts and populations, quantitative rate data were not obtained. k_{ex} (290 K) $\sim$ 120 s^{-1} from an approximate three site lineshape analysis using estimated N-H linewidths at 290 K. Internal rotation for coordinated dmu is evidently much slower than for uncoordinated dmu in CD_3CN. In view of the comments and observations made with the tmu system it is clear that, although it may be important, steric interaction between coordinated urea molecules[115] is probably not the major determinant of the energy barrier to internal rotation for coordinated tmu and dmu. Otherwise, internal rotation for coordinated tmu in CD_3CN should be detectable also. It is conceivable that differences in the extent of specific interactions (dipole-dipole and hydrogen bonding[119-121]) between CD_3CN and coordinated dmu compared to the extent of those between CD_3CN and free dmu are important in determining the relative free energies of ground and transition states for coordinated and free dmu. The making or breaking of hydrogen bonds will accompany the rotational process and a significant entropy of activation may be observed as well[119]. In the case of tmu, where the extent of hydrogen bonding is negligible, specific interactions with diluent probably only affect the energetics marginally. Electronic effects due to the metal are probably significant for coordinated tmu and dmu but it is difficult to assess their energetic contribution for each ligand.

Figure 4.10 shows N-CH_3 decoupled ^1H n.m.r. spectra of the N-H region of a sample which consisted of $[Sc(dmu)_6](ClO_4)_3 \cdot EtOH$ (0.025 mol dm^{-3}) and dmu (0.261 mol dm^{-3}) in CD_3CN. There was some precipitation of dmu at the lower temperatures. Three resonances

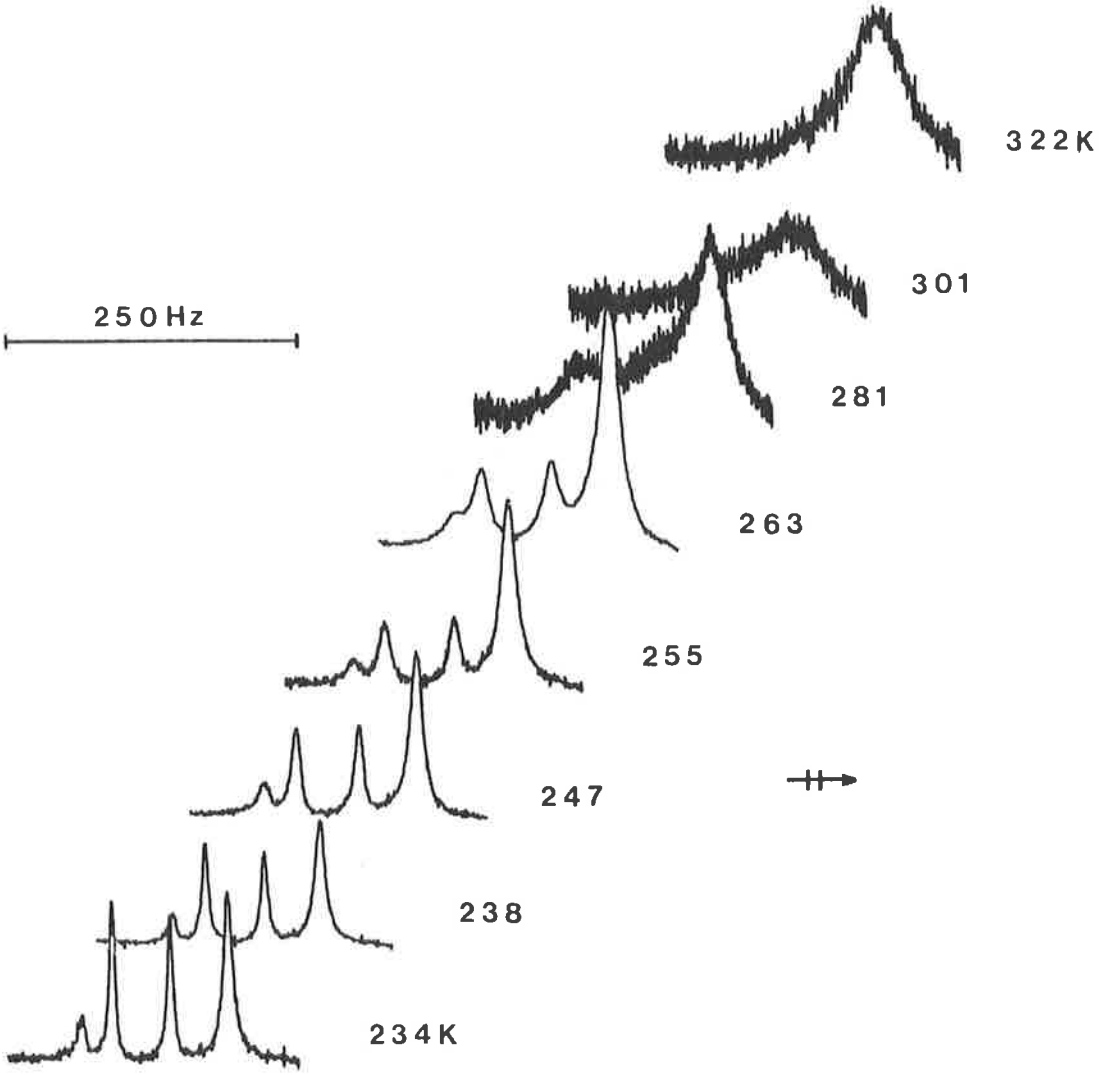

FIGURE 4.10 N-H (N-CH_3 decoupled) ^1H n.m.r. lineshapes for a solution of $[Sc(dmu)_6](ClO_4)_3 \cdot EtOH$ (23 mg/ml) and dmu (23 mg/ml) in CD_3CN. The experimental temperatures appear to the right of the Figure.

ascribed to coordinated dmu ($[Sc(dmu)_6]^{3+}$ is the most likely scandium(III) species) appear downfield from the singlet resonance of free dmu at 234 K. The minor coordinated dmu peak is now, however, further downfield and comparatively larger than before (cf. Figure 4.9). A shift of this magnitude caused simply by the addition of free dmu is unlikely and therefore the peak is probably due to the other isomer not observable in Figure 4.9. If rapid rotation occurs in the free ligand during the intermolecular ligand exchange process and the coordinating abilities of I, II and III are similar, then the observed relative proportions of dmu rotamers in the coordinated environment at 234 K are a measure of the relative populations of I, II and III outside the first coordination sphere. As may be discerned from Figure 4.10, there exists a complicated intermolecular and rotational exchange coalescence pattern and so kinetic data were unobtainable. Both exchange processes are within the ^1H n.m.r. time scale at 90 MHz. Intermolecular exchange of dmu on scandium(III), under the experimental conditions, also appears to be more facile than exchange of tmu.

4.8 N,N-dimethylformamide, N,N-diethylformamide and N,N-di-n-butylformamide complexes of scandium(III)

Of the three complexes, $[Sc(dmf)_6](ClO_4)_3$ [110], $[Sc(def)_6](ClO_4)_3$ and $[Sc(dbf)_6](ClO_4)_3$, the first was very hygroscopic, the second was moderately hygroscopic and the last was only mildly moisture sensitive. All were soluble in CD_2Cl_2 and CD_3CN. Somewhat surprisingly, as for the sulphoxide complexes in Section 4.5, ligand exchange on scandium(III) was in the fast exchange limit over the liquid temperature range of CD_2Cl_2 and CD_3CN. The N-methylformamide complex[122] also displays this behaviour in CH_3CN/nmf.

4.9 Exchange of N-methylacetamide on $[Sc(nma)_6]^{3+}$

For free nma in CD_3CN at 300 K the *trans* : *cis* isomer proportion was approximately 97 : 3. On the other hand, ^1H n.m.r. (90 MHz) spectra of a CD_3CN solution of the air-stable complex $[Sc(nma)_6](ClO_4)_3$ (Figure 4.11) showed that the amount of coordinated *cis* isomer varied from ∿7% at 250 K to ∿9.5% at 350 K.

^1H spectra of $[Sc(nma)_6](ClO_4)_3$/nma in CD_3CN (Table 4.5) displayed coordinated ligand resonances downfield from the resonances of free ligand under slow exchange conditions ($T \lesssim 240$ K). Integration of these resonances indicated that $[Sc(nma)_6]^{3+}$ was the outstanding scandium(III) species present. (Rotation about the C-N bond in coordinated and free nma was in the slow exchange limit in the temperature range of this study.) At 225 K the chemical shift separation between coordinated and free *trans* nma N-methyl resonances varied from 6.8 Hz for solution (i) to 6.2 Hz for solution (v). For the analogous acetyl shift separation (18.1 Hz) there was little variation with concentration. The temperature dependence of this separation was only slight (ca. 0.1 Hz increase per 5 K). Because both coordinated and free nma exist primarily in the *trans* configuration, the probability of direct exchange between *cis* isomers in the two environments will be relatively low compared to the other ligand exchange probabilities. Coalescence of the *cis* ligand resonances occurs as a consequence of both direct and indirect exchange but since this coalescence pattern was superimposed upon that for the *trans* ligand (which was much greater in amplitude) it was not practicable to obtain accurate kinetic parameters for the *cis* ligand exchange process. Instead, the superimposed *cis* coalescence lineshape was simply subtracted from the *trans* coalescence lineshape

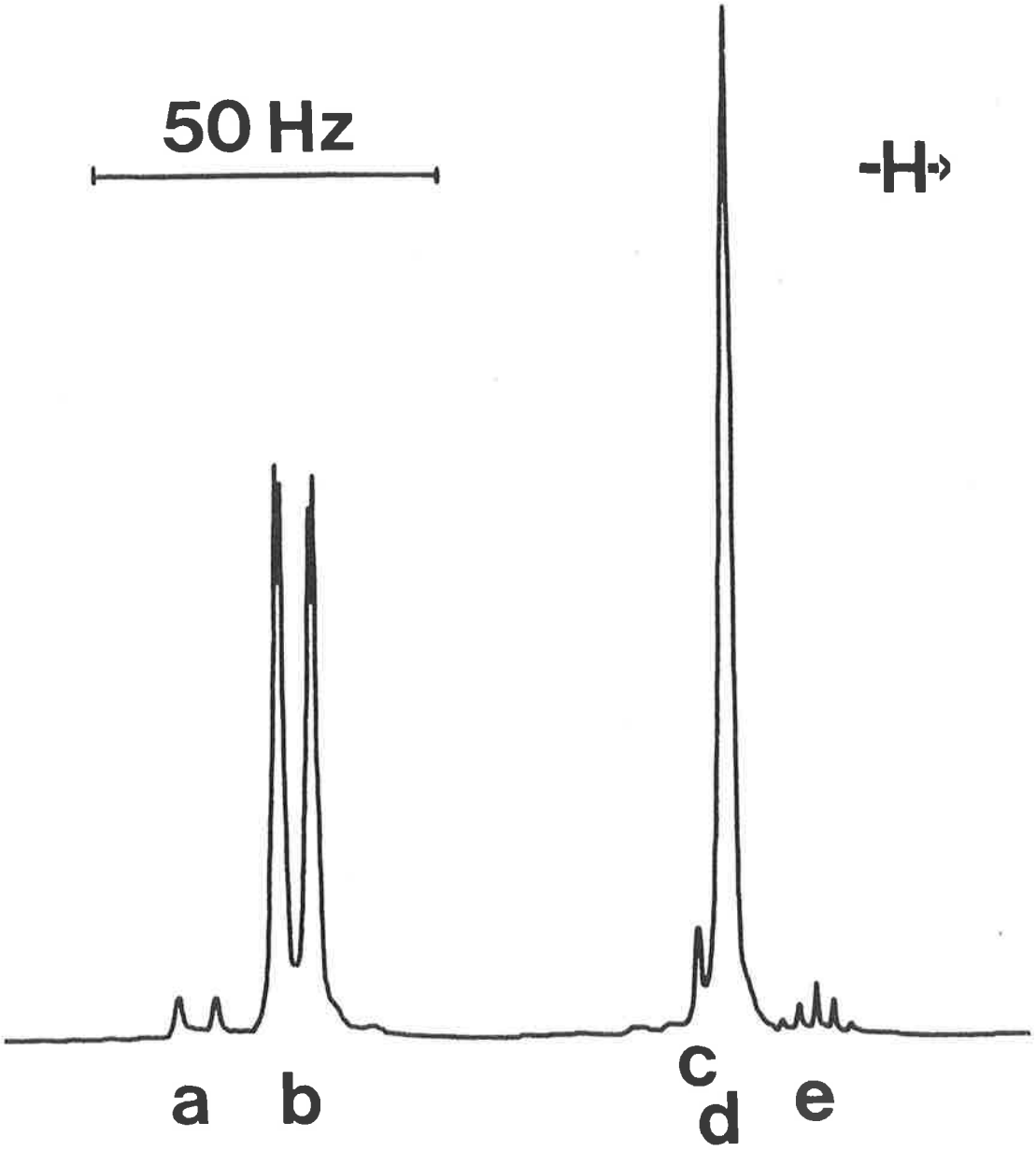

FIGURE 4.11 A ^{1}H n.m.r. (90 MHz) spectrum of $[Sc(nma)_6]^{3+}$ in CD_3CN solution at 302 K. The N-CH_3 resonances of *cis* and *trans* nma are labelled (a) and (b), the acetyl resonances (c) and (d) and the proton impurity resonance (e) respectively. For *trans* and *cis* nma $J(NC\underline{H}_3 - N\underline{H})$ = 4.9 and 5.3 Hz, and $J(NC\underline{H}_3 - C\underline{H}_3)$ = 0.7 and <0.4 Hz respectively.

TABLE 4.5 *Solution compositions and kinetic parameters for nma exchange on* $[Sc(nma)_6]^{3+}$

Solution	$[Sc(nma)_6^{3+}]$ mol dm^{-3}	[nma] mol dm^{-3}	$[CD_3CN]$ mol dm^{-3}	C.N.[a]
(i)	0.0634	0.403	17.6	5.8 ± 0.2
(ii)	0.0882	0.391	17.3	5.9 ± 0.2
(iii)	0.0403	0.207	17.9	5.9 ± 0.2
(iv)	0.0134	0.0883	18.1	5.9 ± 0.2
(v)	0.0039	0.0260	18.3	5.8 ± 0.2

	k_1(300 K)[b] s^{-1}	k_2(300 K)[b] dm^3 mol^{-1} s^{-1}	$\Delta H^{\ddagger}$[b] kJ mol^{-1}	$\Delta S^{\ddagger}$[b] J K^{-1} mol^{-1}
	87 ± 6	-	27.3 ± 0.9	-117 ± 4
	-	419 ± 38	26.1 ± 1.2	-108 ± 5

a C.N. = coordination number of scandium(III) as determined by integration. The errors represent the maximum observed deviation from the mean value.

b Kinetic parameters evaluated from DATAFIT analysis. The errors quoted represent one standard deviation.

(LINSHP interactive program). Kinetic parameters for the exchange of *trans* ligands were derived from complete lineshape analysis (ignoring minor couplings) of the coalescence of either the N-methyl resonances (solutions (ii) - (v)) or acetyl resonances (solution (i)) arising from coordinated and free *trans* nma. Figure 4.12 shows semilogarithmic plots of $\tau_c T$ versus 1/T whilst Figure 4.13 reveals that the observed rate constants (which refer predominantly to the direct exchange of *trans* nma) characterize a two term rate law.

$$\text{i.e. exchange rate} = 6(k_1 + k_2[\text{nma}])[\text{Sc(nma)}_6^{3+}]$$

Activation enthalpies and entropies for this system were then computed by DATAFIT utilizing Equation 2.17. The k_1 term for nma exchange is assigned to a D mechanism whilst either an I_D or, more probably, an A mechanism is responsible for the k_2 term.

In CD_3NO_2 diluent the coordinated and free nma resonances were found to be just coalesced at 250 K (the lower temperature limit) and the fast exchange limit applied at higher temperatures. Hence, it was not practicable to acquire accurate kinetic parameters.

4.10 Exchange of N,N-dimethylacetamide on $[Sc(dma)_6]^{3+}$

The mildly hygroscopic perchlorate salt $[Sc(dma)_6](ClO_4)_3$ [123] was soluble in CD_3CN and CD_3NO_2 but insoluble in CD_2Cl_2. As per normal, solutions of $[Sc(dma)_6](ClO_4)_3$ and dma in CD_3CN or CD_3NO_2 exhibited ^1H resonances arising from coordinated ligands downfield from those of the free ligands under conditions of slow exchange. $[Sc(dma)_6]^{3+}$ was found to be the vastly predominant scandium(III) species in all of the solutions studied (Table 4.6). In CD_3NO_2 solutions ((i) - (v)) quantitative determinations of the species in

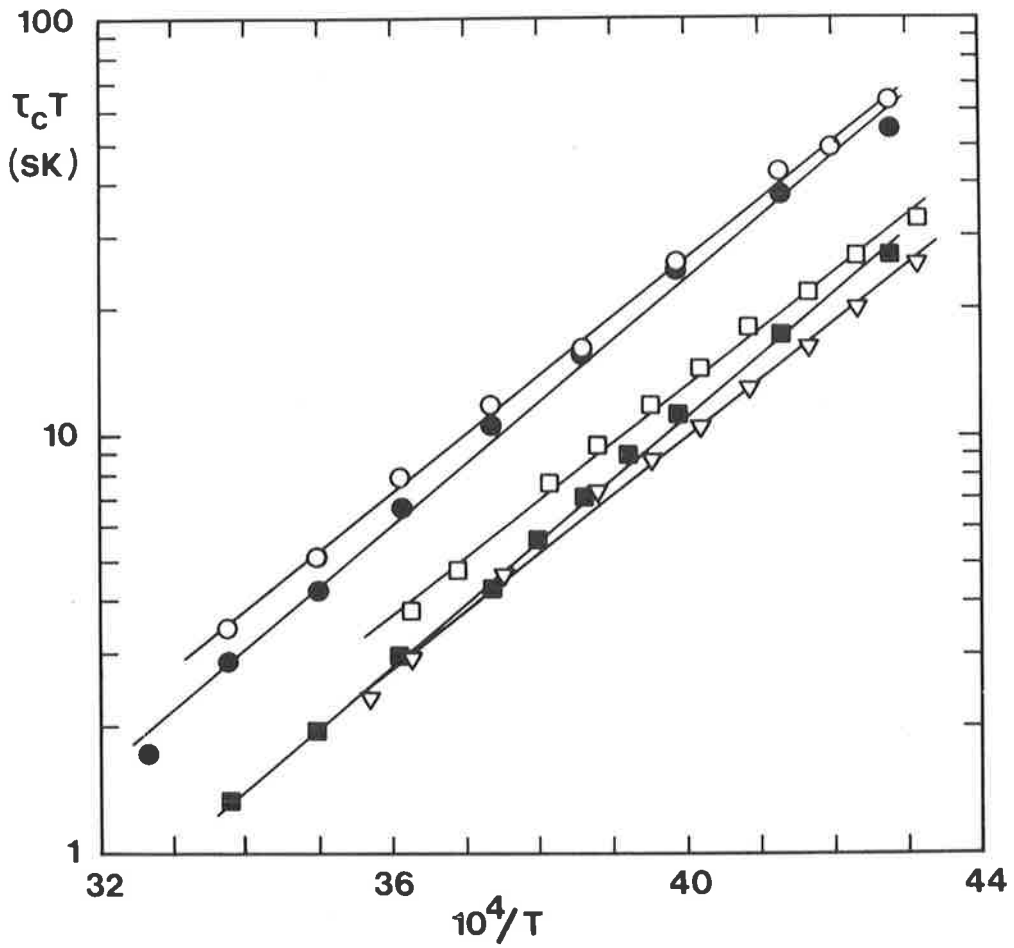

FIGURE 4.12 Semilogarithmic plots of $\tau_c T$ against 1/T for nma exchange on $[Sc(nma)_6]^{3+}$ in CD_3CN solution. Data for solutions (i) to (v) are represented as (i) ■ , (ii) ▽ , (iii) □ , (iv) ● and (v) ○ . The solid lines are linear regression lines.

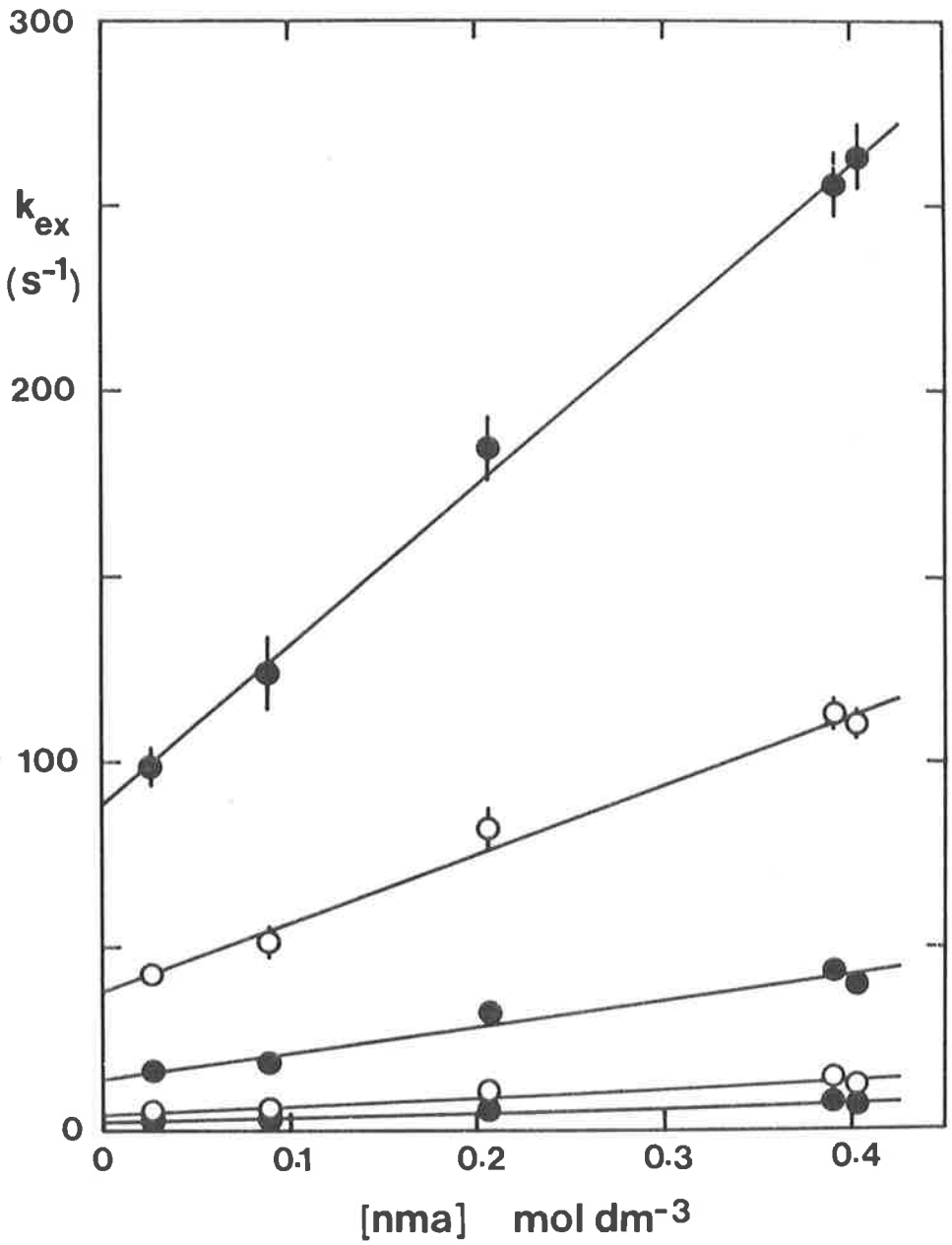

FIGURE 4.13 Plots of interpolated k_{ex} values for ligand exchange on $[Sc(nma)_6]^{3+}$ against [nma]. k_{ex} decreases in the sequence 300, 280, 260, 240 and 230 K for a given [nma] value and the solid lines represent linear regression lines.

TABLE 4.6 *Solution compositions and kinetic parameters for dma exchange on* $[Sc(dma)_6]^{3+}$

Solution	$[Sc(dma)_6^{3+}]$ mol dm^{-3}	[dma] mol dm^{-3}	$[CD_3NO_2]$ mol dm^{-3}	$[CD_3CN]$ mol dm^{-3}	C.N.[a]
(i)	0.0395	0.357	17.0	-	6.0 ± 0.1
(ii)	0.0415	0.256	17.1	-	6.1 ± 0.1
(iii)	0.0198	0.109	17.5	-	5.9 ± 0.2
(iv)	0.0103	0.0635	17.5	-	5.9 ± 0.2
(v)	0.0071	0.0390	18.0	-	6.0 ± 0.2
(vi)	0.1567	0.790	-	15.0	6.0 ± 0.2
(vii)	0.0505	0.255	-	16.2	5.9 ± 0.1
(viii)	0.0324	0.163	-	17.9	5.8 ± 0.2
(ix)	0.0195	0.0981	-	18.0	5.9 ± 0.1

Diluent	k_1(300 K)[a] s^{-1}	k_2(300 K)[a] dm^3 mol^{-1} s^{-1}	$\Delta H^{\ddagger}$[a] kJ mol^{-1}	$\Delta S^{\ddagger}$[a] J K^{-1} mol^{-1}
CD_3NO_2	4.1 ± 0.4	-	30.8 ± 2.0	-131 ± 6
CD_3NO_2	-	114 ± 3	26.0 ± 0.6	-119 ± 2
CD_3CN	13.3 ± 1.6	-	32.2 ± 3.5	-116 ± 12
CD_3CN	-	167 ± 9	27.2 ± 1.2	-112 ± 4

a Specifications as per Table 4.5.

solution were based upon the acetyl ^1H resonances of coordinated and free dma (separated typically by 30 Hz, a shift which exhibited a negligible temperature dependence). In CD_3CN solutions ((vi) - (ix)) the residual proton impurity signals arising from the diluent were in the vicinity of the acetyl resonances thus precluding determinations based upon the latter resonances for all but the most concentrated solution (vi). Measurements were therefore based upon the N-methyl resonances for solutions (vii) - (ix); these resonances being devoid of effects due to rotation about the C-N bond below 340 K. It is seen in Figure 4.14 that the high- and low-field components of the N-methyl doublets of coordinated and free dma respectively are almost coincident. This pattern was observed consistently for solutions (vii)- (ix).

Complete lineshape analysis of the coalescence of either N-methyl or acetyl dma resonances yielded the mean site lifetimes of a single coordinated ligand. Typical experimental spectra and best fit calculated lineshapes for solution (viii) are depicted in Figure 4.14 along with corresponding τ_c values. It was found that in both diluents $k_{ex} = k_1 + k_2[dma]$. Plots of k_{ex} versus [dma] for CD_3NO_2 solutions are shown in Figure 4.15. Kinetic parameters were obtained using DATAFIT as usual and are presented in Table 4.6. It is worthwhile to reiterate now that the mathematical model of the rate data is simple and does not explicitly take into account small environmental kinetic effects (such as those arising from liquid structural changes upon alteration of the concentration of the exchanging species) which may manifest themselves as apparent systematic perturbations of kinetic parameters. k_1 values are not likely to be significantly affected since they are essentially derived by extrapolation to infinite dilution. The derived k_2 values may incorporate small environmental

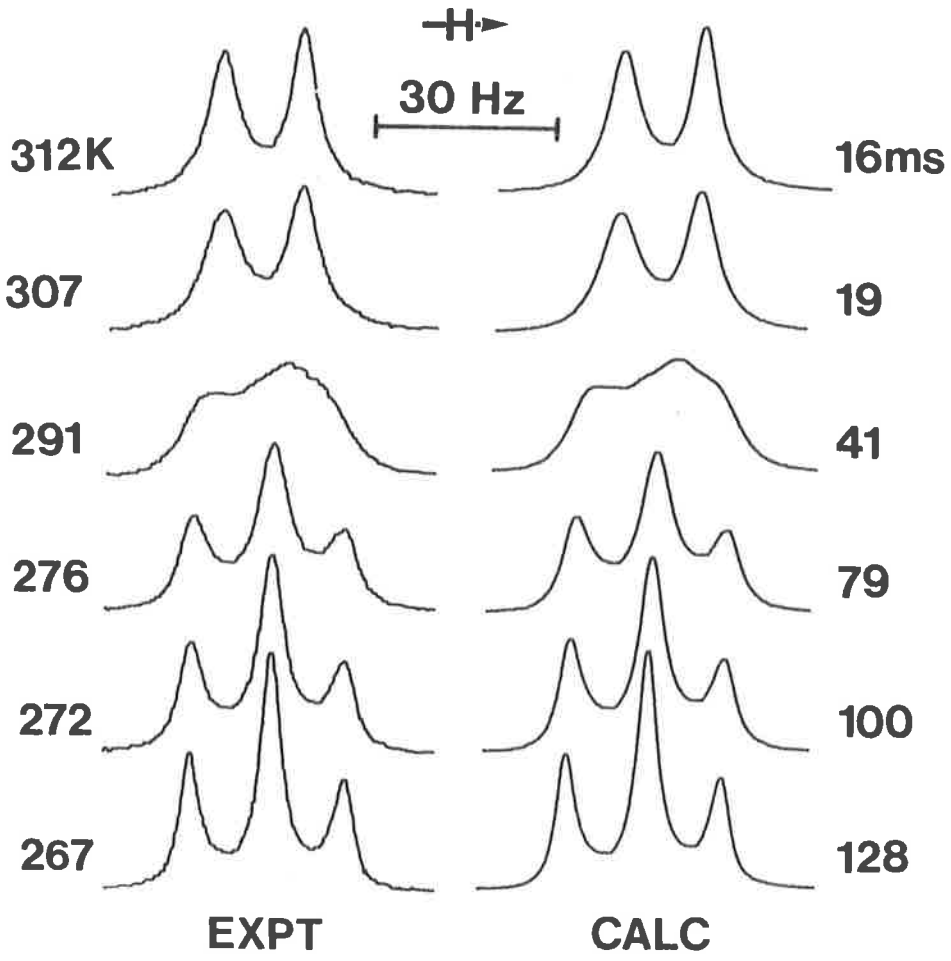

FIGURE 4.14 ^{1}H (90 MHz) n.m.r. N-CH_3 spectra characterizing ligand exchange on $[Sc(dma)_6]^{3+}$ in a solution in which $[Sc(dma)_6{}^{3+}]$, [dma] and $[CD_3CN]$ were respectively 0.0324, 0.163 and 17.9 mol dm^{-3}. The experimental spectra and the corresponding temperatures appear to the left of the Figure and the best fit calculated lineshapes and the corresponding τ_c values appear to the right of the Figure. The N-methyl doublet of coordinated dma is at low-field.

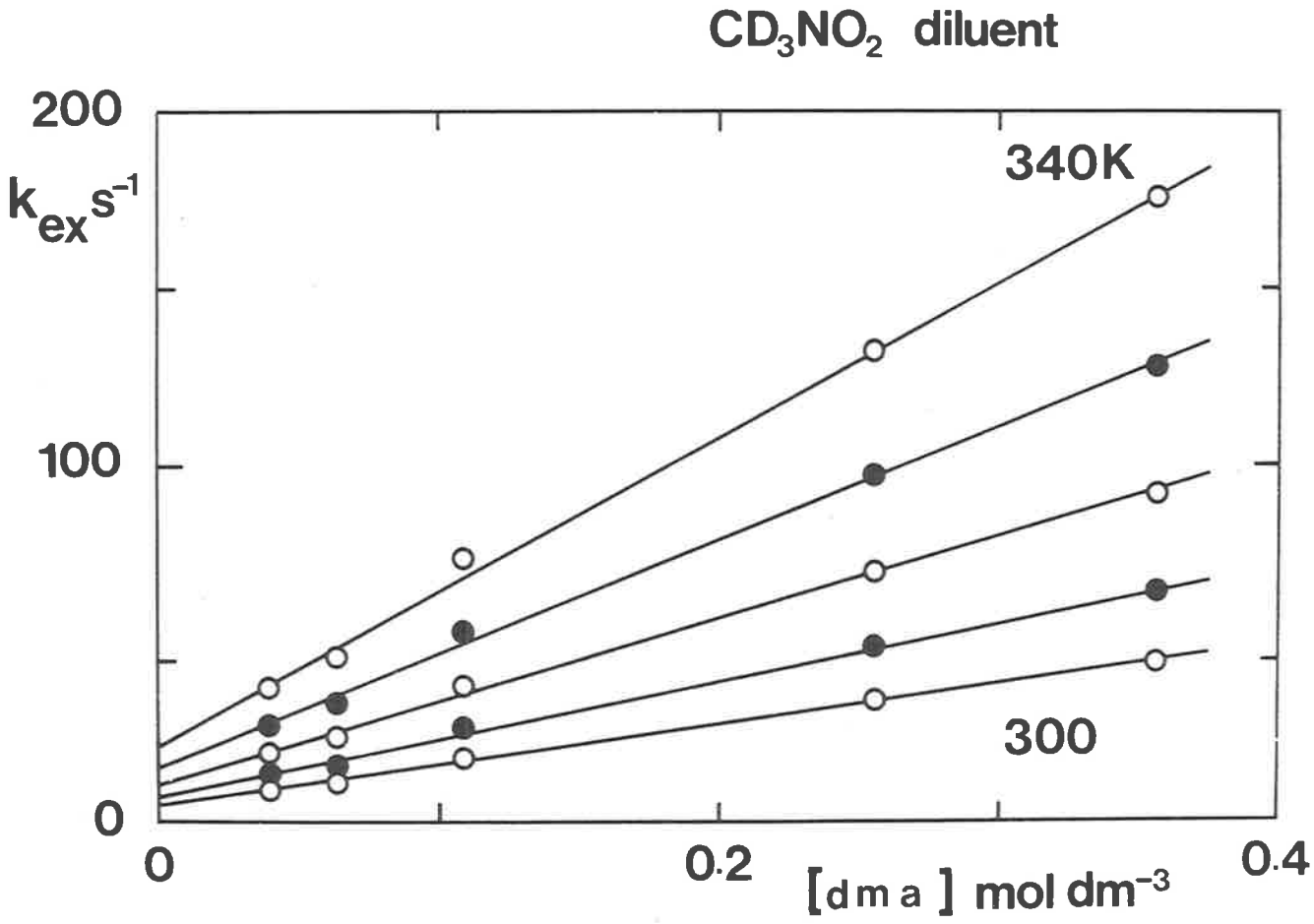

FIGURE 4.15 Plots of interpolated k_{ex} values for ligand exchange on $[Sc(dma)_6]^{3+}$ in CD_3NO_2 diluent. The top data set refers to 340 K and then in decreasing sequence to 330, 320, 310 and finally 300 K for the bottom data set. The solid lines represent the linear regression lines.

effects but when there is a strong dependence of k_{ex} upon the concentration of free ligand, as in these scandium(III) systems, the corresponding calculated activation parameters should refer predominantly to the second order process characterized by k_2.

The observation of two ligand exchange paths suggests similar energies for the intermediates $[Sc(dma)_5]^{3+}$ and $[Sc(dma)_7]^{3+}$ associated with D and A mechanisms respectively. It could be argued that the k_2 term arises from an I_D mechanism under the limiting condition in which [encounter complex] $\ll$ $[Sc(dma)_6^{3+}]$ such that $k_2 = k_{int}K$. An inspection of Table 4.6 and Figure 4.15 will indicate that if an I_D mechanism were operative it would be necessary for $k_{int} > 10k_1$* which seems implausible since the primary energetic step in both the D and I_D mechanisms is the fission of the metal-ligand bond. As coordination numbers greater than six[103-105] have been observed in the solid state for scandium(III) species the k_2 term probably arises from an A mechanism.

4.11 Exchange of N,N-diethylacetamide on $[Sc(dea)_6]^{3+}$

^1H n.m.r. spectra of samples of the virtually air stable compound $[Sc(dea)_6](ClO_4)_3$ and dea in either CD_3CN or CD_3NO_2, at temperatures below about 290 K, exhibited coordinated ligand resonances downfield from free ligand resonances. A comparison of the integrated areas of the acetyl signals (measurements based upon the ethyl resonances were not feasible due to overlap) for the CD_3NO_2 solutions

---

* If [encounter complex] $\ll$ $[Sc(dma)_6^{3+}]$ and $K[dma] \ll 1$ for all of the solutions studied then for a solution with [dma] = 0.5, $K \ll 2$. At 300 K (Table 4.6), k_2/k_1 (= $k_{int}K/k_1$) $\sim$29 in CD_3NO_2 solution and $\sim$13 in CD_3CN which means that k_{int}/k_1 would have to be greater than 10.

studied revealed that $[Sc(dea)_6]^{3+}$ was the vastly preponderant complex species in solution (Table 4.7). In CD_3CN samples the small ^1H resonances arising from incompletely deuterated diluent severely hampered acetyl signal integration procedures except for the most concentrated solutions (vii) and (viii). It became necessary to simulate experimental acetyl lineshapes (LINSHP) that were not significantly exchange broadened and then visually subtract the interfering resonances (difference display of LINSHP) to confirm that the coordination number was in fact six for all solutions.

The variation of the observed exchange rate constant with temperature and [dea] (solutions in CD_3NO_2), as determined from the coalescence of the acetyl resonances, is shown in Figure 4.16. There is seen to be a distinct curvature in the semilogarithmic plots of $\tau_c T$ versus 1/T which is symptomatic of a two term rate law of the form

$$\text{exchange rate} = 6(k_1 + k_2[\text{dea}])[Sc(\text{dea})_6^{3+}]$$

for which first and second order exchange processes are characterized by substantially different $\Delta H^{\ddagger}$ values. Table 4.7 lists kinetic parameters obtained from DATAFIT analysis of the data. If the linear interpolation procedure[78] (cf. Chapter 2) is adopted in lieu of the DATAFIT method, errors are introduced due to the curvature of $\ln(\tau_c T)$ versus 1/T plots. The DATAFIT kinetic parameter estimates for the CD_3NO_2 solutions may be compared with those derived through the linear interpolation procedure below, but despite the disaccord the general mechanistic interpretation is the same:

$k_1(300\ K) = 0.18 \pm 0.05\ s^{-1}$, $\Delta H_1^{\ddagger} = 77 \pm 4\ kJ\ mol^{-1}$,

$\Delta S_1^{\ddagger} = -1 \pm 10\ J\ K^{-1}\ mol^{-1}$; $k_2(300\ K) = 19.5 \pm 0.3\ dm^3\ mol^{-1}\ s^{-1}$,

$\Delta H_2^{\ddagger} = 22.6 \pm 0.9\ kJ\ mol^{-1}$ and $\Delta S_2^{\ddagger} = -145 \pm 2\ J\ K^{-1}\ mol^{-1}$.

(The errors here are estimated total errors.)

TABLE 4.7 *Solution compositions and kinetic parameters for dea exchange on* $[Sc(dea)_6]^{3+}$

Solution	$[Sc(dea)_6^{3+}]^a$ mol dm^{-3}	[dea] mol dm^{-3}	$[CD_3NO_2]$ mol dm^{-3}	$[CD_3CN]$ mol dm^{-3}	C.N.^{b}
(i)	0.193	1.489	11.2	-	5.8 ± 0.2
(ii)	0.158	0.876	14.1	-	5.9 ± 0.2
(iii)	0.0901	0.504	15.9	-	5.9 ± 0.1
(iv)	0.0407	0.314	17.0	-	6.0 ± 0.1
(v)	0.0173	0.0965	17.5	-	6.0 ± 0.2
(vi)	0.0064	0.0495	17.6	-	5.8 ± 0.2
(vii)	0.219	1.471	-	10.6	5.9 ± 0.2
(viii)	0.181	1.095	-	13.6	6.0 ± 0.2
(ix)	0.105	0.636	-	14.8	6.0 ± 0.2^c
(x)	0.084	0.600	-	15.5	6.0 ± 0.2^c
(xi)	0.048	0.289	-	17.0	6.0 ± 0.2^c
(xii)	0.018	0.126	-	17.3	6.0 ± 0.2^c

Diluent	k_1(300 K)^b s^{-1}	k_2(300 K)^b dm^3 mol^{-1} s^{-1}	$\Delta H^{\ddagger b}$ kJ mol^{-1}	$\Delta S^{\ddagger b}$ J K^{-1} mol^{-1}
CD_3NO_2	0.13 ± 0.02	-	81.6 ± 2.6	9.9 ± 7.2
CD_3NO_2	-	14.9 ± 0.3	28.1 ± 0.6	-129 ± 2
CD_3CN	12.5 ± 0.4	-	43.9 ± 1.0	-78 ± 3
CD_3CN	-	18.1 ± 0.7	23.5 ± 0.9	-142 ± 3

a The chemical shift separation between the coordinated and free dea acetyl resonances varied systematically from 22.5 Hz in solution (vii) to 16.8 Hz in solution (xii) at 250 K. The analogous separation of 33.6 Hz was virtually independent of concentration in solutions (i) - (vi) at 250 K.

b Specifications as per Table 4.5.

c C.N. determined by lineshape analysis. The errors represent the estimated total uncertainty.

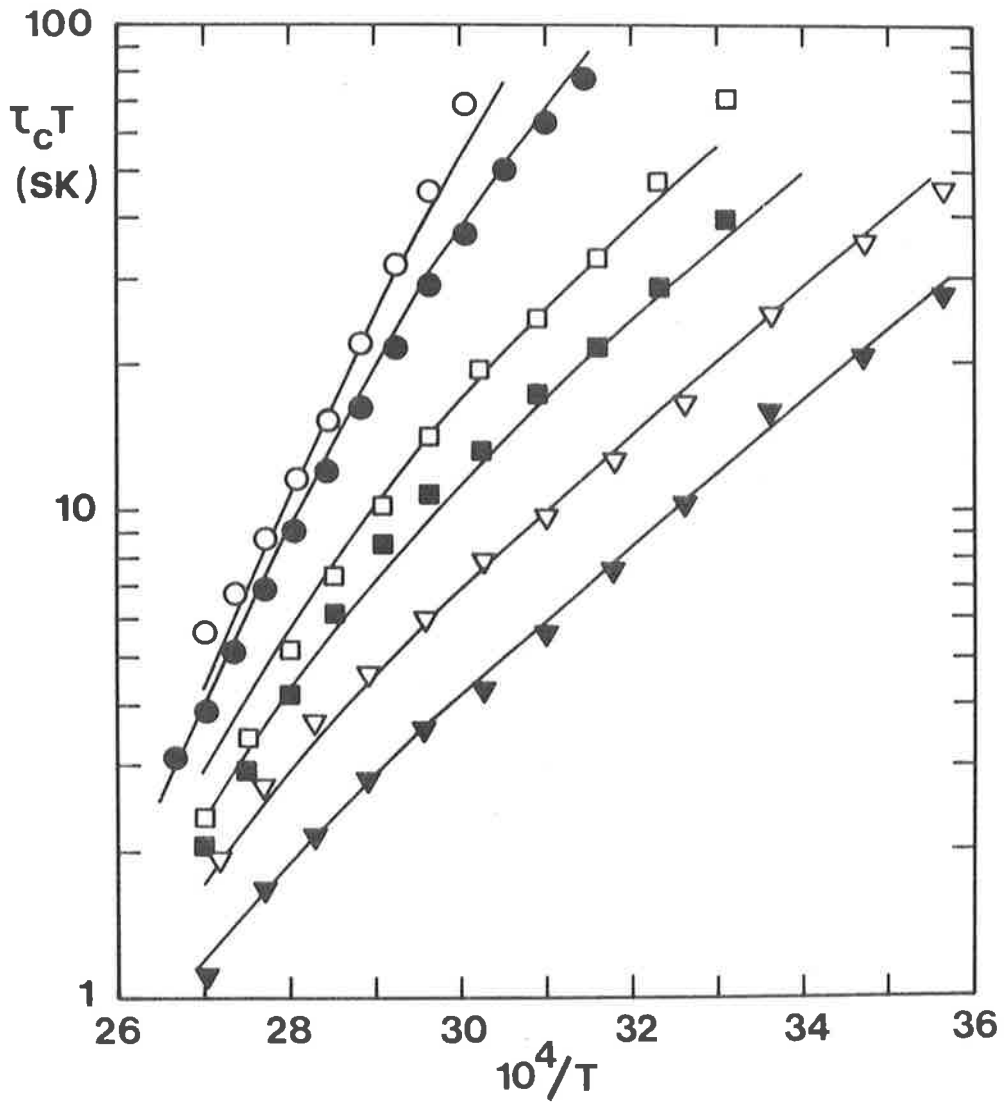

FIGURE 4.16 Semilogarithmic plots of $\tau_c T$ against 1/T for dea exchange on $[Sc(dea)_6]^{3+}$ in CD_3NO_2 solution. The data for solutions (i) - (vi) are represented as (i) ▼, (ii) ▽, (iii) ■, (iv) □, (v) ● and (vi) ○. The solid curves are those derived from a simultaneous fit of all the data to Equation 2.17.

By virtue of the interference of the diluent's proton impurity signals in the lineshape analysis of the acetyl region, the rate data for CD_3CN solutions could only be acquired over a limited [dea] range. In practice, the visual subtraction technique was less reliable at low $[dea]_{total}$ and under intermediate exchange rate conditions. DATAFIT was again used to analyse the data since the plots of $\ln(\tau_c T)$ versus $1/T$ were slightly curved. The rate law in CD_3CN was the same as that in CD_3NO_2. Using the arguments put forward in the last Section, k_1 and k_2 terms may be assigned to D and A mechanisms respectively.

4.12 The N-phenylacetamide complex of scandium(III)

N-phenylacetamide (acetanilide) has been shown to exist predominantly as the *trans* isomer in $CDCl_3$ (at 250 K)[124] or pyridine[125]. Consequently, the rate of internal rotation about the carbonyl carbon-nitrogen bond has not been measured. (The rate of rotation about the benzene-nitrogen axis is rapid[126].) N-phenylacetamide was not particularly soluble in CD_3CN (<30 mg/ml below 250 K). Nevertheless, ^1H n.m.r. spectra of npa in CD_3CN at 225 K were consistent with the presence of only one isomer and rapid intramolecular exchange is unlikely at 225 K[126]. The concentration dependent linewidth of the N-H singlet varied from 8 Hz at 230 K to 38 Hz at 320 K for a ca. 0.3 mol dm^{-3} solution.

The mildly hygroscopic complex $[Sc(npa)_6](ClO_4)_3$ was moderately soluble in CD_3CN ($\sim$60 mg/ml below 250 K), sparingly soluble in CD_3NO_2 (8 mg/ml at 300 K) and practically insoluble in CD_2Cl_2. ^1H n.m.r. spectra (N-H region) of $[Sc(npa)_6](ClO_4)_3$ in CD_3CN at low temperature consisted of a major singlet and a minor upfield ($\sim$37 Hz) singlet. The ratio of areas was temperature dependent with the proportion of the

minor singlet increasing slightly with temperature. At 270 K the minor signal was 4% of the major signal and coalescence occurred above 300 K. Coordinated npa N-H linewidths were found to be smaller than the free npa N-H linewidth: Whilst the free npa linewidth increased almost linearly with temperature, coordinated npa linewidths increased monotonically but in a non-linear fashion and at a lesser rate. In the case of a sample of $[Sc(npa)_6](ClO_4)_3$ (0.05 mol dm^{-3}) in CD_3CN the N-H linewidth (major signal) was 5 Hz at 230 K; at 260 K, 11 Hz; and at 320 K it was 13 Hz. From these data it appears that the relaxation times of ^{14}N nuclei associated with coordinated npa are shorter than those of ^{14}N nuclei in free npa.

The spectrum of the acetyl region was complex due to the presence of the proton impurity signals arising from incompletely deuterated diluent. Despite this complication, at temperatures below 250 K, there appeared to be a major singlet and at least one minor downfield ($\sim$14 Hz) singlet (which was masked to some extent by the ^1H signals from the diluent). In CD_3NO_2 the observations were similar. A minor upfield N-H resonance and a broad minor downfield acetyl resonance were detected below 270 K.

The conclusion from the observations above is that the minor resonances are due to the *cis* isomer of npa. Because of the disparate proportions of *cis* and *trans* isomers and the temperature dependence of populations, kinetic data for internal rotation could not be accurately obtained.

For 90 MHz ^1H n.m.r. samples of $[Sc(npa)_6](ClO_4)_3$ and npa in CD_3CN, the slow intermolecular ligand exchange condition applied below 270 K. At these temperatures the acetyl signal of free npa appeared downfield from the major acetyl resonance of coordinated npa. In contrast, the N-H signal of free npa appeared upfield from the major

N-H signal of the coordinated ligand. The amount of postulated *cis* npa was substantially reduced when complex and ligand were mixed together in CD_3CN. Figure 4.17 shows the coalescence of the N-H signals with increase in temperature. Unfortunately, accurate kinetic parameters could not be extracted through simulation of either acetyl or N-H coalescence phenomena for several reasons. In the case of the acetyl resonances, the main hindrance was the significant contribution of the ^1H impurity resonances of diluent (which were located in the midst of free and coordinated ligand acetyl resonances) to the total lineshape of the acetyl region. This contribution could not be easily accounted for in the determination of rates. In the case of the N-H resonances, the main obstacle was the sensitivity of N-H linewidths and chemical shifts to changes in concentration and temperature. There was also a variation of site populations with temperature such that as the temperature was raised the mole fraction of free ligand increased. At the lower temperatures integrations were compatible with $[Sc(npa)_6]^{3+}$ being the predominant scandium(III) species. A sizeable [npa] range was not feasible due to the limited solubility of npa in CD_3CN. Hence, determination of the rate law was precluded. Intuitively, the kinetics of npa exchange should be similar to the kinetics of exchange observed for the other acetamides mentioned in this Chapter. At 270 K, $k_{ex} \sim 50\ s^{-1}$ for the solution in Figure 4.17 and this value is comparable with the rate constant (at 270 K) calculated for a $[Sc(nma)_6]^{3+}$/nma/CD_3CN solution of similar concentration (i.e. solution (iii) in Table 4.5): $k_{ex}(270\ K) \simeq 47\ s^{-1}$.

4.13 Conclusions regarding the kinetics of amide systems

The observation that ligand exchange on scandium(III) is within the n.m.r. time scale if the ligand is nma, dma, dea or npa but is in

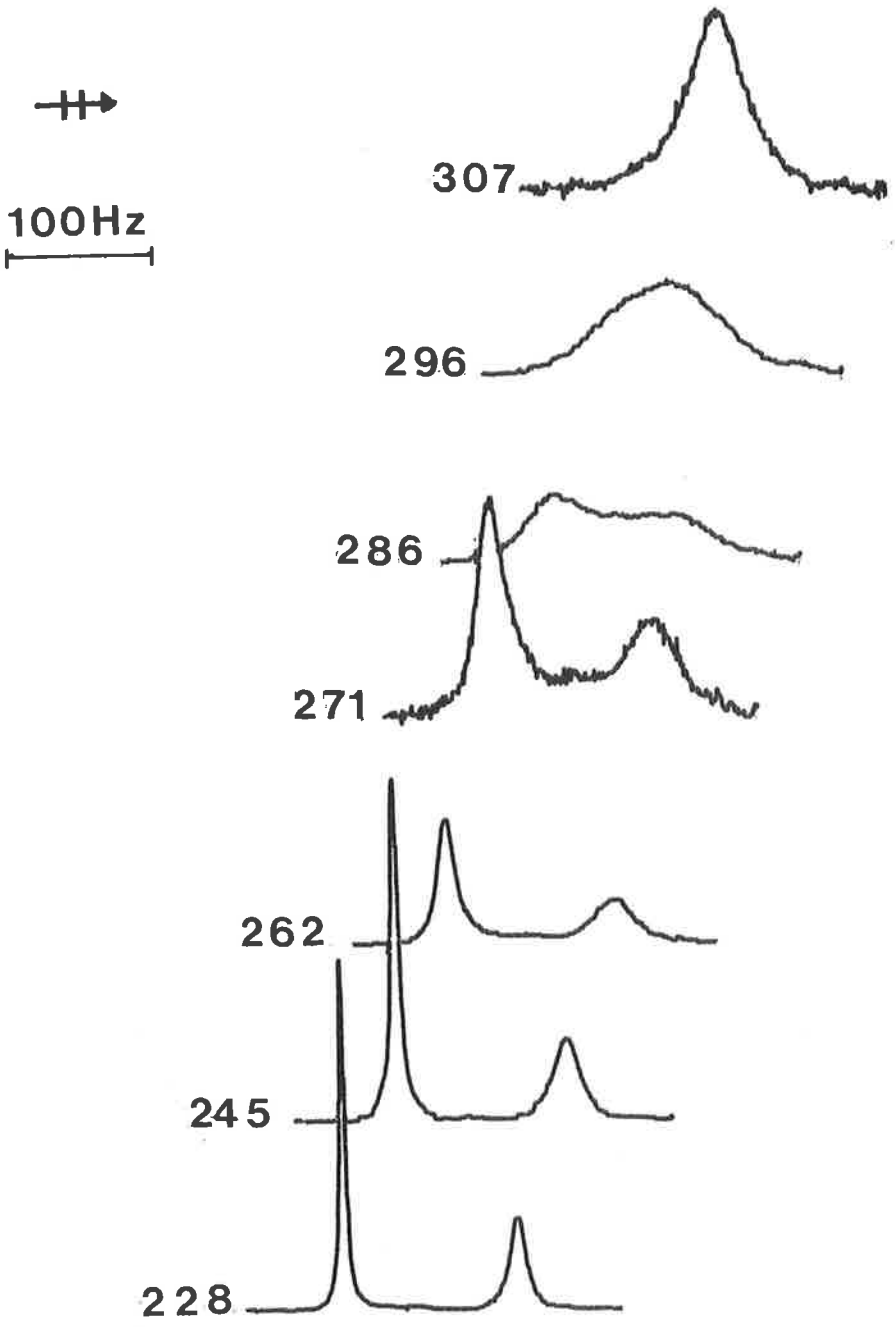

FIGURE 4.17 ^{1}H n.m.r. spectra (N-H region) for a solution of $[Sc(npa)_6](ClO_4)_3$ (0.0538 mol dm^{-3}) and npa (0.233 mol dm^{-3}) in CD_3CN. The experimental temperatures appear to the left of the Figure.

the fast exchange limit of that time scale when the ligand is nmf, dmf, def or dbf emphasizes the importance of the acetyl methyl group and the formyl proton in determining ligand lability. The donor numbers of dmf, dma, def and dea on the Gutmann scale[127] are 26.6, 27.8, 30.9 and 32.2 respectively, from which it may be inferred that electron donating ability is not the major factor determining the relative labilities of these ligands when coordinated to scandium(III). The same conclusion is assumed to be valid for the other amides studied. A discussion of ligand lability based upon steric considerations is now presented.

Although R_2 and R_3 substituents in $O{=}C(R_1)NR_2R_3$ contribute to the total steric interaction of ligands in the first coordination sphere it is clear that the steric interactions which most strongly influence lability arise from R_1. It appears that when R_1 = H an increase in coordination number in either the transition state or the ground state will occur more readily than when R_1 = Me. In the former event a rapid associative exchange process is probable whereas in the latter event a coordination number greater than six will result in ligand labilization through an increase in ground state bond length as discussed elsewhere[10,95]. Alternatively, it is possible that during the formation of a D transition state a relatively greater decrease in metal-ligand bond length for the non-leaving ligands will occur when R_1 = H. Consequently, a greater lability will be conferred upon $[ScS_6]^{3+}$. However, the absence of directly determined coordination numbers and ligand exchange rate laws for the formamide systems precludes further mechanistic discussion for those systems.

At 300 K and over the liquid temperature range (ca. 230 - 340 K) of the CD_3CN solutions studied, $[Sc(nma)_6]^{3+}$ is the most labile of the three acetamide complex ions for which quantitative ligand exchange

data is available (nma, dma, dea; cf. Tables 4.5 - 4.7). This is probably a reflection of the lesser steric crowding (arising from the R_2 and R_3 groups) in this ligand exchange system by comparison to the crowding which is experienced in the dma and dea systems. In contrast, the most sterically hindered species, $[Sc(dea)_6]^{3+}$, exhibits the smallest k_2 term and it is only at the upper extreme of the temperature scale that the k_1 term for $[Sc(dea)_6]^{3+}$ becomes greater than the k_1 term for $[Sc(dma)_6]^{3+}$. For $[ScS_6]^{3+}$ in CD_3CN, $\Delta H_1^{\ddagger}$ decreases and $\Delta S_1^{\ddagger}$ becomes more negative as S is varied in the sequence dea, dma, nma; but the variation in $\Delta H_2^{\ddagger}$ and $\Delta S_2^{\ddagger}$ is less systematic.

When the diluent is changed to CD_3NO_2, activation enthalpies and entropies change markedly in the case of dea but to a lesser extent for dma. This behaviour again indicates that interactions outside the first coordination sphere can make significant and complicated contributions towards observed activation parameters. Hence, a detailed mechanistic interpretation of the variation of the activation parameters is not attempted.

CHAPTER 5 LIGAND EXCHANGE ON YTTRIUM(III)

5.1 Introduction

Geier[95] has determined the rate of substitution of murexide into the first coordination sphere of the aquayttrium(III) ion to be 1.3×10^7 dm^3 mol^{-1} s^{-1} at 310.2 K. The high rate was considered[95] to be a consequence of the great lability of the aqua ligands in $[Y(H_2O)_n]^{3+}$ where $n > 6$. The more recent ^1H n.m.r. work of Fratiello[128] dealing with yttrium(III) salts in aqueous acetone solution has demonstrated that nitrate ion probably enters the first coordination sphere of yttrium(III) in yttrium(III) nitrate solutions (as evidenced by a measured hydration number of less than three) and that in the case of acidified yttrium(III) perchlorate solutions immeasurably rapid water exchange occurs even at 175 K. Coordination numbers of up to eight for yttrium(III) with oxygen donor chelates[129,130] have been observed in solution and up to ten in the solid state[105,131,132]. The latter reports are consistent with the fact that the ionic radius of yttrium(III) is larger than that of scandium(III) and comparable to those of the lanthanides[133]. They also lend support to Geier's early postulate above.

It would appear that considerable uncertainty still exists in the understanding of simple ligand exchange processes on yttrium(III) and that there is a need for more data in this area. Yttrium(III) is expected to be generally more labile than scandium(III) on the basis of relative ionic radii and this Chapter describes studies designed to assess the lability of the metal ion towards ligand substitution in non-aqueous media.

5.2 Exchange of 1,1,3,3-tetramethylurea on $[Y(tmu)_6]^{3+}$

A hygroscopic complex of the formula $[Y(tmu)_6](ClO_4)_3$ (in agreement with Giesbrecht and Kawashita[134]) was easily prepared. Anhydrous solutions of the complex and tmu (compositions are given in Table 5.1) exhibited a 270 MHz ^1H n.m.r. singlet arising from coordinated tmu downfield from the singlet of free tmu at 225 K. The chemical shift separation at 225 K varied systematically from 19.0 Hz for solution (i) to 12.4 Hz for solution (v) (^1H spectra were run at 270 MHz because of the small separation at 90 MHz). For all solutions the separation increased with increase in temperature (ca. 1.5 Hz/10 K). As for the $[Sc(tmu)_6]^{3+}$ system there appeared to be rapid rotation about the C-N bonds for coordinated tmu. The relative areas of the singlets were consistent with $[Y(tmu)_6]^{3+}$ being the vastly predominant yttrium(III) species in solution. Complete lineshape analysis of their coalescence over the temperature range 225 - 270 K (spectra were recorded at 5 K intervals) yielded the kinetic parameters in Table 5.1. The observed exchange rate constants at 250 K are seen to vary little with change in [tmu]. Kinetic data for solution (i) are different from the others but this difference may be due to afore-mentioned environmental effects at high [tmu]. The results are compatible with a rate law of the form

$$\text{exchange rate} = 6k_1[Y(tmu)_6^{3+}]$$

This rate law typifies a D or I_D exchange mechanism in which $K > 300$ dm^3 mol^{-1}. However, no direct experimental evidence for the formation of an encounter complex exists.

At 250 K, $[Y(tmu)_6]^{3+}$ is considerably more labile than

TABLE 5.1 *Solution compositions and kinetic parameters for tmu exchange on* $[Y(tmu)_6]^{3+}$ *in* CD_3CN

Solution	$[Y(tmu)_6^{3+}]$ mol dm^{-3}	[tmu] mol dm^{-3}	$[CD_3CN]$ mol dm^{-3}	C.N.[a]	k_{ex}(250 K)[b,d] s^{-1}	$\Delta H^{\ddagger}$[c,d] kJ mol^{-1}	$\Delta S^{\ddagger}$[c,d] J K^{-1} mol^{-1}
(i)	0.140	0.786	14.7	6.0 ± 0.1	52 ± 3	31.4 ± 0.9	-85 ± 3
(ii)	0.0602	0.429	16.2	6.0 ± 0.2	23 ± 1	26.5 ± 0.7	-111 ± 3
(iii)	0.0460	0.259	17.4	6.0 ± 0.1	25 ± 1	26.3 ± 0.5	-111 ± 2
(iv)	0.0195	0.139	17.6	6.0 ± 0.2	26 ± 2	24.6 ± 0.9	-118 ± 4
(v)	0.0039	0.028	18.3	5.9 ± 0.1	25 ± 1	27.1 ± 0.5	-108 ± 2
From Table 4.4:	$[Sc(tmu)_6^{3+}]$						
	0.0138	0.0732	17.4		2.7×10^{-3}[e]	70.7 ± 1.6	-9.8 ± 4.8

a C.N. = number of tmu ligands coordinated to Y^{3+} as determined by integration and lineshape analysis in the temperature range 225 - 240 K. The errors represent the estimated total uncertainty.

b k_{ex}(250 K) interpolated from the Eyring plots. 250 K is the middle coalescence temperature.

c $\Delta H^{\ddagger}$ and $\Delta S^{\ddagger}$ obtained from the Eyring plots.

d The errors represent one standard deviation (ACTENG).

e Calculated from the activation parameters.

$[Sc(tmu)_6]^{3+}$ as a consequence of its remarkably smaller $\Delta H^{\ddagger}$ and more negative $\Delta S^{\ddagger}$ magnitudes. Perhaps all that can be said here, with allusion to an electrostatic model, is that this reflects the fact that the effective ionic radius of yttrium(III) (r = 0.900Å)[91] is greater than that of scandium(III) (r = 0.68Å)[135]. As a result of a larger metal ion surface charge density the electrostatic interaction between tmu and scandium(III) is greater. In addition, greater steric repulsion between ligands in the first coordination sphere, due to electrostriction, will be experienced for $[Sc(tmu)_6]^{3+}$. The activation parameters in Table 5.1 probably also reflect the softer acid nature of yttrium(III) (cf. Section 3.4). However, the interpretation of activation parameter magnitudes (in particular $\Delta S^{\ddagger}$) is not simple since those parameters may incorporate contributions emanating from outside the first coordination sphere as will be discussed in the next Chapter.

5.3 Exchange of methylmethylphenylphosphinate on $[Y(mmpp)_6]^{3+}$

In contrast to $[Y(tmu)_6](ClO_4)_3$, the hygroscopic complex $[Y(mmpp)_6](ClO_4)_3$ was quite soluble in CD_2Cl_2. 90 MHz ^1H n.m.r. spectra of a CD_2Cl_2 solution of this compound showed only the expected resonances. On the other hand, ^1H decoupled ^{31}P n.m.r. spectra of the same solution at low temperature exhibited a doublet resonance (J (^{89}Y - ^{31}P) = 11.4 Hz; I (^{89}Y) = ½) attributable to $[Y(mmpp)_6]^{3+}$ and also a much smaller upfield resonance due to another yttrium(III) species (probably of lower coordination number) as in Figure 5.1. Coalescence of all signals to a singlet was seen to occur with elevation of temperature. Intermolecular mmpp exchange was thus proceeding but there was no apparent resonance for free mmpp at any temperature.

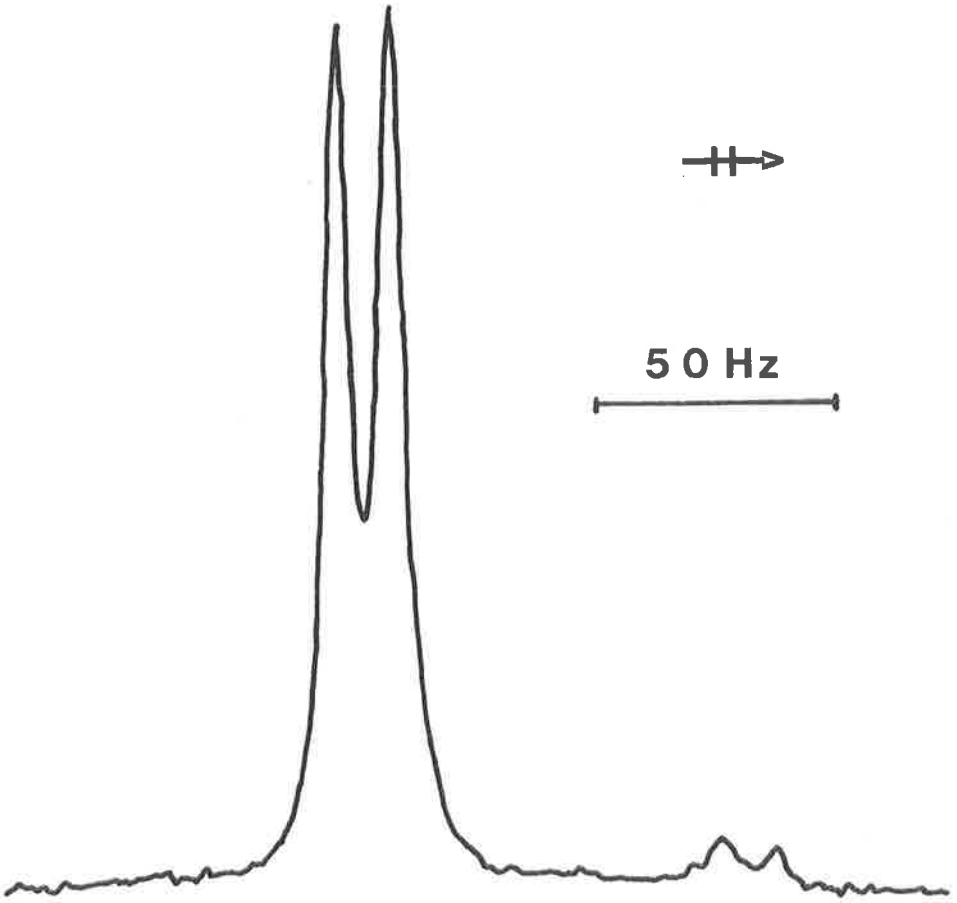

FIGURE 5.1 Proton decoupled ^{31}P FT n.m.r. spectrum of a 0.13 mol dm^{-3} solution of $[Y(mmpp)_6](ClO_4)_3$ in d_2-dichloromethane at 185 K. The major doublet resonance is assigned to $[Y(mmpp)_6]^{3+}$.

It was quickly realized that a quantitative 90 MHz ^{1}H n.m.r. study of mmpp exchange was not practicable when ^{1}H spectra of samples of $[Y(mmpp)_6](ClO_4)_3$/mmpp in CD_2Cl_2 at 180 K indicated intermediate to fast intermolecular exchange. Fortunately, ^{31}P n.m.r. at 36.43 MHz provided much larger chemical shifts than those from 90 MHz ^{1}H n.m.r. for this system and so quantitative rate data were obtainable using the ^{31}P probe. At 200 K for all solutions studied (Table 5.2), the ^{31}P doublet resonance of coordinated mmpp (the minor upfield resonance was absent) appeared about 340 Hz downfield from the singlet resonance of the free ligand. The chemical shift separation increased with temperature (ca. 5 Hz per 10 K). $[Y(mmpp)_6]^{3+}$ was determined to be, by integration, the predominant yttrium(III) species present in solutions (i) - (v). Ligand exchange causes the coordinated and free ligand resonances to coalesce as in Figure 5.2. The mean lifetime of a ligand in $[Y(mmpp)_6]^{3+}$ was derived through lineshape analysis using a three site exchange treatment (Appendix 2). Whilst there are only two chemically distinct ligand environments, namely coordinated and free, the two spin states of ^{89}Y produce two different magnetic sites for the coordinated ligand which together with that for the free ligand results in a total of three magnetic sites which must be considered in the lineshape analysis. If one labels the low-field component of the coordinated mmpp doublet as site 1, the high-field component as site 2, the free mmpp resonance as site 3 and if $P_1 = P_2 = 0.25$ ($P_3 = 0.5$), the probability transfer matrix $\underline{p}$ is

$$\underline{p} = \begin{bmatrix} -1 & 0 & 1 \\ 0 & -1 & 1 \\ 0.5 & 0.5 & -1 \end{bmatrix}$$

TABLE 5.2 *Solution compositions and kinetic parameters for mmpp exchange on* $[Y(mmpp)_6]^{3+}$.

Solution	$[Y(mmpp)_6^{3+}]$ mol dm^{-3}	[mmpp] mol dm^{-3}	$[CD_2Cl_2]$ mol dm^{-3}	C.N.[a]
(i)	0.146	1.970	8.14	6.0 ± 0.2
(ii)	0.0911	0.671	12.2	6.1 ± 0.2
(iii)	0.0374	0.275	13.3	6.0 ± 0.2
(iv)	0.0286	0.161	14.5	6.0 ± 0.2
(v)	0.0147	0.083	14.7	5.8 ± 0.2
	k_1(215 K)[b] s^{-1}	k_2(215 K)[b] dm^3 mol^{-1} s^{-1}	$\Delta H^{\ddagger}$[b] kJ mol^{-1}	$\Delta S^{\ddagger}$[b] J K^{-1} mol^{-1}
	312 ± 13	-	31.4 ± 1.4	-49 ± 7
	-	455 ± 31	35.3 ± 2.8	-27 ± 13

a C.N. = coordination number of yttrium(III) as determined by integration. The errors represent the maximum observed deviation from the mean value .

b Kinetic parameters evaluated from DATAFIT analysis. The errors quoted represent one standard deviation. 215 K is the approximate middle coalescence temperature.

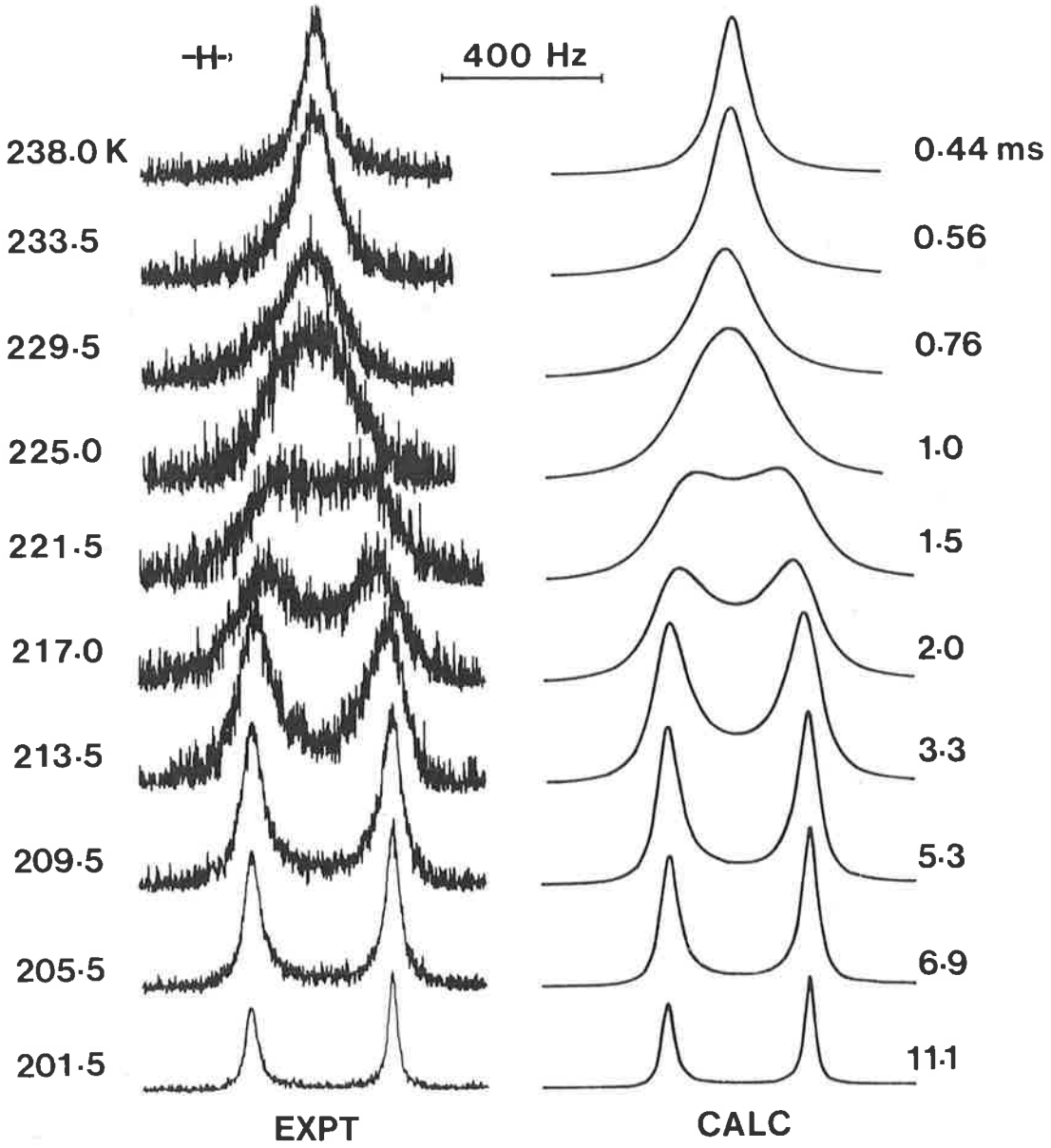

FIGURE 5.2 Experimental and calculated ^{31}P FT n.m.r. lineshapes for a solution of $[Y(mmpp)_6]^{3+}$ (0.0286 mol dm^{-3}) and mmpp (0.161 mol dm^{-3}) in CD_2Cl_2. The experimental temperatures and best fit τ_c values appear to the left and right of the Figure respectively. The free mmpp signal is upfield.

We choose τ to be the mean site lifetime of a coordinated ligand. The matrix above is only applicable, however, when $\tau_C = \tau_F$, the lifetime of a ligand in the free state. These two lifetimes are related as follows

$$\tau_C/P_C = \tau_F/P_F \quad \text{and} \quad P_C = P_1 + P_2$$

where P is the appropriate mole fraction. Thus the matrix above may be generalized by multiplying elements p_{31}, p_{32} and p_{33} by P_C/P_F to give:

$$\underline{p} = \begin{bmatrix} -1 & 0 & 1 \\ 0 & -1 & 1 \\ P_C/2P_F & P_C/2P_F & -P_C/P_F \end{bmatrix}$$

The exchange rate = $6k_{ex}[Y(mmpp)_6^{3+}]$ where $k_{ex} = 1/\tau_C$.

It is seen in Figure 5.3 that τ_C decreases with an increase in temperature or free ligand concentration. Since a two term rate law appears to operate over the 24-fold range in [mmpp] for this system, the kinetic parameters were obtained from DATAFIT analysis. As can be seen from Table 5.2 the errors associated with kinetic parameters are larger than those for the other ligand exchange systems in this thesis. There are a number of possible reasons for this. Firstly, the signal to noise ratio for experimental spectra (Figure 5.2) was relatively low principally because the observed nucleus, ^{31}P, is less sensitive than ^{1}H. Secondly, the fit of the rate data to the DATAFIT two term rate equation was not as good as that for the other systems but is obviously better than the fit to a one term rate equation (cf. Figure 5.3). The k_1 path is ascribed

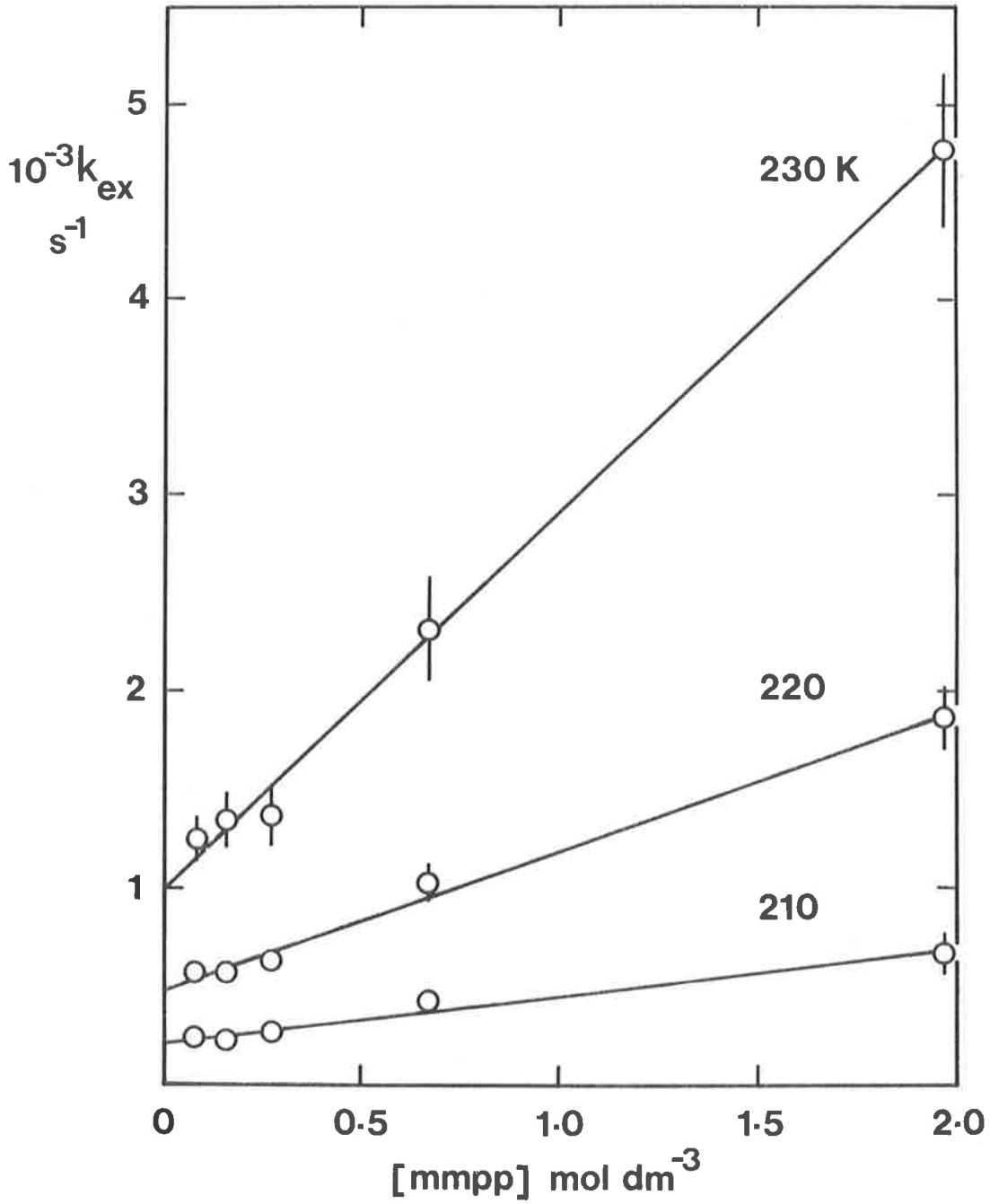

FIGURE 5.3 Plots of interpolated k_{ex} values for ligand exchange on $[Y(mmpp)_6]^{3+}$ against [mmpp]. The lines represent linear regression lines.

to a D mechanism and the k_2 path to either an A or an I_D mechanism (limit (a)). An associative mechanism seems more attractive than the interchange mechanism in view of the high coordination numbers which have been observed for yttrium(III)[105,131,132].

5.4 The yttrium(III)/hexamethylphosphoramide system

In contrast to the result expected from the work of Scholer and Merbach[106] the hmpa complex isolated using the usual preparative procedure was found to be $[Y(hmpa)_{5.12}](ClO_4)_3$. The solid state infrared spectrum of $[Y(hmpa)_{5.12}](ClO_4)_3$ (apparently non-stoichiometric) exhibited signals characteristic of coordinated unidentate perchlorate and no signals due to water. In CH_2Cl_2 solution the coordinated perchlorate signals were absent.

^1H decoupled ^{31}P n.m.r. spectra of $[Y(hmpa)_{5.12}](ClO_4)_3$ in CD_2Cl_2, for sample temperatures below 230 K, exhibited three distinct coordinated hmpa doublet resonances and a downfield singlet resonance due to free hmpa as in Figure 5.4. ^1H n.m.r. spectra were compatible with the ^{31}P spectra. As the temperature was increased coalescence of all ^{31}P resonances occurred, but even at room temperature discrete broad signals were evident. In order to be consistent with the solid state stoichiometry doublet (a) in Figure 5.4 should arise from $[Y(hmpa)_6]^{3+}$ (J (^{89}Y - ^{31}P) = 17.2 Hz), (b) from $[Y(hmpa)_5]^{3+}$ (J = 15.1 Hz) and (c) from $[Y(hmpa)_4]^{3+}$ (J = 15.1 Hz). All of these species were found to exist according to an equilibrium that strongly favours the lower coordination number complexes with increase in temperature or decrease in [hmpa]. As for the scandium(III)/hmpa system there was no evidence for slow intramolecular exchange (at 190 K) in $[Y(hmpa)_5]^{3+}$. Unlike the scandium(III)/hmpa system,

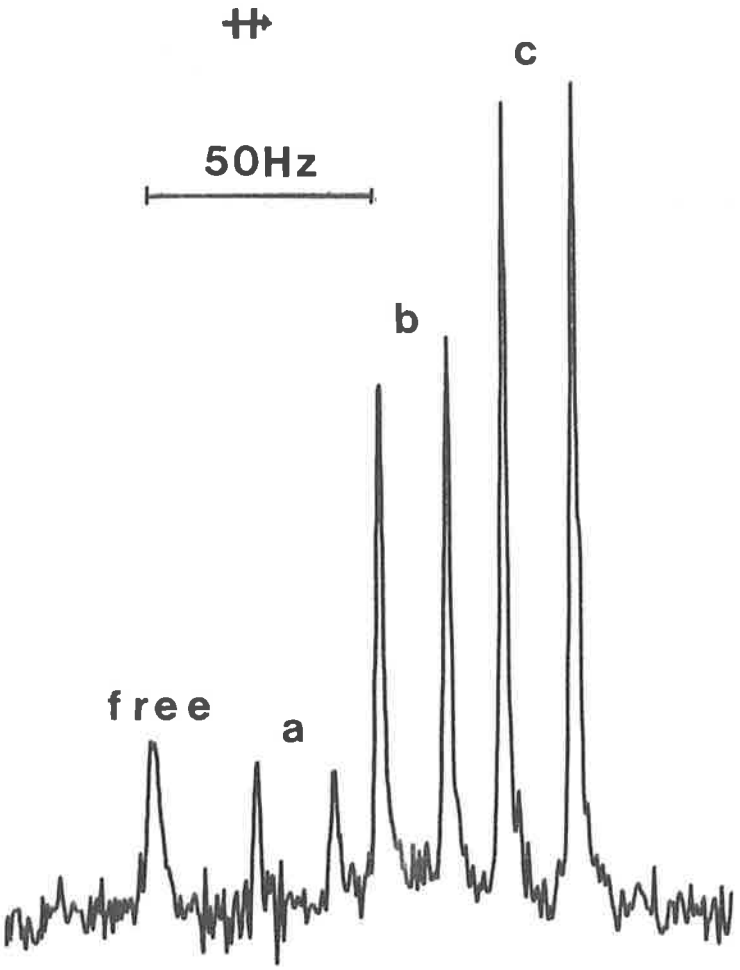

FIGURE 5.4 ^{1}H decoupled ^{31}P FT n.m.r. spectrum of a solution of $[Y(hmpa)_{5.12}](ClO_4)_3$ (37 mg/ml) in CD_2Cl_2 at 200 K. Doublet (a) is assigned to $[Y(hmpa)_6]^{3+}$, (b) to $[Y(hmpa)_5]^{3+}$ and doublet (c) is assigned to $[Y(hmpa)_4]^{3+}$.

however, a six-coordinate hmpa complex ion appears to be present along with the four- and five-coordinate species. $[Y(hmpa)_6]^{3+}$ is likely to be more stable than $[Sc(hmpa)_6]^{3+}$ on steric grounds.

Bearing in mind, now, the unusual observations made with the hmpa complexes of scandium(III), yttrium(III), gallium(III) and indium(III)[107] in solution, it seems that the peculiar nature of the hmpa molecule itself is mainly responsible for the 'abnormally' low ligand exchange rates and the presence of more than one solvento complex of hmpa. For the same reasons given for the scandium(III)/hmpa system no attempt was made here to extract kinetic data from the coalescing lineshapes.

5.5 The yttrium(III)/triphenylphosphineoxide system

The air stable complex $[Y(tppo)_4](ClO_4)_3$ was very soluble in CD_2Cl_2. The solid state infra-red spectrum of the complex (Appendix 1) was consistent with the absence of water and coordinated perchlorate. The latter result could be considered a puzzling one since $[Sc(tppo)_4](ClO_4)_3$ [110] reportedly has coordinated perchlorate whilst $[In(tppo)_4](ClO_4)_3$ [136] does not. For indium(III) and yttrium(III), the bulk of the tppo molecule and concomitant crystal packing effects presumably prevent these ions from achieving a higher coordination number than four in the solid state, but it is hard to comprehend the result for the smaller scandium(III) ion in steric terms. ^1H n.m.r. spectra of a solution of $[Y(tppo)_4](ClO_4)_3$ in CD_2Cl_2 were difficult to interpret because of the complexity of the aromatic region. ^1H decoupled ^{31}P n.m.r. spectra, on the other hand, were much simpler. Throughout the liquid temperature range of CD_2Cl_2 only one sharp ^{31}P doublet resonance (J (^{89}Y - ^{31}P) = 12.4 Hz) was

exhibited. The situation became much more complicated when free tppo was added to the solution above. Figure 5.5 is a ^{31}P spectrum of a CD_2Cl_2 solution of $[Y(tppo)_4](ClO_4)_3$ and tppo at 228 K. Doublet (a) (J = 13.5 Hz) is assigned to $[Y(tppo)_6]^{3+}$, doublet (b) (J = 12.5 Hz) to $[Y(tppo)_5]^{3+}$ (again, no evidence for slow intramolecular exchange) doublet (c) (J = 12.4 Hz) to $[Y(tppo)_4]^{3+}$ and the relatively broad upfield singlet is due to free tppo. (There is no apparent reason for the broadness.) As the temperature was increased or [tppo] decreased the yttrium(III) species of lower coordination number were favoured. At 200 K for the solution in Figure 5.5, the average coordination number was 4.8 and at 240 K it was 4.4. For all solutions examined the apparent coordination number at 300 K was four. Coalescence of resonances from free and coordinated tppo occurred well above room temperature and hence intermolecular tppo exchange on yttrium(III) is slow compared to that on magnesium(II). The width at half height, $w_{\frac{1}{2}}$, of the coordinated tppo ^{31}P signal at 300 K remained constant at about 37 Hz over the fourfold [tppo] range investigated. The natural ^{31}P linewidth for $[Y(tppo)_4]^{3+}$ < 1 Hz so that the rate constant at 300 K for ligand exchange on $[Y(tppo)_4]^{3+}$ may be approximately evaluated using the relationship below.

$$k_{ex} \simeq \Pi w_{\frac{1}{2}} \simeq 116\ s^{-1} \quad \text{(at 300 K)}$$

There is an obvious similarity between this system and the hmpa system discussed in the last Section. Both hmpa and tppo are unusually powerful bases and much more bulky than most of the other ligands mentioned in this report. The slowness of ligand exchange on yttrium(III) when the ligand is hmpa or tppo suggests that the exchange of these ligands on other labile metal ions such as lanthanum(III) could also be slow.

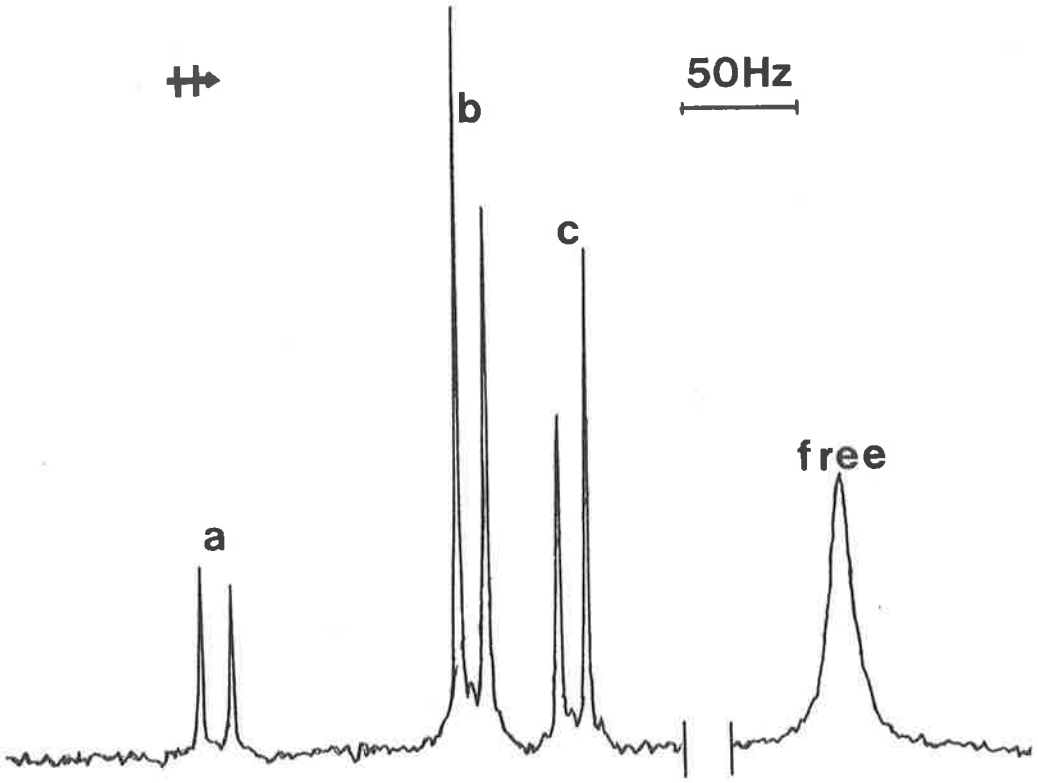

FIGURE 5.5 ^{1}H decoupled ^{31}P FT n.m.r. spectrum of a solution of $[Y(tppo)_4](ClO_4)_3$ (80 mg/ml) and tppo (55 mg/ml) in CD_2Cl_2 at 228 K. Doublet (a) is assigned to $[Y(tppo)_6]^{3+}$, (b) to $[Y(tppo)_5]^{3+}$ and doublet (c) is assigned to $[Y(tppo)_4]^{3+}$. The chemical shift separation between the centre of doublet (c) and free tppo is 382 Hz.

5.6 N-methylacetamide, N,N-dimethylacetamide, N,N-diethylacetamide and dimethylsulphoxide complexes of yttrium(III)

The hygroscopic complexes $[Y(nma)_6](ClO_4)_3$, $[Y(dma)_6](ClO_4)_3$ and $[Y(dea)_6](ClO_4)_3$ were easily prepared according to the usual procedure and all had ionic perchlorate only. Moeller and Vicentini[137] using a synthetic method involving a large excess of dma have prepared $[Y(dma)_7](ClO_4)_3$. They detected no coordinated perchlorate and demonstrated that all seven dma ligands bond to yttrium(III) through the carbonyl oxygen of the amide.

Under the experimental conditions given in Chapter 7, an air stable compound of stoichiometry $[Y(dmso)_{7.37}](ClO_4)_3$ was isolated (all the dmso ligands appeared to be directly coordinated). Krishnamurthy and Soundararajan[138] have prepared $[Y(dmso)_7](ClO_4)_3$ but Kawashita Kuya and coworkers[139] noted that the conditions of precipitation and the choice of solvent seem to be important in determining composition. They have also prepared non-stoichiometric dmso hexafluorophosphate complexes with a range of lanthanides[139].

For the four above-mentioned ligands, exchange on yttrium(III) was found to be in the fast exchange limit of the ^1H n.m.r. time scale even over extended free ligand concentration ranges. As a result of the observed solubilities of the complexes in CD_2Cl_2, CD_3CN and CD_3NO_2, the lowest temperature attainable for the dma and dea systems was 180 K; for nma, 225 K and for the dmso system, 245 K. The proportion of *cis* nma observed for a solution of $[Y(nma)_6](ClO_4)_3$ in CD_3CN varied from $\sim$6.0% at 230 K to $\sim$7.7% at 330 K. These isomer values are slightly less than those noted for $[Sc(nma)_6](ClO_4)_3$ in CD_3CN and much less than the value for $[Al(nma)_6](ClO_4)_3$ [140] in CD_3NO_2 at 300 K (16.3%). One possible explanation is as follows:-

Cis nma is expected to be more sterically favoured to coordinate to a metal ion since the N-methyl group is oriented away from the metal centre. When the steric crowding near the metal centre increases as the ionic radius of the metal ion decreases, the proportion of *cis* isomer will tend to increase.

5.7 Trimethylphosphate and dimethylmethylphosphonate complexes of yttrium(III)

$[Y(tmp)_6](ClO_4)_3$ was the hygroscopic product obtained using the standard synthesis and tmp as ligand. Recrystallization from a dichloromethane/tmp/ether solution (see Chapter 7) yielded a hygroscopic complex of the formula $[Y(tmp)_6](ClO_4)_3 - 1.87 - tmp$. The extra 1.87 tmp molecules in the lattice are not directly coordinated to yttrium (i.e. tmp of crystallization) as may be ascertained from the following two pieces of evidence. The first is the presence of a shoulder (at higher wavenumber) on the main phosphoryl infra-red absorption band for the compound (Appendix 1). Secondly, when $[Y(tmp)_6](ClO_4)_3 - 1.87 - tmp$ was subjected to a rarefied atmosphere it was eventually reduced to $[Y(tmp)_6](ClO_4)_3$.

The air stable complex, $[Y(dmmp)_6](ClO_4)_3$, was prepared in a straightforward manner.

^1H and ^{31}P n.m.r. spectra of $[Y(tmp)_6](ClO_4)_3$ and tmp in CD_2Cl_2 at 180 K were consistent with the occurrence of rapid tmp exchange between coordinated and free sites. No kinetic data could be acquired. A similar predicament arose for $[Y(dmmp)_6](ClO_4)_3$/dmmp/CD_3CN solutions.

CHAPTER 6 GENERAL REMARKS CONCERNING THE LABILITIES OF MG(II), SC(III) AND Y(III) IONS

6.1 The extrathermodynamic relationship between $\Delta H^{\ddagger}$ and $\Delta S^{\ddagger}$

If all ligand exchange reactions on a given metal ion proceeded at the same rate at some particular temperature and if the characteristic rates for all metal ions had been established at the universal temperature, it would be a simple matter to meaningfully compare metal ion labilities. Unfortunately, the rate determining factors arise not only from the properties of the metal ion but also from characteristics of the ligand and diluent. Nevertheless, the pedagogic concept of a definite 'overall' metal ion lability does appear to have merit for many metal ions interacting with certain simple ligands[122,141].

The accumulation of kinetic data for magnesium(II), scandium(III) and yttrium(III) complexes with various unidentate oxygen donor ligands now facilitates comparisons of the overall labilities of these metal ions with those of well-known ions towards ligand exchange. A method of comparison, based on plots of $\Delta H^{\ddagger}$ versus $\Delta S^{\ddagger}$ (Figure 6.1) for ligand exchange on the relevant metal ions will now be discussed.

Several authors[40,141] have found that an apparent linear relationship exists between $\Delta H^{\ddagger}$ and $\Delta S^{\ddagger}$ for dissociative-type exchange processes on a given metal ion. This extrathermodynamic relationship, $\Delta H^{\ddagger} = \Delta G^{\ddagger} + T\Delta S^{\ddagger}$, is sometimes called the isokinetic effect. In particular, for ligand exchange on bivalent metal ions such correlations have been noted and several explanations proposed[40,142,144]. Bennetto and Caldin have interpreted the isokinetic effect on the basis of structural properties of the solvent (which are represented by its

FIGURE 6.1 $\Delta H^{\ddagger}$ versus $\Delta S^{\ddagger}$ for ligand exchange on scandium(III) (upper data set) and magnesium(II) (lower data set). Individual exchange systems are identified as: identifying number: exchanging ligand: diluent; and the following diluent abbreviations are used; CD_3CN, an; CD_3NO_2, nm; CD_2Cl_2, cd; $C_2H_2Cl_4$, ch; $(CD_3)_2CO$, ac. For six-coordinate scandium(III), circles denote systems in which exchange occurs through a D mechanism alone: 1): tmu: nm; 2): tmu: an; 3): tmp: ch; 4): tmp: an. Squares denote that exchange occurs through an A mechanism alone: 5): dmmp: nm; 6): tmp: nm. Inverted triangles and triangles respectively denote the A and D data from two term rate laws: 7): dea: nm; 8): dea: an; 9): dmmp: an; 10): nma: an; 11): dma: an; 12): dma: nm. All of the six-coordinate magnesium(II) systems undergo ligand exchange through D mechanisms: 13): dmf: cd; 14): MeOH: no diluent; 15): tmp: cd; 16): EtOH: no diluent; 17): acetone: no diluent; 19) H_2O: no diluent; 20): tmp: ac; 21): dmf: ac. System 18) refers to ligand exchange on $[Mg(tppo)_5]^{2+}$ in cd. The solid line through the scandium(III) data is the linear regression line for systems 1) - 4) inclusive, and that through the magnesium(II) data is the linear regression line for systems 13) - 21) excluding 14).

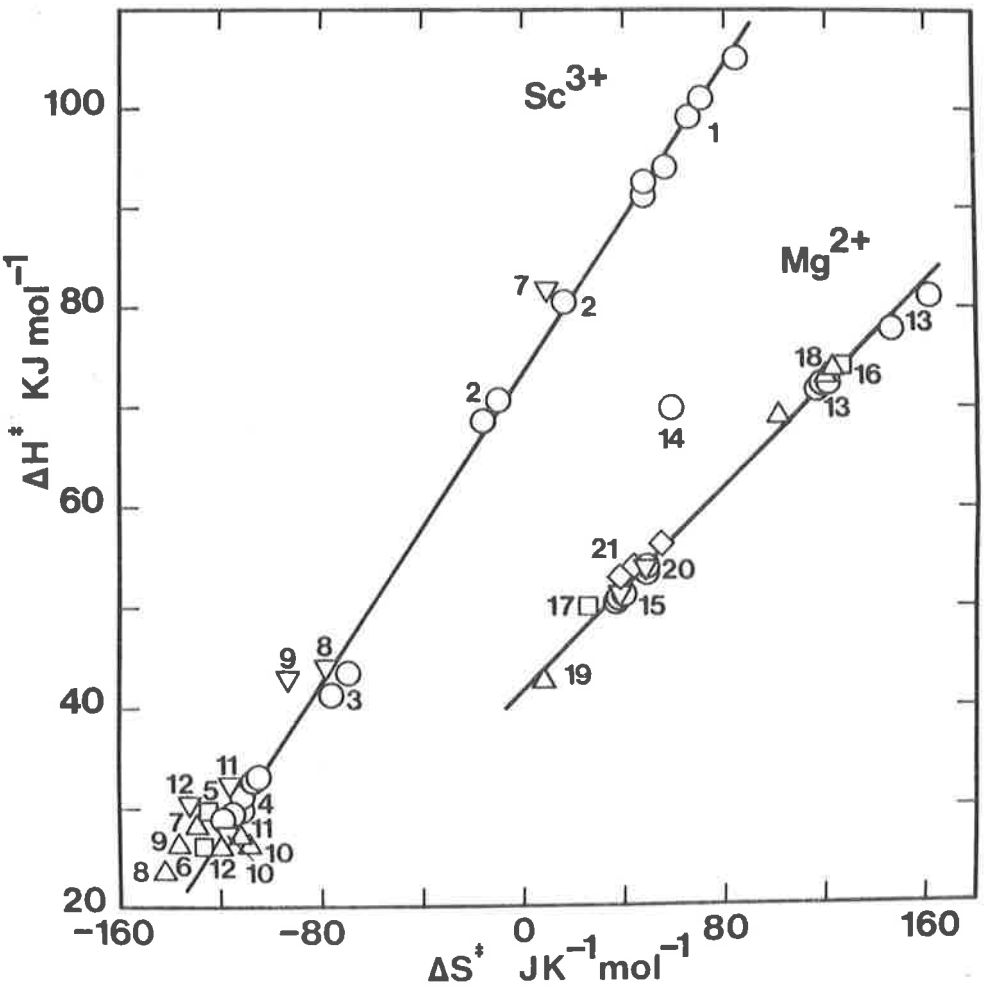
Sc3+
Mg2+
ΔH‡ KJ mol-1
ΔS‡ JK-1mol-1
100
80
60
40
20
-160
-80
0
80
160

heat of vapourization and fluidity)[40]. Fischer, Hoffmann and Platz[144] have asserted that changes in the degrees of freedom for rotation and vibration in the transition state are responsible for their $\Delta H^{\ddagger}/\Delta S^{\ddagger}$ correlation. If this linearity is real, the implication is that at a particular temperature, the isokinetic temperature (given by the slope of the $\Delta H^{\ddagger}/\Delta S^{\ddagger}$ plot), the rate constants of all reactions which have associated $\Delta H^{\ddagger}/\Delta S^{\ddagger}$ points on this line will be identical. Hence it has been implied[141,145] that the overall lability comparisons between metal ions may be made by referring to $\Delta H^{\ddagger}$ intercepts ($\Delta G^{\ddagger}$) for respective lines provided that they are roughly parallel. The higher the intercept, the less labile is the ion. Lincoln[76,141] has interpreted empirical results largely in terms of electrostatic interactions. On the basis of the relative position of $\Delta H^{\ddagger}/\Delta S^{\ddagger}$ data for the uranyl ion, he has inferred that the surface charge density of this ion is between those of typical bivalent and trivalent metal ions.

Ligand exchange $\Delta H^{\ddagger}/\Delta S^{\ddagger}$ data for magnesium(II) (including the data for $[Mg(tppo)_5]^{2+}$) which are thought to characterize D mechanisms exhibit a fair linear relationship ($R^2 = 0.936$; Table 6.1). The exclusion of the datum point for $[Mg(MeOH)_6]^{2+}$ greatly improves the linearity ($R^2 = 0.994$). It is possible to test whether the apparent linear relationship is of chemical origin (*vide supra*) or arises solely out of an enthalpy-entropy compensation effect by the application of the hypothesis test of Krug, Hunter and Grieger[146]. They have shown that if the temperature range over which rate measurements are made is small, large statistical errors associated with $\Delta H^{\ddagger}$ and $\Delta S^{\ddagger}$ will generate a highly linear $\Delta H^{\ddagger}/\Delta S^{\ddagger}$ plot such that the slope or isokinetic temperature is close to the harmonic mean of

TABLE 6.1 *Statistical data for Mg(II) and Sc(III) ligand exchange systems*

	N[a]	T_{hm} K	m[b]	$\hat{\beta}$[c] K	95% C.I. of $\hat{\beta}$ K	$\Delta G^{\ddagger}$ kJ mol^{-1}	R^2[d]
All Mg^{2+} systems	228	226.6	22	247.7	277.8, 217.6	43.0	0.936
All Mg^{2+} systems except $[Mg(MeOH)_6]^{2+}$	209	223.9	21	252.8	262.4, 243.2	42.0	0.994
All Sc^{3+} systems	-	-	31	376.8	391.1, 362.5	73.7	0.990
All dissociative Sc^{3+} systems	-	-	17	385.3	394.7, 375.9	73.3	0.998

a N = number of experimental temperatures.

b m = number of $\Delta H^{\ddagger}/\Delta S^{\ddagger}$ pairs.

c $\hat{\beta}$ = estimate of isokinetic temperature by linear regression.

d R^2 = square of linear correlation coefficient.

the experimental temperatures. The application of the hypothesis test is of some relevance since, as far as the author is aware, no statistical assessment of $\Delta H^{\ddagger}/\Delta S^{\ddagger}$ plots has been undertaken for such solvent exchange systems. Previous arguments have been founded on comparisons of the estimated error limits in experimental $\Delta H^{\ddagger}$ and $\Delta S^{\ddagger}$ values (ca. ± 2 kJ mol^{-1} in $\Delta H^{\ddagger}$) with the range of $\Delta H^{\ddagger}$ and $\Delta S^{\ddagger}$ values observed.[40] (The variation in $\Delta H^{\ddagger}$ may exceed 70 kJ mol^{-1}.) According to Krug, Hunter and Grieger the null hypothesis is that the slope of the $\Delta H^{\ddagger}/\Delta S^{\ddagger}$ line, β, is equal to the harmonic mean of the experimental temperatures, T_{hm}.

$$H_0 : \beta = T_{hm}$$

If T_{hm} lies outside the 95% confidence interval for $\hat{\beta}$ (the estimated slope by linear regression) then the null hypothesis may be rejected with 95% certainty and the linear relationship between $\Delta H^{\ddagger}$ and $\Delta S^{\ddagger}$ is of some chemical origin. Using this method, the results for magnesium(II) systems may be seen from Table 6.1. The hypothesis may be rejected with 95% confidence if the data for $[Mg(MeOH)_6]^{2+}$ are neglected. Otherwise, a statistical compensation effect could be the sole cause for the observed linearity. The reason for the behaviour of the $[Mg(MeOH)_6]^{2+}$ system is not understood.

In the case of the $\Delta H^{\ddagger}$ and $\Delta S^{\ddagger}$ data for scandium(III) systems which undergo exchange through a D mechanism alone there is an excellent linear correlation ($R^2 = 0.998$). Since the upper limit of the 95% confidence interval for $\hat{\beta}$ is 375.9 K, which is greater than the highest temperature examined, the null hypothesis may be rejected despite the fact that the harmonic mean of the experimental temperatures is not given. Furthermore, it is significant that if

all $\Delta H^{\ddagger}/\Delta S^{\ddagger}$ information (regardless of mechanism) is analysed in this way the null hypothesis may still be rejected. The harmonic mean of the experimental temperatures is certainly less than 362.5 K. There seems to be no justification in examining the yttrium(III) data because there are only seven points at present which are 'bunched together'.

If $\Delta H^{\ddagger}/\Delta S^{\ddagger}$ data for specific dissociative ligand exchange systems (Figure 6.1) are considered, there is for some systems a systematic variation in $\Delta H^{\ddagger}$ and $\Delta S^{\ddagger}$ as the concentrations of species are varied (e.g. $[Sc(tmu)_6]^{3+}$/tmu/CD_3CN system) whereas for others there is some randomness in the variation of $\Delta H^{\ddagger}$ and $\Delta S^{\ddagger}$. For the latter cases it is possible that experimental error produces a substantial amount of internal $\Delta H^{\ddagger}/\Delta S^{\ddagger}$ compensation resulting in an apparent isokinetic relationship within the measured $\Delta H^{\ddagger}/\Delta S^{\ddagger}$ limits of the exchange system (e.g. for $[Sc(tmu)_6]^{3+}$ in CD_3NO_2). In the former systems the systematic $\Delta H^{\ddagger}/\Delta S^{\ddagger}$ variation could reflect changes in the environment beyond the first coordination sphere[75].

Having established that an extrathermodynamic relationship does exist for all available scandium(III) $\Delta H^{\ddagger}/\Delta S^{\ddagger}$ data, it is likely that it exists for data for other metal ions as well (e.g. aluminium(III)). Therefore, lines corresponding to different metal ions may be drawn on a graph of $\Delta H^{\ddagger}$ versus $\Delta S^{\ddagger}$ and some kinetic conclusions reached based on the empirical observations. Figure 6.1 depicts the two lines for magnesium(II) and scandium(III). It has become clear from Chapter 3 and Chapter 4 that six-coordinate magnesium(II) is generally more labile than six-coordinate scandium(III) and this is reflected in the $\Delta H^{\ddagger}$ intercepts (as has been predicted[141,145]). The yttrium(III) 'line' is not shown in Figure 6.1 for sake of clarity.

Data for the $[Y(tmu)_6]^{3+}$ system are not meaningfully distinguishable from some of the data for scandium(III) systems whilst data for the more labile mmpp system are displaced down from the scandium(III) line.

The aluminium(III) line, derived from a recent compilation of data for ligand exchange on Al^{3+} (slope ≃ 410 K, intercept ≃ 69.5 kJ mol^{-1}), is in close proximity to that for scandium(III). The limitations of a simple electrostatic interpretation now become clearer. If the relationship between the $\Delta H^{\ddagger}$ intercept and the surface charge density of the ion were exact, the smaller aluminium(III) centre should produce a significantly greater intercept than does scandium(III), but this is not what is observed. The discrepancy has been ascribed to differences in bonding which are superimposed upon the ion-dipole interaction[122].

Beryllium(II) $\Delta H^{\ddagger}/\Delta S^{\ddagger}$ data (Chapter 1) also lie near the scandium(III) line implying a comparable overall lability for this ion. As far as gallium(III) and indium(III) are concerned there is probably not enough information to really use, although, on the grounds of respective ionic radii, indium(III) and yttrium(III) should be similar in overall lability.

6.2 Concluding remarks

Four- , five- and six-coordinate complexes of magnesium(II), scandium(III) and yttrium(III) have been observed in non-aqueous solution. The coordination number reflects a balance of many forces, the major ones arising from the character of the metal-ligand bond and steric interactions. The kinetics of ligand exchange also

depends on the interplay of many competing forces. Interactions both within and outside the first coordination sphere may influence the energetics. It seems that, with few exceptions, the kinetic importance of interaction decreases with distance away from the metal centre. This has been dramatically highlighted by the behaviour of the scandium(III)/amide systems which represent the most methodically studied ligand exchange systems to date.

Ligand exchange on magnesium(II) has been seen to be primarily dissociative in nature whereas the exchange on scandium(III) and yttrium(III) may be dissociatively and/or associatively activated.

CHAPTER 7 EXPERIMENTAL DETAILS

7.1 Origin and purification of chemicals

7.1.1 *Perchlorates*

Hydrated magnesium perchlorate
Hydrated scandium perchlorate
Hydrated yttrium perchlorate
} (G. Frederick Smith)

These perchlorates were used without further purification and were analysed for metal content by an ion exchange method described by Vogel[147].

7.1.2 *Dehydrating agents*

Triethylorthoformate (Koch-Light) was used as received. Linde 4A molecular sieves were soaked in distilled water and ethanol to remove surface impurities and then activated by heating in a furnace at 620 K for ten hours.

7.1.3 *Liquid ligands*

Nmf (B.D.H.), nma (B.D.H.), dmf (B.D.H.), dma (B.D.H.), def (Fluka), dea (Fluka), dbf (Aldrich), dmso (B.D.H.), tmp (B.D.H.), dmmp (Pfaltz and Bauer), mmpp (Strem) and hmpa (Koch-Light) were firstly dried by agitation over molecular sieves then fractionally distilled under reduced pressure. They were stored over molecular sieves in a dry box.

7.1.4 *Solid ligands*

Npa (Aldrich), dmu (Fluka), tmtu (Fluka) and tso (Aldrich) were dried *in vacuo* over P_2O_5 for several days before use. Tppo was recrystallized from ethanol/ether solution. It was subsequently dried at 350 K *in vacuo* over P_2O_5 for one week.

7.1.5 *Diluents*

CD_2Cl_2 (C.E.A., France, 99.4%), $(CD_3)_2CO$ (C.E.A., France, 99.8%), CD_3CN (C.E.A., France, 99.6% and Aldrich, 99%) and CD_3NO_2 (C.E.A., France, 99.3%) were purified by distillation and then thoroughly dried over molecular sieves. 1,1,2,2-tetrachloroethane (B.D.H.) was purified according to a published procedure[148] and then stored over molecular sieves.

7.2 Preparation of solvento complexes

7.2.1 *Précis*

The synthetic procedure used was basically that of van Leeuwen and Groeneveld[149]. Ideally, the hydrated metal perchlorate salt is dissolved in excess triethylorthoformate at 330 K whereupon an acid catalysed dehydration reaction occurs converting aqua ligands to ethanol. If an appropriate alternative ligand is added to the reaction mixture replacement of coordinated ethanol ensues producing the required solvento complex. The main synthetic difference between individual metal complex preparations in this report lies in the method of isolating the solvento complex as a crystalline salt.

7.2.2 *Details of individual preparations*

Number	Name of complex
1.	Hexakis(dimethylsulphoxide)scandium(III) perchlorate
2.	Hexakis(N-methylacetamide)scandium(III) perchlorate
3.	Hexakis(N,N-dimethylacetamide)scandium(III) perchlorate
4.	Hexakis(N,N-diethylacetamide)scandium(III) perchlorate
5.	Hexakis(1,1,3,3-tetramethylurea)scandium(III) perchlorate
6.	Hexakis(1,3-dimethylurea)scandium(III) perchlorate-ethanol
7.	Hexakis(trimethylphosphate)scandium(III) perchlorate

8. Hexakis(dimethylmethylphosphonate)scandium(III) perchlorate

9. Hexakis(N-methylacetamide)yttrium(III) perchlorate

10. Hexakis (N,N-dimethylacetamide)yttrium(III) perchlorate

11. Hexakis(N,N-diethylacetamide)yttrium(III) perchlorate

12. Hexakis (1,1,3,3-tetramethylurea)yttrium(III) perchlorate

13. Hexakis(trimethylphosphate)yttrium(III) perchlorate

14. Hexakis(dimethylmethylphosphonate)yttrium(III) perchlorate

General preparative scheme:-

The hydrated metal perchlorate (x mol) was dissolved in triethylorthoformate (20 x mol) and stirred at 330 K for about one hour. Atmospheric moisture was excluded by the use of a silica gel guard tube. The appropriate dry ligand (ca. 6.6 x mol, unless otherwise specified) was subsequently added to the mixture.

Complexes 1 - 14 precipitated from solution at this point. The crystalline product was filtered and washed with sodium-dried ether before being vacuum-dried (except complex 6) to remove volatile impurities. All operations subsequent to the dehydration step were performed in a dry box under a dry nitrogen atmosphere. Yields for all preparations were virtually quantitative unless otherwise specified.

15. Tetrakis(triphenylphosphineoxide)magnesium(II) perchlorate

16. Tetrakis(triphenylphosphineoxide)yttrium (III) perchlorate

These two complexes were prepared in a similar manner to the ones above except that

(a) tppo was added as a solution in dry ethanol and

(b) sodium-dried benzene was used to wash excess tppo from the filtered complex.

17. Pentakis(N-methylacetamide)magnesium(II) perchlorate

18. Hexakis(N-methylformamide)magnesium(II) perchlorate

19. Hexakis(N,N-dimethylformamide)magnesium(II) perchlorate

20. Hexakis(N,N-dimethylformamide)scandium(III) perchlorate

21. Hexakis(4,4'-ditolylsulphoxide)scandium(III) perchlorate

Complexes 17 - 21 were prepared according to the preparative scheme above but dry ether was required to induce crystallization (solvento complexes 18 and 21 initially appeared as oils). Tso was added as a solution in dry ethanol.

22. 5.75(trimethylphosphate)magnesium(II) perchlorate

23. Hexakis(N,N-diethylformamide)scandium(III) perchlorate

24. Hexakis(N,N-di-n-butylformamide)scandium(III) perchlorate

25. Hexakis(methylmethylphenylphosphinate)yttrium(III) perchlorate

Complexes 22 - 25 were synthesized according to the scheme above except that after the ligand was added, the reaction mixture was reduced in volume (∿60%) on a vacuum line to induce crystallization of the complex.

26. Hexakis(N-phenylacetamide)scandium(III) perchlorate

This compound initially formed as an oil when npa was added to the dehydration mixture. The oil was treated with dry ether and then with dry dichloromethane whereupon off-white crystals were obtained. Recrystallization from a mixture of acetonitrile, npa and ether yielded white crystals which were vacuum-dried for several hours to remove acetonitrile of crystallization.

27. Hexakis(1,3-dimethylurea)scandium(III) perchlorate - dichloromethane

Complex 6 was used as the starting material. $[Sc(dmu)_6](ClO_4)_3.EtOH$ was dissolved in a minimum volume of CH_3CN/dmu (10:1 by weight) and dichloromethane then added to precipitate complex 27. The crystals

were washed with dichloromethane but not vacuum-dried (Complex 27 loses dichloromethane slowly giving $[Sc(dmu)_6](ClO_4)_3$.).

28. 4.32(hexamethylphosphoramide)scandium(III) perchlorate

The general preparative scheme was employed (hydrated scandium perchlorate : 3.7 mmol; triethylorthoformate : 135 mmol; hmpa : 28 mmol).

29. 4.97(hexamethylphosphoramide)scandium(III) perchlorate

Complex 28 was used as the starting material. It was dissolved in CH_3CN/hmpa (the hmpa : Sc^{3+} mole ratio ~10:1) and upon addition of sodium-dried ether complex 29 was obtained.

30. 5.12(hexamethylphosphoramide)yttrium(III) perchlorate

The general preparative scheme was again employed (hydrated yttrium perchlorate : 5.1 mmol; triethylorthoformate : 148 mmol; hmpa : 35 mmol).

31. 7.37(dimethylsulphoxide)yttrium(III) perchlorate

The general preparative scheme was used (hydrated yttrium perchlorate : 2.4 mmol; triethylorthoformate : 60 mmol; dmso : 23 mmol).

32. Hexakis(trimethylphosphate)yttrium(III) perchlorate — 1.87 — tmp

Compound 13 was used as the starting material. It was dissolved in CH_2Cl_2/tmp (mole ratio tmp : Y^{3+} ~16:1) and after addition of ether, compound 32 formed as a precipitate. The yield was 80%.

No suitable synthetic route was found for the preparation of crystalline complexes with the following metal/ligand combinations:-

Combination	Observations
Scandium - mmpp	oil failed to crystallize
Scandium - tmtu	
Yttrium - tmtu	
Magnesium - tmu	unstable solid tending to form an oil especially under reduced pressure
Yttrium - dmf	
Magnesium - tmtu	precipitation of $[Mg(EtOH)_6](ClO_4)_2$

The handling of all of the perchlorate salts above is potentially dangerous. However, high temperatures (usually in excess of 470 K) or quite violent shocks are required[109] to cause explosion and hence under normal circumstances they should be considered safe to use. No problems were encountered with the dehydration step although this reaction is potentially dangerous due to possible oxidation of the organic species present.

7.3 Elemental analyses

Complexes were analysed for metal content by an ion exchange/titration method (using Dowex 50 W ion exchange resin) described by Vogel[147]. Those which had poor solubility in water (marked with an asterisk below) were loaded on the column as solutions in 50% v/v ethanol/water. Measurements of pH performed in aqueous ethanol (up to 90% ethanol[150]) are known to accurately reflect aqueous pH values and hence this technique is applicable to the compounds designated in Table 7.1. Microanalyses of complexes were executed by the Australian Microanalytical Service, Melbourne.

TABLE 7.1 *Analytical results*

Compound		% Metal	% C	% H	% N, P or S
1. $[Sc(dmso)_6](ClO_4)_3$	calcd.	5.54	17.75	4.47	23.7
	found.	5.59	17.59	4.53	23.9
2. $[Sc(nma)_6](ClO_4)_3$	calcd.	5.75	27.65	5.41	10.8
	found.	5.81	27.49	5.40	10.6
3. $[Sc(dma)_6](ClO_4)_3$	calcd.	5.19	33.29	6.29	9.7
	found.	5.18	32.96	5.97	9.6
4. $[Sc(dea)_6](ClO_4)_3$	calcd.	4.35	41.80	7.60	8.1
	found.	4.37	42.03	7.15	8.0
5. $[Sc(tmu)_6](ClO_4)_3$	calcd.	4.32	34.64	6.98	16.2
	found.	4.36	34.24	6.52	15.8
6. $[Sc(dmu)_6](ClO_4)_3.EtOH$	calcd.	4.90	26.17	5.93	18.3
	found.	5.03	25.94	5.74	18.4
7. $[Sc(tmp)_6](ClO_4)_3$	calcd.	3.80	18.25	4.60	15.7
	found.	3.80	18.35	4.60	15.4
8. $[Sc(dmmp)_6](ClO_4)_3$	calcd.	4.13	19.87	5.00	17.1
	found.	4.14	19.60	4.96	16.8
9. $[Y(nma)_6](ClO_4)_3$	calcd.	10.77	26.18	5.13	10.2
	found.	10.71	25.92	4.94	10.2
10. $[Y(dma)_6](ClO_4)_3$	calcd.	9.77	31.68	5.98	9.2
	found.	9.77	31.44	5.97	9.2
11. $[Y(dea)_6](ClO_4)_3$	calcd.	8.25	40.10	7.29	7.8
	found.	8.31	39.52	7.41	7.6
12. $[Y(tmu)_6](ClO_4)_3$	calcd.	8.20	33.23	6.69	15.5
	found.	8.20	33.12	6.60	15.6

TABLE 7.1 *(cont.)*

Compound		% Metal	% C	% H	% N, P or S
13. $[Y(tmp)_6](ClO_4)_3$	calcd.	7.24	17.61	4.43	15.1
	found.	7.08	17.83	4.70	14.5
14. $[Y(dmmp)_6](ClO_4)_3$	calcd.	7.86	19.10	4.81	16.4
	found.	7.72	19.16	4.81	16.2
15. $[Mg(tppo)_4](ClO_4)_2$*	calcd.	1.82	64.71	4.53	9.3
	found.	1.82	64.33	4.52	9.6
16. $[Y(tppo)_4](ClO_4)_3$*	calcd.	5.93	57.64	4.03	8.3
	found.	5.87	57.96	4.21	8.2
17. $[Mg(nma)_5](ClO_4)_2$	calcd.	4.13	30.60	5.99	11.9
	found.	4.02	30.95	6.21	12.0
18. $[Mg(nmf)_6](ClO_4)_2$	calcd.	4.21	24.95	5.24	14.6
	found.	4.19	24.68	5.21	14.8
19. $[Mg(dmf)_6](ClO_4)_2$	calcd.	3.67	32.67	6.40	12.7
	found.	3.73	31.77	6.46	12.3
20. $[Sc(dmf)_6](ClO_4)_3$	calcd.	5.75	27.65	5.41	10.8
	found.	5.75	27.58	5.47	10.4
21. $[Sc(tso)_6](ClO_4)_3$*	calcd.	2.61	58.49	4.91	
	found.	2.64	58.06	4.91	
22. $[Mg(tmp)_{5.75}](ClO_4)_2$	calcd.	2.37	20.14	5.07	17.3
	found.	2.37	20.08	5.13	17.3
23. $[Sc(def)_6](ClO_4)_3$	calcd.	4.73	37.92	7.00	8.8
	found.	4.80	37.75	6.83	8.8
24. $[Sc(dbf)_6](ClO_4)_3$*	calcd.	3.49	50.40	8.93	6.5
	found.	3.53	50.31	8.56	6.4

TABLE 7.1 *(cont.)*

Compound		% Metal	% C	% H	% N, P or S
25.	$[Y(mmpp)_6](ClO_4)_3$	calcd. 6.31	40.94	4.72	
		found. 6.41	40.80	4.75	
26.	$[Sc(npa)_6](ClO_4)_3$	calcd. 3.90	49.95	4.72	7.3
		found. 3.90	49.67	4.80	7.2
27.	$[Sc(dmu)_6](ClO_4)_3.CH_2Cl_2$ [a]	calcd. 4.70			
		found. 4.78			
28.	$[Sc(hmpa)_{4.32}](ClO_4)_3$	calcd. 4.02			
		found. 4.02			
29.	$[Sc(hmpa)_{4.97}](ClO_4)_3$	calcd. 3.64			
		found. 3.64			
30.	$[Y(hmpa)_{5.12}](ClO_4)_3$	calcd. 6.81	28.28	7.12	16.5 (N)
		found. 6.81	27.66	6.99	15.9
31.	$[Y(dmso)_{7.37}](ClO_4)_3$	calcd. 9.23	18.38	4.63	24.5
		found. 9.23	18.46	4.57	24.7
32.	$[Y(tmp)_6](ClO_4)_3.1.87$ tmp	calcd. 5.97			
		found. 5.97			

[a] loses CH_2Cl_2 of crystallization

7.4 Preparation of n.m.r. samples

Solutions for n.m.r. study generally consisted of solid complex/ligand/inert diluent mixtures. They were prepared by weight in 2 cm^3 volumetric flasks and hence accurate molalities and somewhat less accurate molarities were recorded. Portions ($\sim$0.4 cm^3) of each solution

were degassed and sealed under vacuum in 5 mm o.d. n.m.r. tubes. All operations were performed in a dry box under a dry nitrogen atmosphere to exclude moisture. Non-volumetric glassware was baked in an oven at about 390 K for at least six hours before use. All other items used in the preparation of solutions were thoroughly dried over P_2O_5.

7.5 Spectroscopic measurements

^1H n.m.r. measurements on freshly prepared samples were made with Bruker HX-90-E or Bruker HX-270 instruments at 90 and 270 MHz respectively. Operations were either in pulsed free precession (PFP) or PFT modes. An internal ^2H lock was used with deuterated diluents and an ^1H lock in the case of $C_2H_2Cl_4$. ^{31}P and ^{13}C FT n.m.r. spectra (with ^1H broad band decoupling) were run at 36.43 and 22.63 MHz respectively on the HX-90-E spectrometer with an internal ^2H lock. The sample temperature was monitored by a copper-constantan thermocouple which was periodically checked with standard methanol and ethylene glycol samples[151]. The sample temperature stability was better than ± 0.3 K. Digitized spectra were initially recorded as 1 K (1024 points) data blocks on a Diablo magnetic disk and were later subjected to lineshape analysis utilizing the computer programs for CYBER 173 or Nicolet BNC-12 computers. When necessary, transfer of spectral information between computers was achieved by paper tape.

Infra-red spectra (Appendix 1) were recorded on a Perkin Elmer 457 grating spectrophotometer. All mulls (in nujol) and solutions (using sodium chloride i.r. cells) were prepared under anhydrous conditions immediately prior to infra-red measurements.

APPENDIX 1 SOLID STATE INFRA-RED SPECTRA OF SELECTED COMPLEXES

Infra-red spectroscopy was used to assist characterization of the complexes prepared. This technique should allow differentiation of perchlorate in ionic (T_d symmetry), unidentate (C_{3v}) or bidentate (C_{2v}) forms. Nearly all complexes prepared appeared to have perchlorate in pure ionic form. However, solid state infra-red spectra of the hmpa complexes of scandium and yttrium (*vide infra*) exhibited some bands characteristic of coordinated perchlorate[106].

The expected decrease in C = O, P = O or S = O stretching frequency upon coordination was observed, and is indicative of bonding through oxygen[137,139]. As might be predicted, no O - H stretch due to water was evident in the infra-red spectra. It should be noted that spectra presented in this Appendix relate only to previously unreported complexes or to discussions elsewhere in the text. The corresponding complex numbers (see Chapter 7) appear to the right of the spectra.

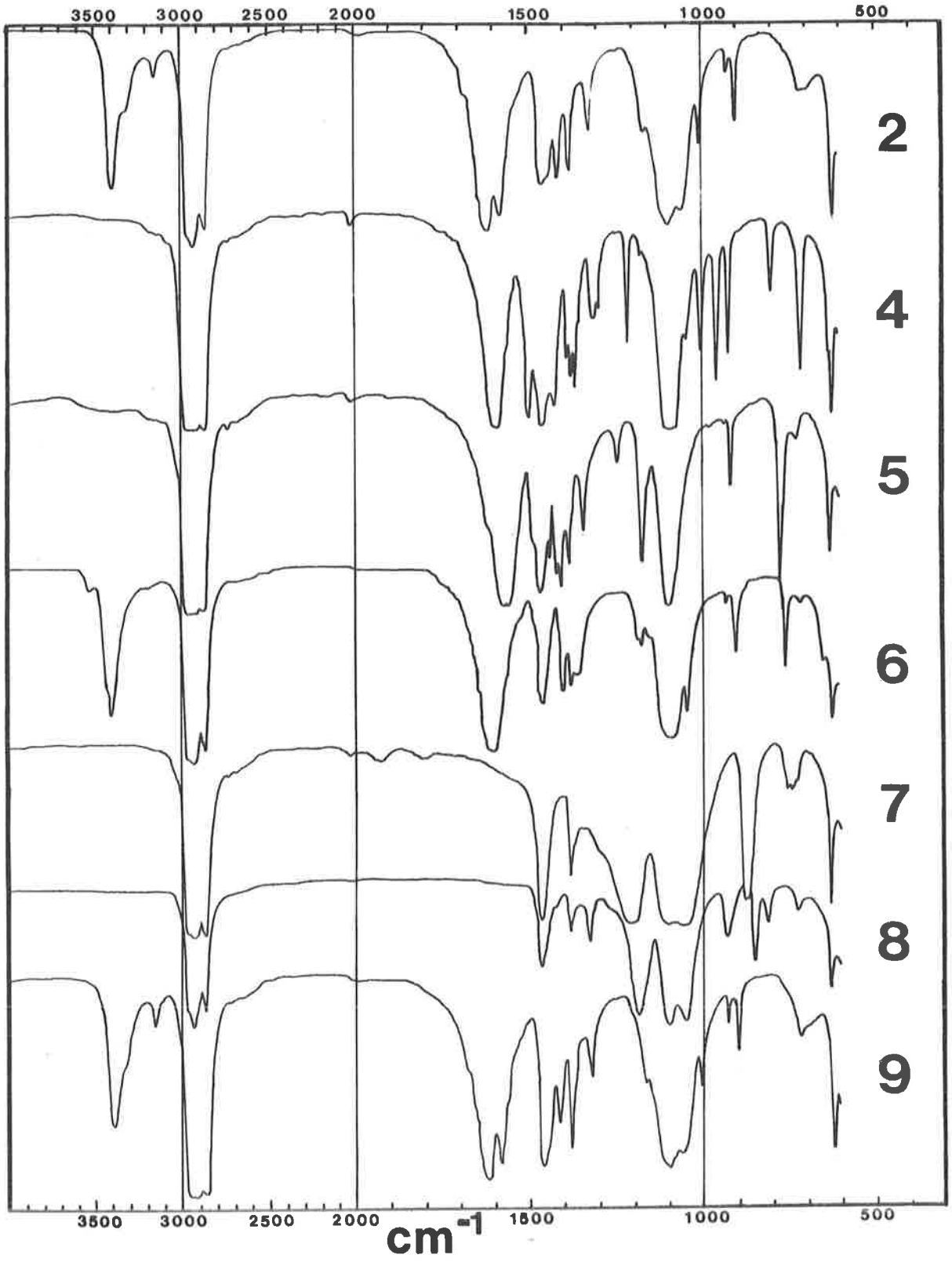
3500
3000
2500
2000
1500
1000
500
2
4
5
6
7
8
9
cm⁻¹

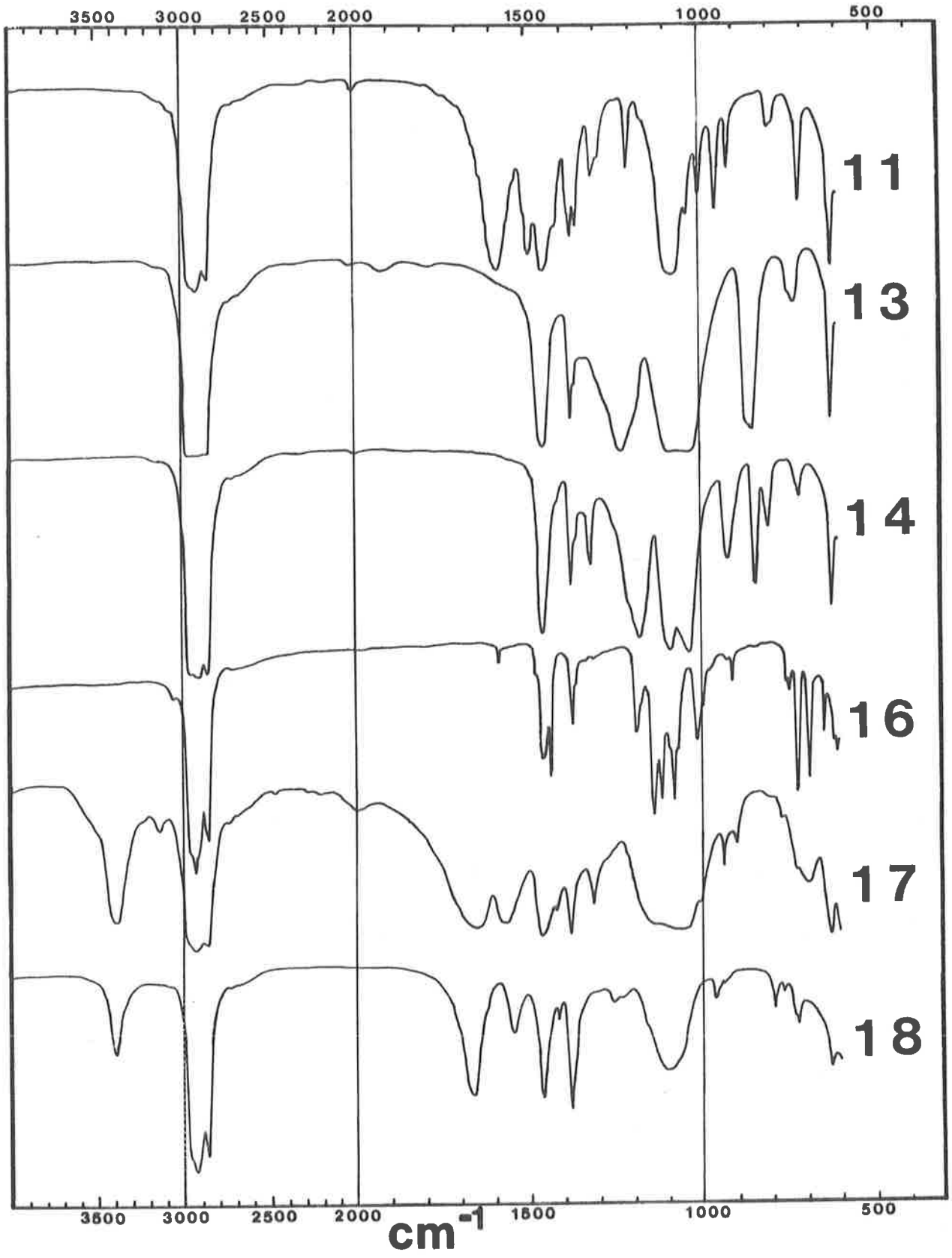
3500
3000
2500
2000
1500
1000
500
11
13
14
16
17
18
cm-1

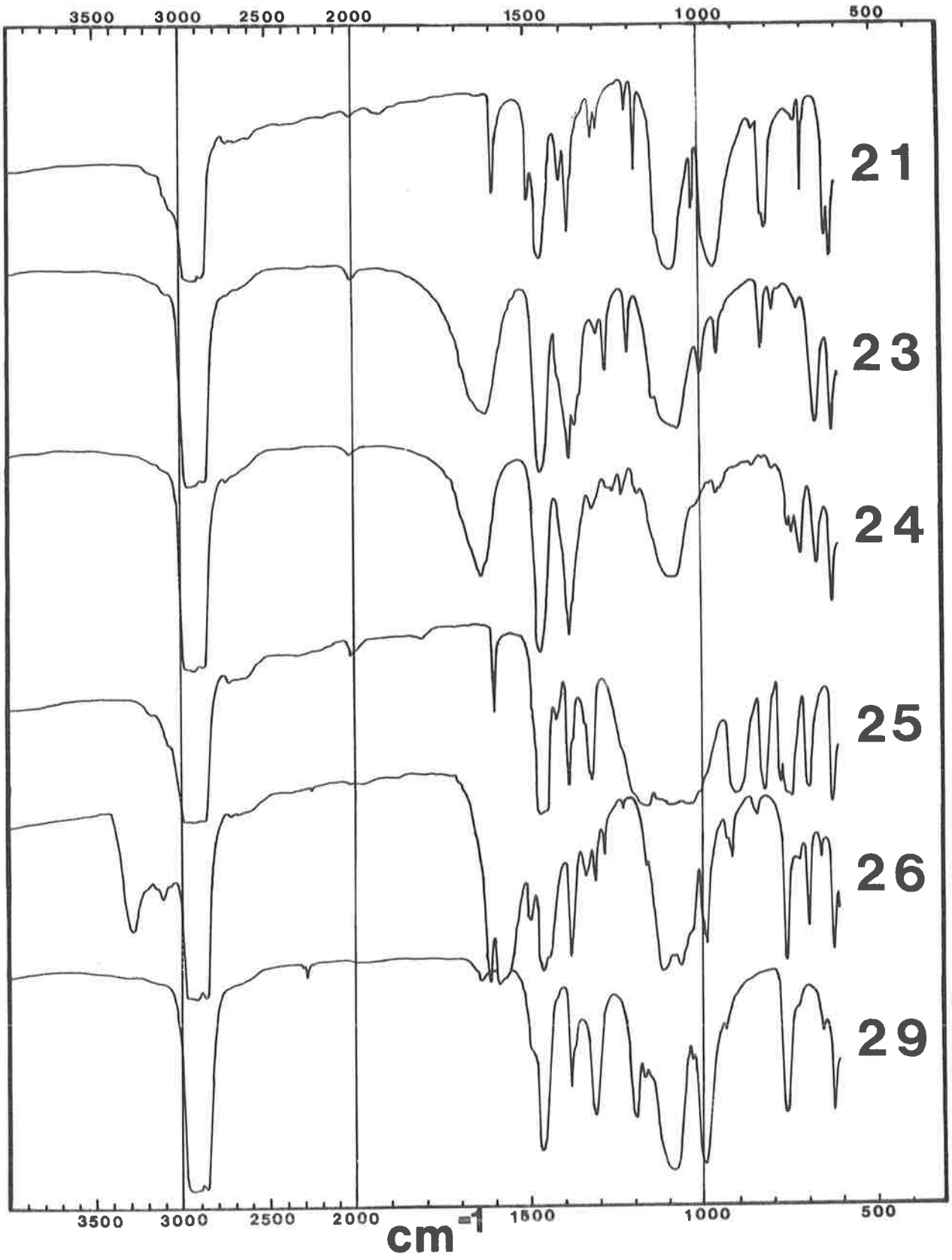
3500
3000
2500
2000
1500
1000
500
21
23
24
25
26
29
cm⁻¹

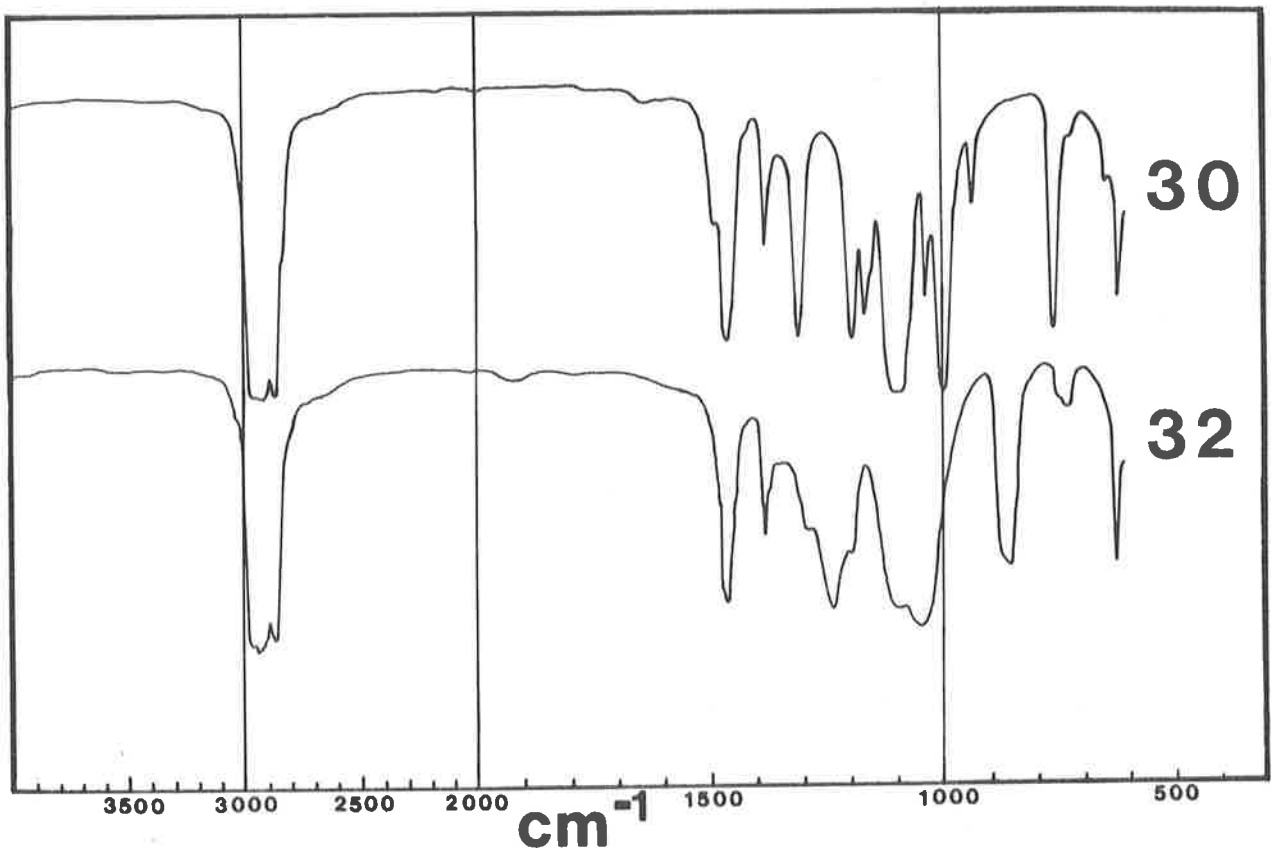
30
32
3500
3000
2500
2000
1500
1000
500
cm-1

APPENDIX 2 THREE SITE EXCHANGE

The Kubo-Sack[56,62-64,152,153] method of introducing chemical exchange into the classical lineshape equations[53] has proved to be very convenient. It handles any number of uncoupled sites through a simple matrix formalism.

The absorption mode lineshape (v) is proportional to

$$\mathrm{Re}(\underline{P} \cdot \underline{A}^{-1} \cdot \underline{1})$$

where Re is the "real part of"

$\underline{P}$ is a row matrix of length N comprising the mole fractions of sites 1 - N

$\underline{A}$ is a N x N complex matrix (Kubo-Sack matrix)

and $\underline{1}$ is the unity column matrix of length N.

$\underline{A}$ is formulated according to

$$\underline{A} = \underline{\Omega} + \underline{D} \qquad \text{(A2.1)}$$

where $\Omega_{ij} = -\delta_{ij}\,\alpha_i$ ($\delta_{ij} = 1$ if $i = j$, otherwise 0)

$D_{ij} = p'_{ij}/\tau_i$ $(i \neq j)$

$D_{ii} = -1/\tau_i$

$\alpha_i = 1/T_{2i} - i(\omega_{0i} - \omega)$ $(i = \sqrt{-1})$

τ_i = mean lifetime of site i

and p'_{ij} = fraction of transfers from site i which terminate in site j.

If we consider a three site situation and if each site is assigned the same lifetime, τ, multiplied by the probability of transfer from that site to another site, p_{11}, p_{21} etc., $\underline{A}$ may be decomposed as in Equation A2.2[53].

$$\underline{A} = \begin{bmatrix} -\alpha_1 & 0 & 0 \\ 0 & -\alpha_2 & 0 \\ 0 & 0 & -\alpha_3 \end{bmatrix} + \begin{bmatrix} p_{11} & p_{12} & p_{13} \\ p_{21} & p_{22} & p_{23} \\ p_{31} & p_{32} & p_{33} \end{bmatrix} \times \tau^{-1} \qquad \text{(A2.2)}$$

Here the exchange rate = τ^{-1}. The problem now simplifies to selecting the transfer probabilities characterizing the three site exchange process. Procedures for deriving transfer probabilities, p_{ij}, have been described by Johnson and Moreland[71]. In practice, subroutine THRSITE of a modified version of MATCH was used to compute the lineshape. The IMSL (International Mathematical and Statistical Library) subroutine LEQT1C performed the 3 × 3 complex matrix inversion for every point of the theoretical spectrum.

LIST OF PUBLICATIONS

Some of the material in this thesis has already appeared in the chemical literature. The relevant papers are listed below.

1. *"Nuclear Magnetic Resonance Study of Ligand Exchange on the Hexakis(trimethylphosphate)scandium(III) Ion"*., by D.L. Pisaniello, S.F. Lincoln and E.H. Williams, *J. Chem. Soc. Chem. Commun.*, 1047 (1978).

2. *"Exchange of Trimethylphosphate on Magnesium(II). A Phosphorus-31 Nuclear Magnetic Resonance Study"*., by D.L. Pisaniello, S.F. Lincoln and E.H. Williams, *Inorg. Chim. Acta.*, 31, 237 (1978).

3. *"A Nuclear Magnetic Resonance Study of Trimethylphosphate Exchange on the Hexakis(trimethylphosphate)scandium(III) Ion"*., by D.L. Pisaniello, S.F. Lincoln and E.H. Williams, *J. Chem. Soc. (Dalton)*., 1473 (1979).

4. *"A Proton Magnetic Resonance Study of Ligand Exchange on the Hexakis(N,N-dimethylformamide)magnesium(II) Ion"*., by D.L. Pisaniello and S.F. Lincoln, *Aust. J. Chem.*, 32, 715 (1979).

5. *"A Nuclear Magnetic Resonance Study of Ligand Exchange on the Hexakis(dimethylmethylphosphonate)scandium(III) Ion"*., by D.L. Pisaniello and S.F. Lincoln, *Inorg. Chim. Acta.*, 36, 85 (1979).

6. *"A Proton Magnetic Resonance Study of Ligand Exchange on the Hexakis(1,1,3,3-tetramethylurea)scandium(III) Ion and its N,N-dimethylacetamide Analogue"*., by D.L. Pisaniello and S.F. Lincoln, *J. Chem. Soc. (Dalton)*, 699 (1980).

REFERENCES

1. S.F. Lincoln, *Coord. Chem. Rev.*, 6, 309 (1971).
2. H.S. Frank and W.Y. Wen, *Discuss. Faraday. Soc.*, 24, 133 (1957).
3. C.H. Langford and J.P.K. Tong, *Acc. Chem. Res.*, 10, 258 (1977).
4. M. Eigen and R.G. Wilkins, in *"Mechanisms of Inorganic Reactions"*, *Adv. Chem. Ser.*, 49, 55 (1965).
5. M. Eigen and K. Kustin, *I.C.S.U. Review*, Elsevier, Amsterdam, 5, 106 (1963).
6. D.H. Hewkin and R.H. Prince, *Coord. Chem. Rev.*, 5, 45 (1970).
7. T.R. Stengle and C.H. Langford, *Coord. Chem. Rev.*, 2, 349 (1967).
8. J.P. Hunt, *Coord. Chem. Rev.*, 7, 1 (1971).
9. M. Eigen, *Pure Appl. Chem.*, 6, 97 (1963).
10. H. Diebler, M. Eigen, G. Ilgenfritz, G. Maas and R. Winkler, *Pure Appl. Chem.*, 20, 93 (1969).
11. H. Strehlow and W. Knoche, *Ber. Bunsenges. Phys. Chem.*, 73, 427 (1969).
12. C.H. Langford and H.B. Gray, in *"Ligand Substitution Processes"*, W.A. Benjamin, New York, N.Y., 1966.
13. C.K. Ingold, in *"Structure and Mechanism in Organic Chemistry"*, Cornell University Press, Ithaca, N.Y., 1953, Chapter 7.
14. J. Burgess, in *"Metal Ions in Solution"*, Ellis Horwood, Chichester, 1978, Chapter 11.
15. D.R. Stranks, *Pure Appl. Chem.*, 38, 303 (1974).
16. F.K. Meyer, K.E. Newman and A.E. Merbach, *J. Amer. Chem. Soc.*, 101, 5588 (1979).
17. C. Ammann, P. Moore and A.E. Merbach, *Helv. Chim. Acta.*, 63, 268 (1980).
18. A.J. Brown, O.W. Howarth, P. Moore and W.J.E. Parr, *J. Chem. Soc. (Dalton).*, 1776 (1978).

19. D.L. Pisaniello and S.F. Lincoln, *J. Chem. Soc. (Dalton).*, 699 (1980).

20. R.G. Wilkins, in *"The Study of Kinetics and Mechanism of Reactions of Transition Metal Complexes"*, Allyn and Bacon, Boston, 1974.

21. J. Frahm and H.-H. Füldner, *Ber. Bunsenges. Phys. Chem.*, 84, 173 (1980).

22. N.A. Matwiyoff and W.G. Movius, *J. Amer. Chem. Soc.*, 89, 6077 (1967).

23. J.-J. Delpuech, A. Péguy, P. Rubini and J. Steinmetz, *Nouv. J. Chim.*, 1, 133 (1977).

24. J. Crea and S.F. Lincoln, *J. Chem. Soc. (Dalton)*, 2075 (1973).

25. J.W. Neely, *Ph.D. dissertation*, University of Berkeley, 1971.

26. A.E. Merbach, P. Moore, O.W. Howarth and C.H. McAteer, *Inorg. Chim. Acta.*, 39, 129 (1980).

27. J.-J. Delpuech, M.R. Khaddar, A.A. Péguy and P.R. Rubini, *J. Amer. Chem. Soc.*, 97, 3373 (1975).

28. L.S. Frankel and E.R. Danielson, *Inorg. Chem.*, 8, 1964 (1972).

29. L. Rodehüser, P.R. Rubini, and J.-J. Delpuech, *Inorg. Chem.*, 16, 2837 (1977).

30. M.N. Tkaczuk and S.F. Lincoln, *Aust. J. Chem.*, 32, 1915 (1979).

31. J. Neely and R. Connick, *J. Amer. Chem. Soc.*, 92, 3476 (1970).

32. E.F. Caldin, *Pure Appl. Chem.*, 51, 2067 (1979).

33. A. McAuley and J. Hill, *Quart. Rev.*, 23, 18 (1969).

34. R.G. Pearson, *J. Amer. Chem. Soc.*, 85, 3533 (1963).

35. U. Mayer and V. Gutmann, *Struct. Bonding. (Berlin)*, 12, 113 (1972).

36. R.H. Erlich, E. Roach and A.I. Popov, *J. Amer. Chem. Soc.*, 92, 4989 (1970).

37. R.H. Erlich and A.I. Popov, *J. Amer. Chem. Soc.*, 93, 5620 (1971).

38. V. Gutmann and E. Wychera, *Inorg. Nucl. Chem. Lett.*, 2, 257 (1966).

39. R.S. Drago and B.B. Wayland, *J. Amer. Chem. Soc.*, 87, 3571 (1965).

40. E.F. Caldin and H.P. Bennetto, *J. Soln. Chem.*, 2, 217 (1973).

41. J.P. Hunt and H. Taube, *J. Chem. Phys.*, 18, 757 (1950).

42. D.R. Stranks, in *"Modern Coordination Chemistry"*, ed. J. Lewis and R.G. Wilkins, Interscience, N.Y., p. 78.

43. E.F. Caldin, in *"Fast Reactions in Solution"*, Wiley, New York, 1964.

44. A.K.S. Ahmed and R.G. Wilkins, *J. Chem. Soc.*, 3700 (1959), 2895, 2901 (1960).

45. A.G. Davies and W.M. Smith, *Proc. Chem. Soc.*, 380 (1961).

46. M. Eigen and L. de Maeyer, in *"Techniques of Organic Chemistry"*, ed. S.L. Friess, E.S. Lewis and A. Weissberger, 2nd edn., Interscience, N.Y., 1963, Vol. 8, p. 895.

47. G. Czerlinski and M. Eigen, *Z. Electrochem.*, 63, 652 (1959).

48. G. Atkinson and S. Petrucci, *J. Phys. Chem.*, 70, 3122 (1966).

49. M. Eigen, *Discuss. Faraday. Soc.*, 17, 194 (1954).

50. J. Burgess and M.C.R. Symons, *Quart. Rev.*, 3, 276 (1968).

51. A.J. Brown, D.A. Couch, O.W. Howarth and P. Moore, *J. Mag. Res.*, 21, 503 (1976).

52. T.C. Farrar and E.D. Becker, in *"Pulse and Fourier Transform NMR"*, Academic Press, New York, 1971.

53. S.F. Lincoln, *Prog. React. Kinetics*, 9, 1 (1977).

54. H.M. McConnell and D.D. Thomson, *J. Chem. Phys.*, 31, 85 (1959).

55. R.A. Hoffmann and S. Forsén, *Prog. NMR. Spectrosc.*, 1, 15 (1966).

56. C.S. Johnson, *Adv. Mag. Res.*, 1, 33 (1965).

57. F.A. Anet and A.J.R. Bourne, *J. Amer. Chem. Soc.*, 89, 760 (1967).

58. L.M. Jackman, T.E. Kavanagh and R.C. Haddon, *Org. Mag. Res.*, 1, 109 (1969).

59. H.S. Gutowsky, D.M. McCall and C.P. Slichter, *J. Chem. Phys.*, 21, 279 (1953).

60. E.L. Hahn and D.E. Maxwell, *Phys. Rev.*, 88, 1070 (1952).

61. H.M. McConnell, *J. Chem. Phys.*, 28, 430 (1958).

62. R. Kubo, *J. Phys. Soc. Jap.*, 9, 935 (1954).

63. R. Kubo and K. Tomita, *J. Phys. Soc. Jap.*, 9, 888 (1954).

64. R.A. Sack, *J. Chem. Phys.*, 21, 1688 (1953).

65. M.T. Rogers and J.C. Woodbrey, *J. Phys. Chem.*, 66, 540 (1962).

66. I.O. Sutherland, *Ann. Reports. NMR. Spectrosc.*, 4, 71 (1971).

67. J. Crea, *Ph.D. dissertation*, University of Adelaide, 1976.

68. T. Nakagawa, *Bull. Chem. Soc. Jap.*, 39, 1006 (1966).

69. T.H. Siddall, III, W.E. Stewart and F.D. Knight, *J. Phys. Chem.*, 74, 3580 (1970).

70. E.H. Williams, *Ph.D. dissertation*, University of Adelaide, 1980.

71. C.S. Johnson and C.G. Moreland, *J. Chem. Ed.*, 50, 477 (1973).

72. R.K. Gupta, T.P. Pitner and R. Wasylishen, *J. Mag. Res.*, 13, 383 (1974).

73. G. Binsch, in *"Dynamic Nuclear Magnetic Resonance Spectroscopy"* eds. L.M. Jackman and F.A. Cotton, Academic Press, New York, 1975, p. 70.

74. S. Glasstone, K.J. Laidler and H. Eyring, in *"Theory of Rate Processes"*, McGraw-Hill, N.Y., 1941.

75. H.P. Bennetto and E.F. Caldin, *J. Chem. Soc. (A).*, 2198 (1971).

76. J. Crea, R. Di Guisto, S.F. Lincoln and E.H. Williams, *Inorg. Chem.*, 16, 2825 (1977).

77. ACTENG, Quantum Chemistry Program Exchange, 79.

78. G.J. Honan, S.F. Lincoln and E.H. Williams, *Inorg. Chem.*, 17, 1855 (1978).

79. J. Pitha and R.N. Jones, *Can. J. Chem.*, 44, 3031 (1966).

80. M. Eigen and K. Tamm, *Z. Electrochem.*, 66, 107 (1962).

81. J.H. Swinehart, T.E. Rogers and H. Taube, *J. Chem. Phys.*, 38, 398 (1963).

82. S. Nakamura and S. Meiboom, *J. Amer. Chem. Soc.*, 89, 1765 (1967).

83. T.D. Alger, *J. Amer. Chem. Soc.*, 91, 2220 (1969).

84. F.L. Dickert, *Ber. Bunsenges. Phys. Chem.*, 83, 593 (1979).

85. J. Crea, S.F. Lincoln and R.J. West, *Aust. J. Chem.*, 26, 1227 (1973).

86. Y.S. Ng, G.A. Rodley and W.T. Robinson, *Inorg. Chem.*, 15, 303 (1976).

87. Y.S. Ng, G.A. Rodley and W.T. Robinson, *Acta. Cryst.*, B34, 2385 (1978).

88. F. Toma, M. Villemin and J.M. Thiéry, *J. Phys. Chem.*, 77, 1294 (1973).

89. N.M. Karayannis, C.M. Mikulski, M.J. Strocko, L.L. Pytlewski and M.M. Labes, *J. Inorg. Nucl. Chem.*, 32, 2629 (1970).

90. S.F. Lincoln, D.L. Pisaniello, T.M. Spotswood and M.N. Tkaczuk, *submitted for publication, Aust. J. Chem.*

91. R.D. Shannon and C.T. Prewitt, *Acta. Cryst.*, B25, 925 (1969), B26, 1046 (1970).

92. F. Basolo and R.G. Pearson, in *"Mechanisms of Inorganic Reactions"*, 2nd edn., Wiley, N.Y., 1967, p. 23.

93. L.A. LaPlanche and M.T. Rogers, *J. Amer. Chem. Soc.*, 86, 337 (1964).

94. R.H. Barker and G.J. Boudreaux, *Spectrochim. Acta.*, A23, 727 (1967).

95. G. Geier, *Ber. Bunsenges. Phys. Chem.*, 69, 617 (1965).

96. A. Bonsen, W. Knoche, W. Berger, K. Giese and S. Petrucci, *Ber. Bunsenges. Phys. Chem.*, 82, 678 (1978).

97. A. Fratiello, R.E. Lee and R.E. Schuster, *Inorg. Chem.*, 9, 31 (1970).

98. G.A. Melson, D.J. Olszanski and A.K. Rahimi, *Spectrochim. Acta.*, A33, 301 (1977).

99. J. Aveston, *J. Chem. Soc. (A).*, 1599 (1966).

100. L.N. Komissarova, *Zh. Neorg. Khim.*, 25, 143 (1980).

101. W.E. Morf and W. Simon, *Helv. Chim. Acta.*, 54, 794 (1971).

102. T.J. Anderson, M.A. Neuman and G.A. Melson, *Inorg. Chem.*, 13, 158 (1974).

103. D.D. McRitchie, R.C. Palenk and G.J. Palenk, *Inorg. Chim. Acta.*, 20, L27 (1976).

104. T.J. Anderson, M.A. Neuman and G.A. Melson, *Inorg. Chem.*, 13, 1884 (1974).

105. C.C. Addison, A.J. Greenwood, M.L. Haley and N. Logan, *J. Chem. Soc. Chem. Commun.*, 580 (1978).

106. R.P. Scholer and A.E. Merbach, *Inorg. Chim. Acta.*, 15, 15 (1975).

107. A. Nelson, private communication.

108. M.N. Tkaczuk, private communication.

109. F. Kutek, *Colln. Czech. Chem. Commun.*, Eng. Edn., 32, 3767 (1967).

110. N.P. Crawford and G.A. Melson, *J. Chem. Soc. (A)*, 141 (1970).

111. P. Stilbs and M.E. Moseley, *J. Mag. Res.*, 31, 55 (1978).

112. T.H. Siddall, III and W.E. Stewart, *J. Chem. Soc. Chem. Commun.*, 617 (1968).

113. K.A. Jensen and J. Sandström, *Acta. Chem. Scand.*, 23, 1911 (1969).

114. E.A.H. Griffith, W.A. Spofford, III and E.L. Amma, *Inorg. Chem.*, 17, 1913 (1978).

115. G.J. Honan, S.F. Lincoln and E.H. Williams, *J. Chem. Soc. (Dalton)*, 320 (1979).

116. R.H. Barker, G.J. Boudreaux and S.L. Vail, *Appl. Spectr.*, 20, 414 (1966).

117. K. Spaargen, P.K. Korver, P.J. van der Haak and T.J. de Boer, *Org. Mag. Res.*, 3, 639 (1971).

118.
(a) B.N. Figgis, B. Skelton and A.H. White, *Aust. J. Chem.*, 33, 425 (1980).

(b) J. Delaunay, C. Kappenstein and R.P. Hugel, *J. Chem. Soc. Chem. Commun.*, 679 (1980).

119. T. Drakenberg, K.I. Dahlqvist and S. Forsén, *J. Phys. Chem.*, 76, 2178 (1972).

120. J.V. Hatton and R.E. Richards, *Mol. Phys.*, 3, 253 (1960).

121. J.V. Hatton and R.E. Richards, *Mol. Phys.*, 5, 139 (1962).

122. D.L. Pisaniello and S.F. Lincoln, *submitted for publication, Inorg. Chem.*

123. G.A. Melson and R.W. Stotz, *Coord. Chem. Rev.*, 7, 133 (1971).

124. H. Kessler and A. Rieker, *Justus. Liebigs. Ann. Chem.*, 708, 57 (1967).

125. B.F. Pedersen and B. Pedersen, *Tetrahedron Lett.*, 2995 (1965).

126. W.E. Stewart and T.H. Siddall, III, *Chem. Rev.*, 70, 517 (1970).

127. V. Gutmann and R. Schmid, *Coord. Chem. Rev.*, 12, 263 (1974).

128. A. Fratiello, *Prog. Inorg. Chem.*, 17, 57 (1972).

129. N. Serpone and R. Ishayek, *Inorg. Chem.*, 10, 2650 (1971).

130. A. Merbach and F. Gnaegi, *Helv. Chim. Acta.*, 54, 691 (1971).

131. S.F. Bartram, *Inorg. Chem.*, 5, 749 (1966).

132. J.A. Cunningham, D.E. Sands and W.F. Wagner, *Inorg. Chem.*, 6, 499 (1967).

133. F. Albert Cotton and G. Wilkinson, in *"Advanced Inorganic Chemistry"*, 3rd edn., Wiley-Interscience, 1972, p. 1056.

134. E. Giesbrecht and M. Kawashita, *J. Inorg. Nucl. Chem.*, 32, 2461 (1970).

135. T.J. Anderson, M.A. Neuman and G.A. Melson, *Inorg. Chem.*, 12, 927 (1973).

136. A.J. Carty and D.G. Tuck, *J. Chem. Soc.*, 6012 (1964).

137. T. Moeller and G. Vicentini, *J. Inorg. Nucl. Chem.*, 24, 1477 (1965).

138. V.N. Krishnamurthy and S. Soundararajan, *J. Inorg. Nucl. Chem.*, 29, 517 (1967).

139. M. Kawashita Kuya, O.A. Serra and V.K. Lakatos Osorio, *J. Inorg. Nucl. Chem.*, 37, 1998 (1975).

140. J.A. Carver, private communication.

141. S.F. Lincoln, *Pure Appl. Chem.*, 51, 2059 (1979).

142. K. Kustin and J. Swinehart, *Prog. Inorg. Chem.*, 13, 116 (1970).

143. H. Hoffmann, *Pure Appl. Chem.*, 41, 327 (1975).

144. P. Fischer, H. Hoffmann and G. Platz, *Ber. Bunsenges. Phys. Chem.*, 76, 1060 (1972).

145. G.J. Honan, *Ph.D. dissertation*, University of Adelaide, 1979.

146. R.R. Krug, W.G. Hunter and R.A. Grieger, *J. Phys. Chem.*, 80, 2335, 2341 (1976).

147. A.I. Vogel, in *"Quantitative Inorganic Analysis"*, 3rd edn., Longmans Green and Co., London, 1961, p. 702.

148. A.I. Vogel, in *"A Text Book of Practical Organic Chemistry"*, 3rd edn., Longmans Green and Co., London, 1961, p. 176.

149. P.W.N.M. van Leeuwen and W.L. Groeneveld, *Inorg. Nucl. Chem. Lett.*, 3, 145 (1967).

150. R.G. Bates, M. Paabo and R.A. Robinson, *J. Phys. Chem.*, 67, 1833 (1963).

151. A.L. Van Geet, *Analytical Chem.*, 40, 2227 (1968).

152. R. Kubo, *Nuovo Cimento, Suppl.*, 6, 1063 (1957).

153. R.A. Sack, *Mol. Phys.*, 1, 163 (1958).